The study of clay/epoxy nanocomposites: their synthesis, microstructures and properties

Heng Wang

A Thesis

in

The Department

of

Mechanical and Industrial Engineering

Presented in Fulfillment of the Requirements
for the Degree of Master of Applied Science (Mechanical Engineering) at
Concordia University
Montreal, Quebec, Canada

August 2004

ABSTRACT

The study of clay/epoxy nanocomposites: their synthesis, microstructures and properties

Heng Wang

A new type of organoclay (Triclay) to be used in epoxy-based nanocomposites is synthesized by the addition of a multi-functional intercalating agent to primary clay (Cloisite Na+). The purpose is to enhance the interface by introducing primary bonds between the clay layers, the organic intercalating agent and the epoxy. The properties and microstructure were investigated thoroughly allowing the evaluation of the efficacy of this new epoxy-based nanocomposite.

A new Liquid-Liquid method for synthesizing nanocomposites is developed. This new method improves the dispersion and exfoliation of the organoclay in the polymer matrix; thus improving the end-use properties. Rheological tests on the uncured epoxy-Triclay system demonstrate that this method results in a great increase in viscosity, even more than the most advanced high-pressure mixing method used previously. A higher viscosity of the uncured system indicates better exfoliation. In a 5wt% Triclay nanocomposite, the compressive tests on the cured samples show that there is a 45% increase in maximum stress, a 10% increase in yield stress and a 26% increase in modulus over the pure epoxy-amine system.

In order to obtain the optimum nanocomposite properties, the pure epoxy-amine system, Epon828/Epi-cure 3046, is also studied. The effect of epoxy amine ratio on the solid-state micro and nano-structures is studied at the optimum curing temperature for nanocomposite production. Under these conditions it is found that the highest amount of hard phase in the cured epoxy system is not at the stoichiometric point, but rather at an epoxy-rich point.

Acknowledgements

A great debt of gratitude goes to Dr. Paula Wood-Adams and Dr. Suong V. Hoa, who show their scientific research method , and their great influence upon my professional development.

Thanks to the following individuals: Mr. Lixin Wu and Mr. Weiping Liu for lots of technical discussions. Thanks also go to Mr. Ming Xie for his great help in lab instruments' operation.

Table of contents

List of Figures

List of Tables

1. Introduction

The science and technology of nanocomposites has created great excitement and expectations in the last decade. Research in this area is focused on the nanoscale second phase embedded in a polymeric matrix, which gives physical and chemical properties that cannot be achieved by ordinary material synthesis methods. By using new methods of synthesis, as well as tools for characterization and manipulation, nanocomposite science and technology is now in explosive growth [1, 2, 3].

The term nanocomposite describes composites composed of a matrix (usually here meaning polymer—thermoset or thermoplastic) and dispersed particles with at least one dimension in the scale of nanometer (10^{-9}m). For clay/polymer nanocomposites, the clay particles have a layer thickness of 0.95 nm. Clay reinforced nanocomposites have been causing great interest since the successful synthesis of organoclay/ polyamide-6 nanocomposites by researchers from the Toyota research group in Japan [4]. These nanocomposites show great improvement in mechanical properties and chemical/ thermal stability.

In order to achieve optimum properties of clay/epoxy nanocomposites, not only it is necessary to understand the physical/chemical properties of the polymer matrix and the clay particles, but also it is important to be able to design a good interface. The interface plays a very important role because a better interfacial bond will impart

better overall properties, such as tensile strength, inter-laminar shear strength, delamination resistance, and corrosion resistance.

In this study, a new type of multifunctional amine intercalating agent and a new method for preparing nanocomposites are introduced, and properties of the resulting new organoclay/epoxy system are studied. This new organoclay can create primary bonds between the two phases to improve the interface, and thus improve the properties of the composites. The new L-L method can give better particles dispersion and exfoliation, thus improving the overall properties of the nanocomposites. Also, the epoxy matrix properties are investigated to understand the effects of stoichiometry, micro/nano structures and corresponding mechanical properties.

In the following sections, we will introduce the materials we used to synthesize nanocomposites, explain some technical words that are necessary to understand nanocomposites, and illustrate the instruments used to do chemical and mechanical properties measurements.

1.1 Montmorillonite

Montmorillonite, one type of clay, is a good candidate for preparing nanocomposites. First, it has a high aspect ratio—50 to 1000 with an average of 200, high modulus, and high strength [2]. Secondly, it may be exfoliated into separated layers and

dispersed into the matrix after it has been treated with an intercalating agent. As a result, the properties of composites can be improved by adding only minimum amount of organoclay—usually less than 5wt%. Thirdly, montmorillonite is cheap as it is the most abundant soil on earth.

Figure 1 shows the chemical structure of montmorillonite. Natural montmorillonite is self-organized to form layered stacks with a regular gallery height of 0.95 nm. Isomorphic substitution within the layers (e.g.. Al^{3+} replaced by Mg^{2+} or Fe^{2+}) causes the layer to have negative charges that are counterbalanced by exterior cations, such as Na^{+}, Ca^{2+}, or K^{+}, residing in the galleries. As a natural product, variations in chemical compositions exist even in samples from the same source.

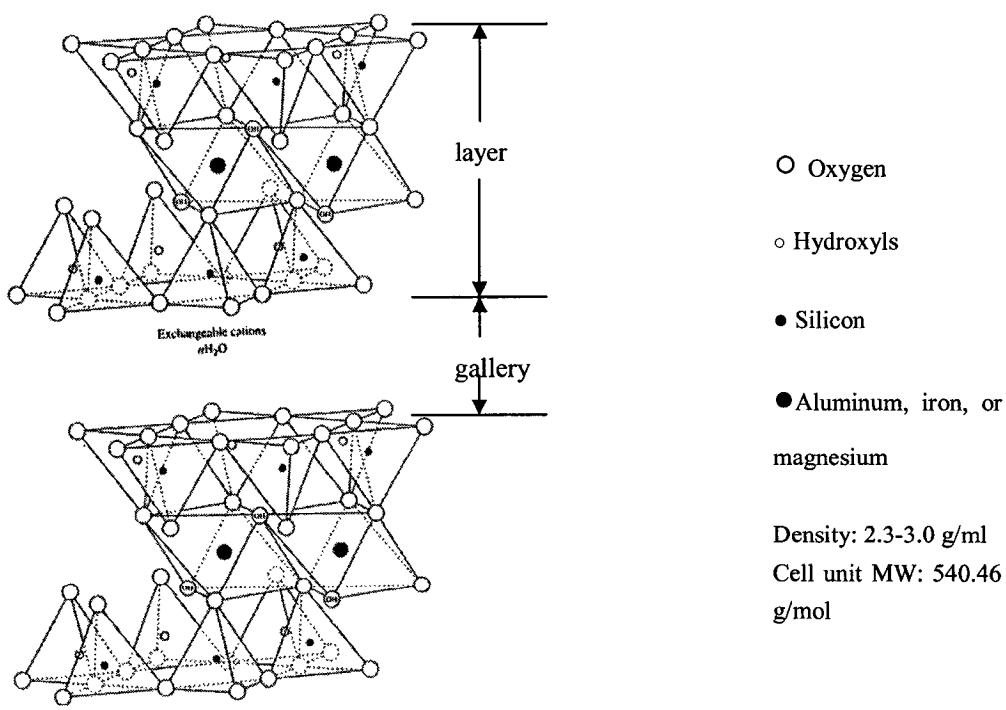

Figure 1: Chemical structure of montmorillonite.

In montmorillonite, all of these gallery cations are normally exchangeable with other species in solution, which means we can use intercalating agents to change the clay's surface chemical composition. The charge density or cation exchange capacity (CEC), which is one important index for montmorillonite, varies from one layer to another. One mean value is given for every batch of montmorillonite. The montmorillonite suitable for preparing nanocomposites should have a CEC of 70 to 150 meq (milliequivalents) /100g [2]. This CEC value means that there are 70-150 x 10^{-3} mol exchangeable inorganic cations that reside in an average 100 gram of montmorillonite.

1.2 Epoxy

The most common polymer matrix for advanced composites is epoxy. It has excellent overall properties including adhesion, strength, chemical/corrosion resistance and low shrinkage. Epoxy is characterized by its epoxide group (Figure 2) that can react with the protons from an amine to form a stable crosslinked structure (Figure 3). If the epoxide group is modified with an additional $-(CH_2)-$, this group is called a glycidyl group.

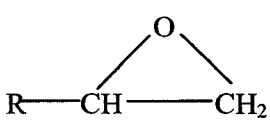

Figure 2: Chemical illustration of epoxide group.

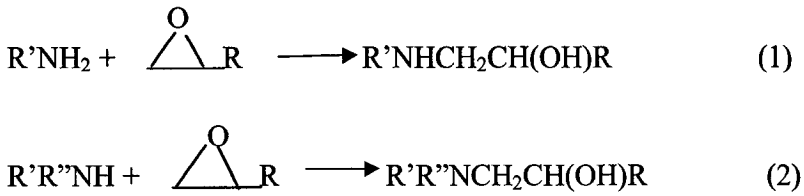

Figure 3: Illustration of chemical reactions between epoxy and amine.

The most commonly used epoxy is diglycidyl ether of bisphenol A (DGEBA), Figure 4. There are also many special epoxy resins, such as TGMDA, and epoxy novalac among others for different industrial applications.

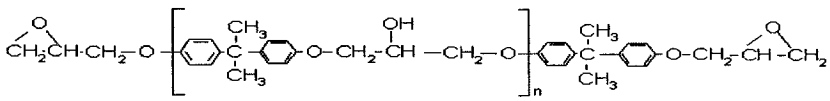

Figure 4: The chemical structure of DGEBA.

Curing agents for epoxies include amines, polyamides, and anhydrides. The cure kinetics and the T_g of a cured system are dependent on the molecular structure of the curing agent (hardener).

The stoichiometry of epoxy to amine is important in polymerization. In order to obtain the optimum properties, there should be no unreacted epoxy or amine when the cure is completed. If there are extra amine or epoxy molecules, those small unreacted molecules will lead to lower T_g and lower mechanical properties of cured epoxy. In practice, it usually requires one hydrogen atom from an amine to react

with one epoxide group. For example, DGEBA which has two epoxide groups has a molecular weight of 350 grams/mole, so its equivalent weight is 175 grams/epoxide. The curing agent DETA (diethylenetriamine) is an aliphatic amine with a molecular weight of 103 grams/mole and it has five active hydrogens, so its equivalent weight is 20.6 grams/hydrogen. For every 175.0 g epoxy, there needs to be 20.6 g DETA, so the stoichiometric ratio is 12 parts DETA for 100 parts DGEBA.

1.3 Intercalating agent and organoclay formation

An intercalating agent is also called a compatibilising agent, a swelling agent, and an intercalant. In some ways, the term swelling agent may be more appropriate than intercalating agent. The most important function of an intercalating agent is to modify the clay surface, changing it from hydrophilic to organophilic, just like industrial surfactants. Accompanying the above change, intercalating agent molecules penetrate into the clay layers and increase the gallery distance. That is why we are calling them intercalating agents.

Figure 5 shows some common intercalating agents. The most commonly used agent for clay is alkyl-ammonium onium. Its cation group ($-NH_3^+$) can replace the clay gallery cations in ion exchange, and form an ionic bond with the surface of the clay.

octadecylammonium onium: $CH_3(CH_2)_{17}NH_3^+$
1,12-diaminododecane onium: $NH_2(CH_2)_{12}NH_3^+$
n-hexadecyl tri-n-butyl phosphonium onium: $(C_4H_9)_3P(C_{16}H_{33})^+$
cetyltrimethylammonium: $CH_3(CH_2)_{12}N(CH_3)_3^+$

Figure 5: Some useful intercalating agents.

The chemical preparation of the intercalating agent is a standard acid-amine reaction to form an amine cation onium. The most useful acids are HCl and HBr, and the most useful amines are long alkyl amine and aminosilane:

$$R\text{-}NH_x + H^+ \rightarrow R\text{-}NH_x^+$$

Where R is a long alkyl chain $-(CH_2)_n-$, usually n>8, or organic silane group.

Because the inorganic cations in the clay galleries are exchangeable, amine cation onium can easily expel the inorganic cations and form ionic bonds between organic onium and clay layers:

$$\mathbf{Na^+\,clay} + \mathbf{AH^+soln} \rightarrow \mathbf{AH^+clay} + \mathbf{Na^+soln}$$

(Primary clay) (Amine cation intercalating agent) (Organoclay) (expelled inorganic ions)

1.4 Organoclay/epoxy nanocomposites

In-situ polymerization is the most promising way to create nanocomposites. In-situ polymerization means that the polymerization occurs in the presence of the clay.

In general, the dispersion of clay layers in a matrix can result in the formation of three types of composites, depending upon the clay concentration, degree of clay layer separation and distribution in the composites. They are:

(a) Conventional Composites where clay tactoids are simply dispersed as a segregated phase, Figure 6 (a).

(b) Intercalating Nanocomposites where one or more polymer molecules are inserted into clay galleries to increase the gallery heights and clay stacks still are in a layered structure, Figure 6 (b).

(c) Exfoliated Nanocomposites where the layers are delaminated and dispersed in the matrix to form a homogeneous structure so the properties of composites can be improved, Figure 6 (c).

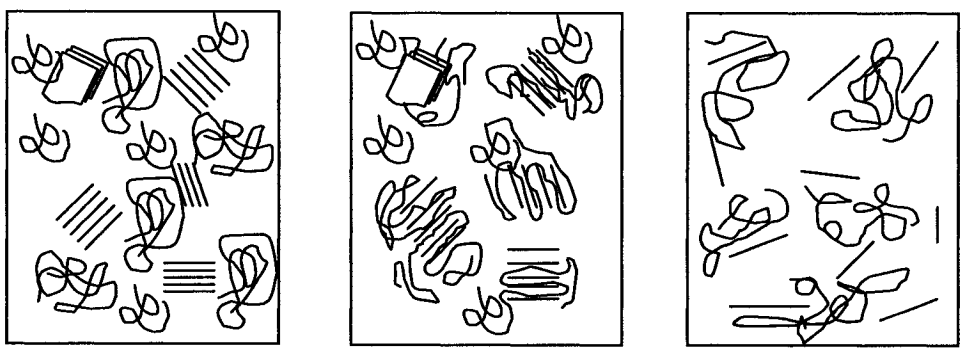

(a) (b) (c)

Figure 6: Illustrations of the three types of clay/polymer composites: (a) conventional type, (b) intercalating type, (c) exfoliated type.

In fact, the above three types of clay layer dispersion co-exist in nanocomposite systems.

1.5 Interface in nanocomposites

An interface exists between the reinforcement (clay) and the polymer matrix, and it plays an important role in determining the final nanocomposite mechanical and chemical properties, such as tensile strength, inter-laminar shear strength, delamination resistance, and corrosion resistance.

The interface is the area around the reinforcement surface. In this area, the local chemical composition, physical properties, morphological features, and mechanical properties change drastically.

A strong bond between the reinforcement and the matrix is desired so that the exterior force can be transferred from the polymer matrix to the reinforcement to improve the mechanical properties of the composite.

1.6 Instruments—DSC, FT-IR, XRD, DMA, Viscometer, AFM, and NanoDMA

In order to investigate the effect of an intercalating agent treatment, different nanocomposite synthesis methods, and the properties of our synthesized clay/epoxy

nanocomposites, Differential Scanning Calorimetry (DSC), Fourier Transformed Infrared (FT-IR), X-ray Diffraction (XRD), Dynamic Mechanical Analysis (DMA), Viscometer, Atomic Force Microscopy and nanoscale dynamic mechanical analysis instruments were performed. Next we give a brief introduction to the above techniques.

Differential scanning calorimetry **(DSC)**: DSC is a technique that determines the variation in the heat flow given out or taken in by a sample when it undergoes temperature scanning in a controlled atmosphere. In polymer science, DSC can be used to analyze polymer crystallization, melting, chemical reactions and the glass transition T_g (see Figure 7).

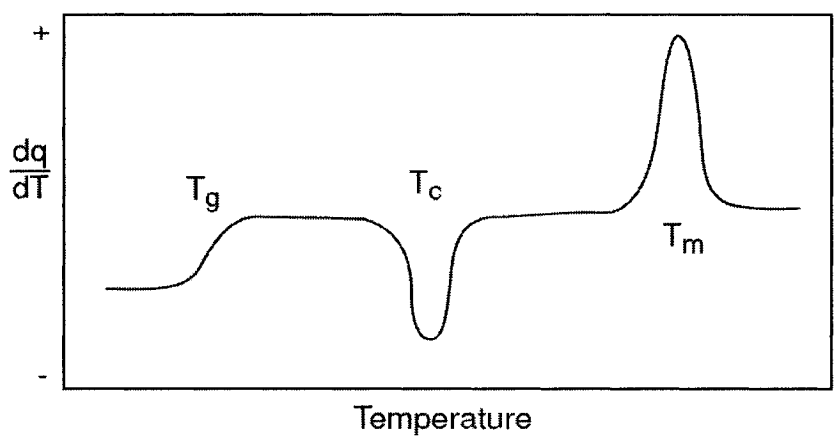

Figure 7: Standard DSC curve for semi-crystalline polymer.

Fourier transform infrared (FT-IR): Molecular bond vibrations at various infra-red frequencies are recorded for identifying types of chemical bonds in a solid or liquid sample by producing an infrared absorption spectrum that is like a molecular

"fingerprint". It is an easy way to identify the presence of certain functional groups in a molecule, since chemical functional groups are known to absorb infrared light at specific frequencies. Hooke's law was used to calculate the frequency of infrared light absorbed:

$$\nu_{osc} = \frac{1}{2\pi}\sqrt{k\frac{m_1 + m_2}{m_1 m_2}}$$

Where k = force constant indicating the strength of the bond, and m_1 and m_2 are the masses of the two atoms.

X-ray diffraction (XRD): XRD uses an incident x-ray beam to interact with the atoms arranged in a periodic manner in 2D to reveal the regular order of crystalline materials. The Bragg equation is used to calculate the basal spacing:

$$2d\sin\theta = n\lambda$$

Where d = Basal spacing distance, θ= x-ray injection angle, λ= wave length of x-ray, and n= 1,2,3...integers.

Dynamic mechanical analysis (DMA): DMA is a thermo-analytical method by which the mechanical behavior of a sample subjected to a specific temperature program is investigated under a sine wave or square wave force. It can determine the storage and loss moduli and the damping factor of a sample as a function of temperature, time, and frequency of an applied oscillating load (see figure 8).

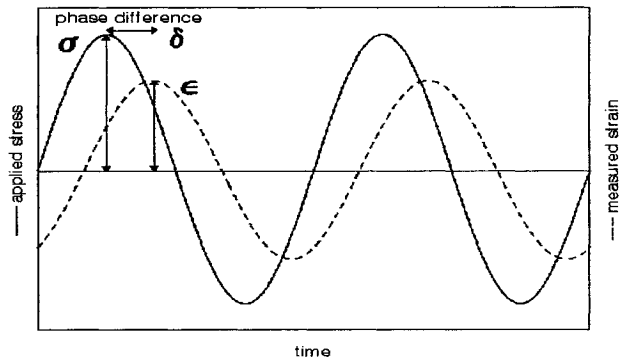

Figure 8: DMA measures the amplitudes of the stress σ and strain ε as well as the phase angle δ between them to resolve the modulus into an in-phase component - the storage modulus (E'), and an out-of-phase component, the loss modulus (E").

Viscometer: Viscometers are used to define the viscous properties of a fluid at ambient or defined temperatures. For rotational viscometry, torque is required to rotate a spindle at constant speed. The torque is proportional to the viscous drag on the immersed spindle, and thus to the viscosity of the fluid. Viscometers can handle both Newtonian and non-Newtonian fluids.

Atomic force microscope (AFM): The AFM utilizes a sharp tip at the end of a cantilever moving over the surface of a sample in a raster scan. The cantilever bends in response to the force between the tip and the sample producing 3-dimensional pictures (see Figure 9).

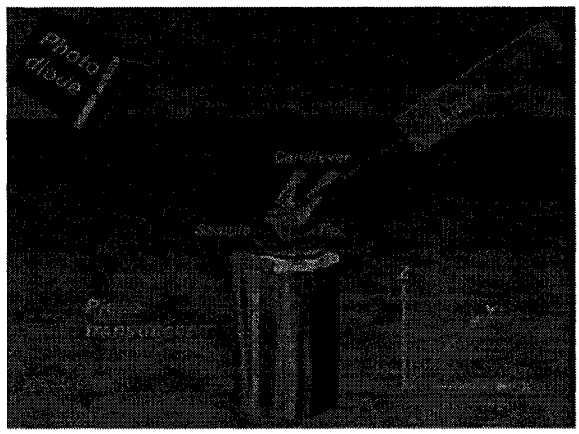

Figure 9: Illustration of AFM measurement theory.

There are three modes in AFM:

1. TappingMode:

The cantilever is oscillated at or near its resonance frequency across the sample surface with an amplitude ranging typically from 20nm to 100nm.

2. Contact Mode:

The tip contacts the surface through the adsorbed fluid layer on the sample surface.

3. Non-contact Mode:

The tip does not contact the sample surface, but oscillates above the adsorbed fluid layer on the surface during scanning.

These three methods have their advantages and disadvantages, and are suitable for different materials. Table 1 gives comparisons and their suitable applications.

Table 1: Comparison of three AFM modes and their applications in material science:

Mode	Sample requirements	Resolution	Damage to the sample	Suitable materials
TappingMode	Rough Z range <7μ m	5nm	Low in air; No scraping;	Polymer, biomaterials
Contact Mode	Suitable for rough samples	Atomic <1nm	Lateral and normal force can damage soft samples	Metal, inorganic (ceramic) materials
Non -contact Mode	smooth	Low due to tip - sample separation	No	Extremely hydrophobic materials

From Table 1, it is clear that TappingMode is used for polymer materials and has a very high resolution on most samples with less damage to soft samples.

The topological and phase images can be obtained in this mode. The topological images reflect the sample surface topological variance. In the phase pictures, the phase lag between the cantilever motion and its driving force is used to show the difference in viscosity/modulus, as well as topography.

The surface roughness can be represented by two indexes: (1) altitude differences, Z (also called z-range), and (2) the average roughness R_A, which is defined as the arithmetic average of the absolute values of the altitude differences compared to a medium plan.

$$R_A = \frac{1}{L}\int_0^L \left|Z - \overline{Z}\right| dx$$

Here, L represents the analyzed length.

Nano Indentation: An indenter tip is driven into the material surface by applying an increasing load up to some preset value. The load is then gradually decreased until partial or complete relaxation of the sample has occurred. The load and displacement are monitored continuously to produce a load displacement curve from which nano-mechanical properties such as hardness, Young's modulus, stress-strain behavior, time dependant creep properties, fracture toughness of plastic and elastic energy of the sample material can be calculated (see Figure 10).

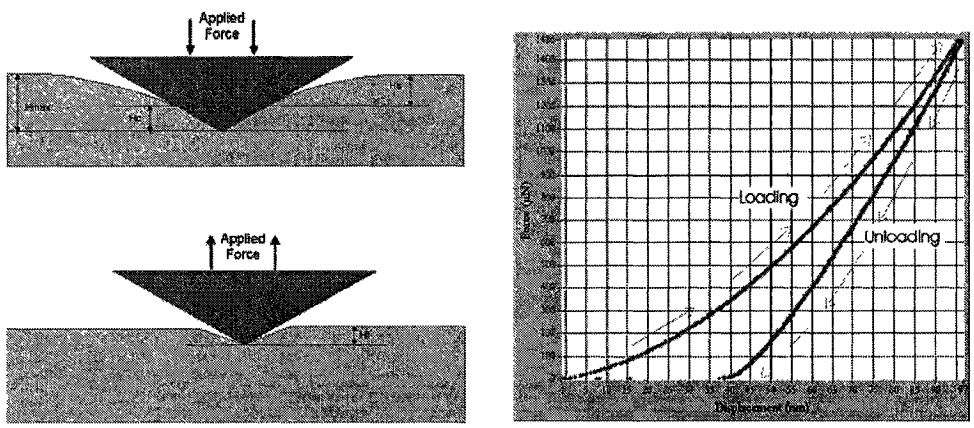

Figure 10: Nano indentation method (provided by Hysitron company).

Nano dynamic mechanical analysis (NanoDMA): NanoDMA allows for dynamic tests such as Frequency Sweep (0.1-300Hz), Proportional AC Load, Variable AC Load and Constant AC Load (see Figure 11). Force amplitude, displacement amplitude and phase lag are measured to give storage modulus, loss modulus, and tan delta. Nanomechanical test methods including Nano indentation and NanoDMA are new techniques under development.

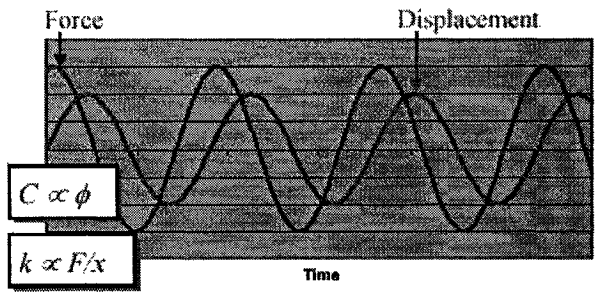

$$E' = \frac{k_s\sqrt{\pi}}{2\sqrt{A_c}} \qquad E'' = \frac{\omega C_s\sqrt{\pi}}{2\sqrt{A_c}}$$

Figure 11: Illustration of a dynamic test by using NanoDMA (provided by Hysitron company).

1.7 Objectives

The research objective is to improve the mechanical and chemical properties of clay/epoxy nanocomposites and to understand the mechanism of reinforcement.

As far as we know, there are two ways to reach our goal: interface design and full exfoliation of clay layers.

The interface plays an important role in all polymer-based composites. With interface design, we can improve not only the mechanical and chemical properties of clay/epoxy nanocomposites, but also other properties, such as barrier enhancement and fire retardation. In this research, we limit our goal to mechanical properties which is one of the most important factors for nanocomposite application. We also

aim to understand the relationship between the micro-/nano-structure and the bulk properties.

Full exfoliation of the clay layers is the highest goal every scientist wants to reach in the area of clay/polymer nanocomposites. It was found that good clay dispersion in polymer matrix is not achieved by direct mixing. Recently the microfludiser was shown to effectively break the agglomerated clay particles and disperse them evenly into the polymer matrix. But this method has two problems: there is a restriction on particle size and the aspect ratio of the clay layers can be decreased due to the high shear force. In this work we develop a new method to improve the dispersion of organoclay and to reach the best exfoliation with minimal damage to the clay layers.

2. Literature Review

2.1 History of clay/polymer nanocomposites

The application of clay in polymers can be traced back to the 1960's. The details of this application include using clay in Epoxy, Nylon 6, PP, ABS, and HDPE where improvements in strength, stability, and cracking resistance were found [5, 6]. Different researchers studied the surface treatments by suitable surfactants such as octadecylammonium and organosilanes. The efficiency of clay to improve the physico-mechanical properties was found to be determined by [6]: 1) the degree of clay dispersion in the matrix; 2) the interface between the reinforcement and matrix; and 3) the clay size. During this stage, researchers used more than 20% clay in the polymer and the clay was regarded as a common filler.

In 1993, researchers from the Toyota research group in Japan successfully synthesized organoclay/ polyamide-6 nanocomposites [4] that showed improvement in mechanical properties and thermal stability when only 4 wt% of clay was introduced in the polymer matrix (see Table 2).

Table 2: The mechanical and thermal properties of clay/nylon6 nanocomposites [4]

Specimen	Montmorillonite (wt%)	Tensile Strength (MPa)	Tensile Modulus (GPa)	Heat Distortion Temperature (°C at 18.5kg/cm^2)
Nylon 6	0	69	1.1	65
Clay/nylon 6 (In-situ polymerization)	4.2	97	1.9	152

Many researchers then expanded this use of organoclay in different polymer matrix nanocomposites, including epoxy [7—10], polypropylene [11], polystyrene [12, 13], polyimide [14,15], polyurethane [16] and dendritic polymers [17, 18]. Results showed that mechanical properties, physical/chemical properties, and fire resistance of the composites were improved at very low clay content.

For clay/epoxy nanocomposites that are regarded as one of the most promising new materials for industrial application, many aspects have been studied. Areas such as the effect of curing processes [19, 20, 21], the promoters [21], the choice of clays [22], the choice of curing agents [23], the choice of intercalating agents by using alkylammonium ion with different alkyl chain length and different head groups (primary, secondary, tertiary and quaternary alkylammonium) [24], and corresponding morphology, mechanical, chemical, thermal, and rheological properties have been thoroughly researched. Because nanocomposite matrix materials offer less curing shrinkage, low thermal expansion, and reduction in micro-cracking and good solvent resistance, clay/carbon-fiber/epoxy composites are currently under investigation [25, 26, 27].

2.2 Organoclay synthesis and properties

The systematic study of the effect of the addition of organoclay on the properties of nanocomposites is a new and attractive topic. Theng gave a very detailed description

of clay, organoclay and organoclay filled polymer as well as of clay-organic chemical reactions in his study of organoclay synthesis and its application [6, 28] for the organoclay filled composites [other researchers: 29, 30].

The most common way to prepare organoclay is [31]:

1) Screen the primary clay (Na^+ montmorillonite) with a sieve at least 325 mesh to remove the impurities;
2) Synthesize intercalating agent—mixing amines with dilute acids like HCl, or HBr in distilled water, the ratio of amine group to acid H^+ is 1:1;
3) Prepare clay/water solution at 60—80 °C, and then mix intercalating agent with clay solution, continue stirring for more than 1 hour;
4) Wash, dry and sieve organoclay.

<u>The effect of alkyl chain length of protonated alkylamines:</u>

It was found that the alkyl chain length must exceed six carbon atoms to attain increased clay gallery spacings. The increased gallery spacings that result when the alkyl chains are longer cause an increase of mechanical properties [32, 33] (Figure 12).

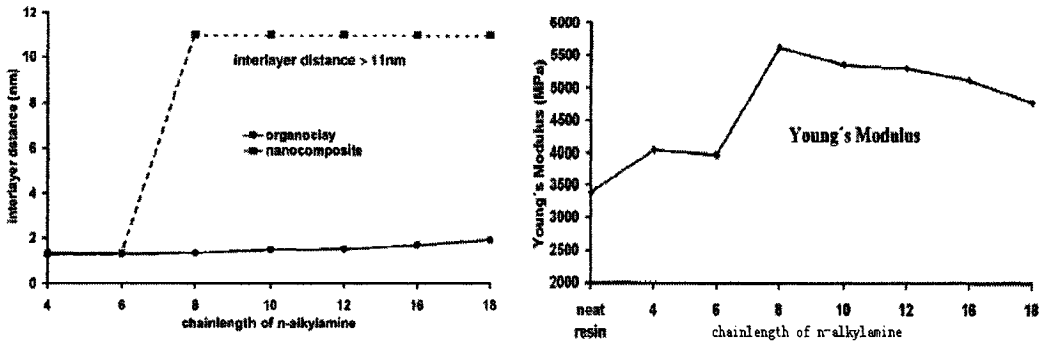

Figure 12: The relationship of the basal spacings distance (left graph) and the mechanical properties of clay/epoxy nanocomposite (right graph) with the onium $CH_3(CH_2)_nNH_3^+$ carbon number n [32,33].

Suh and Park studied the degree of clay surface modification using XRD and TGA to investigate the structures of organoclay (with different amounts of intercalating agent)/PVK (Poly 9-vinyl carbazole) [34]. They found that a lower amount of intercalating agent leads to better exfoliation. Because some of the clay surface remained unmodified, some of the polymer chains intercalated into the gallery spacings and some chains did not have any interaction with the bared clay and kept their coil conformation which lead to gallery spacing expansion. Also a low amount of intercalating agent allows for increased thermal stability.

For the choice of montmorillonites with different CEC, research indicates that the montmorillonite with lower CEC behaves better in final nanocomposites' properties than one with higher CEC, because low charge density clays give better exfoliation and are more readily accessible (they allow more free space) for intragallery polymerization [22, 32].

H.L.Tyan, C.M. Leu, and K.H. Wei studied the adoption of a functional intercalating agent [35,36]. In their clay/polyimide nanocomposite film synthesis, di-functional group, and tri-functional group, intercalating agents were introduced to modify the clay. They observed improvements in the modulus and the maximum stress resistance of clay/polyimide film. Their observations gave ideas about using a functional intercalating agent for epoxy to improve the interface between the clay and the matrix, as well as improving the final mechanical properties of clay/epoxy nanocomposites.

2.3 Study of clay/epoxy nanocomposites

2.3.1 Mechanical properties

Mechanical properties in clay/epoxy nanocomposites—Young's modulus, tensile/ compressive strength and toughness, will be reviewed in the following section.

Modulus: In general, the modulus monotonically increases when more organo clay is added [37, 38], Figure 13. The modulus increase in clay/epoxy is greatly affected by the epoxy matrix properties. For high modulus epoxy, a 10~30% increase can be observed, while a more than 100% increase can be reached in elastomeric epoxy [39], (see Figure 14).

The reinforcement in clay/epoxy nanocomposites modulus depends upon the amount of montmorillonite and the even dispersion of the clay particles in the matrix.

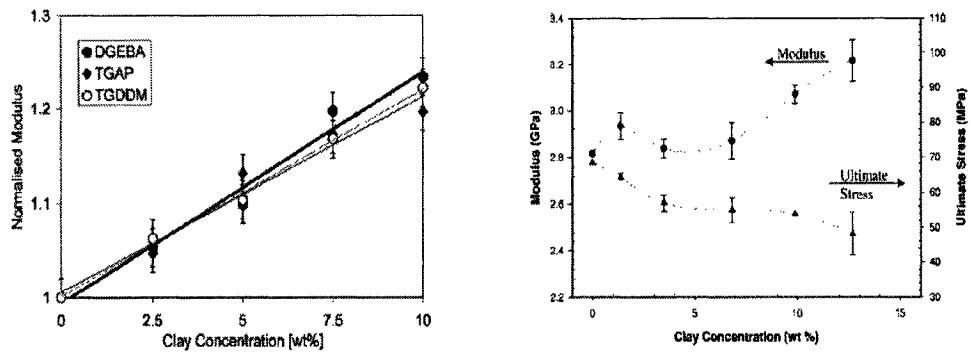

Figure 13: Illustrations of the relationship between the modulus and the amount of organoclay [37,38].

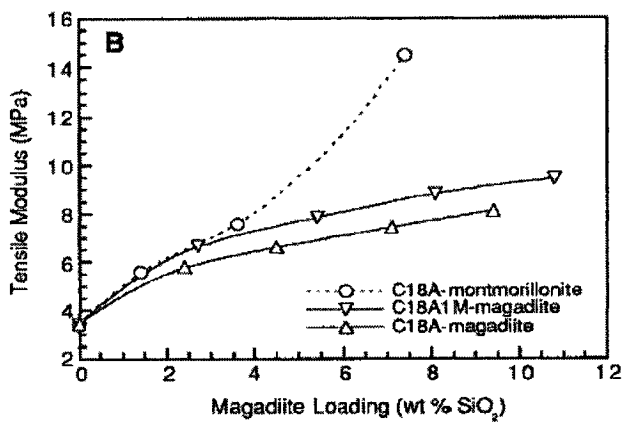

Figure 14: The reinforcement results of nanocomposite modulus for elastomeric epoxy [39].

Tensile strength: For clay/epoxy nanocomposites, the strength usually decreases as more clay is added, except for elastomeric epoxy [39] in which the strength increases more than 3 times compared to unmodified epoxy (see Figure 15).

The reinforced tensile strength mechanism depends upon the strength of the epoxy, the interface between the clay and the epoxy, the shape of the montmorillonites, and

the dispersion of clay in the matrix [6, 27, 33].

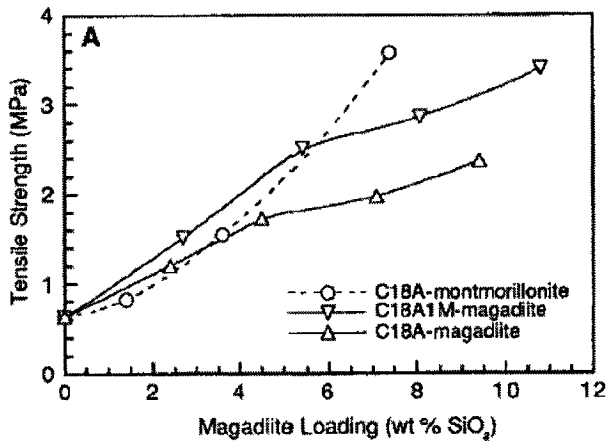

Figure 15: Tensile strengths of nanocomposites of elastomeric epoxy matrix [39].

Fracture toughness: Different research groups have investigated the fracture behavior of clay/epoxy nanocomposites and have reported fracture toughness improvements for brittle matrix [33, 38, and 40]. Zerda and Lesser [38] found that there is little improvement in toughness at low clay concentrations, a significant improvement in the stress-intensity factor K_{1C}, and an energy-release rate of G_{1C} at 3.5 wt% and above (see Figure 16).

The explanation for a reinforcement in toughness may be that the clay particles cause the crack to take a more tortuous path, either around or between regions of clays [38]. From experiments, it was found that the fracture face of clay/epoxy is quite rough and the epoxy fracture face appears very smooth.

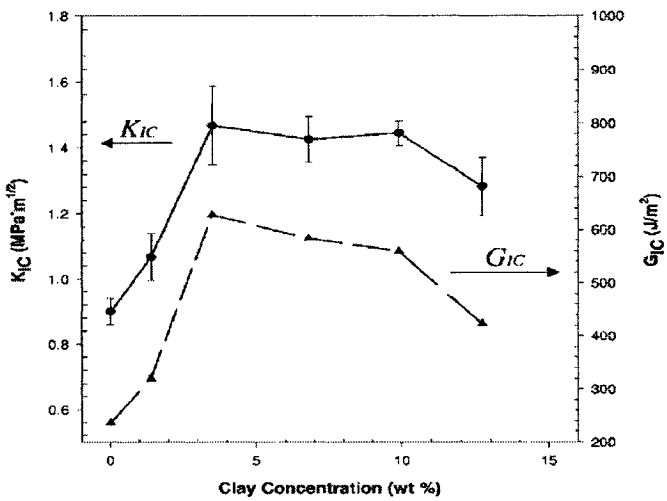

Figure 16: Changes in fracture toughness with increasing clay concentration [38].

2.3.2 Microstructure description

There are many types of microscopes including the scanning electron microscope (SEM), the tunneling electron microscope (TEM), and the atomic force microscope (AFM), as well as X-ray diffraction (XRD) to study clay/epoxy nanocomposites' structure.

<u>XRD studies</u>: X-ray diffraction patterns are widely used in clay/epoxy nanocomposites for clay exfoliation analysis. Clay in full exfoliation will give the most optimum properties, and XRD is an easily available method for evaluating the exfoliation state. XRD can give information about the effect of temperature, curing agents, promoters, processing methods on the clay exfoliation as well as information on the interaction between the organoclay and epoxy resin [41,42] (see Figure 17).

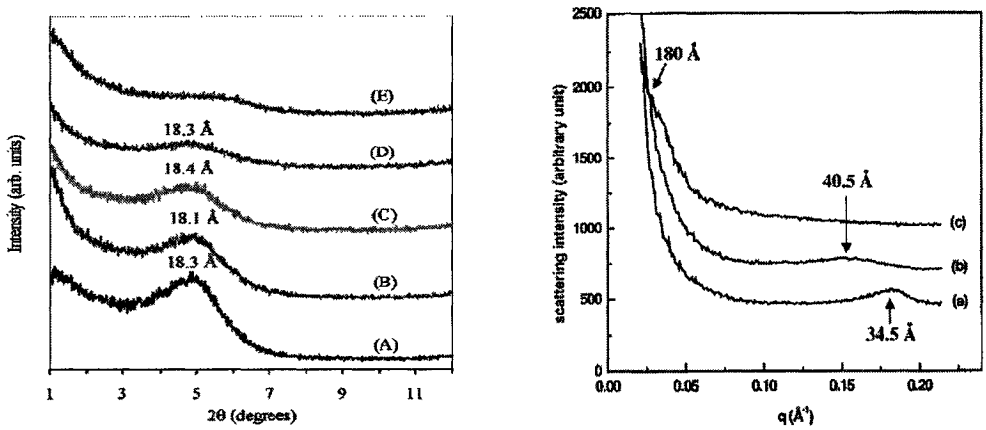

Figure 17: X-ray diffraction patterns reveal the effect of different factors for clay exfoliation. The left picture illustrates the effect of different preparation methods [41]: (A) organoclay, (B) organoclay-Epon 826, (C) organoclay-Epon 826 prepared by acetone solution, (D) organoclay-Epon 826 prepared by ethanol solution, (E) organoclay-Epon 826 prepared by 2-propanol solution, the amount of solvent used was 25 wt% of the epoxy resin, clay 6 wt%. The right picture illustrates the effect of amounts of curing agent [42]: epoxy cured with (a) 25 phr MPDA curing agent, (b) 14.5 phr MPDA, (C) 5 phr MPDA, clay 1 wt%.

SEM studies: Clay particles are difficult to disperse in a polymer matrix evenly and tend to agglomerate and reduce the surface energy. Scanning electron microscopy can be used to investigate clay distribution in the matrix. Figure 18 illustrates the morphology of different contents of clay in an epoxy matrix [38].

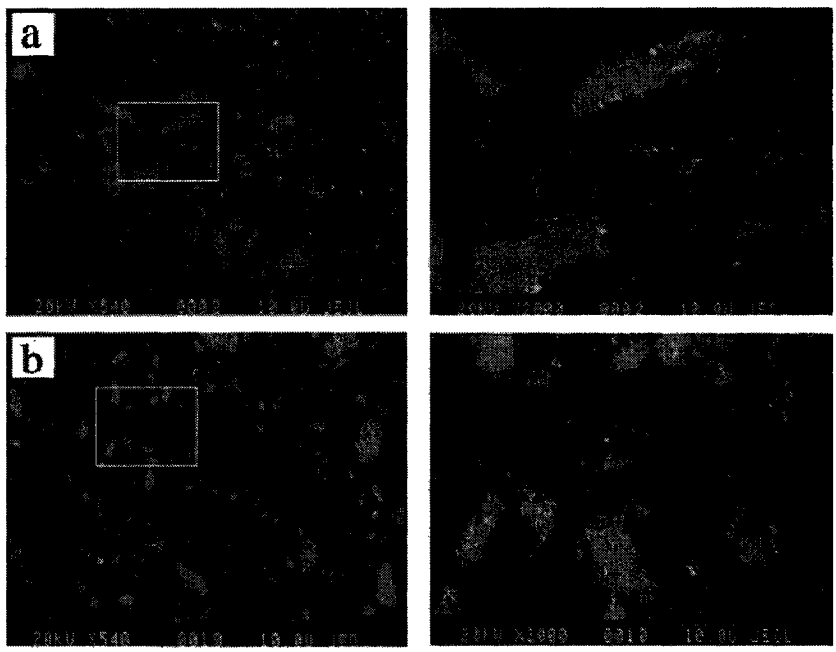

Figure 18: SEM micrographs of clay/epoxy nanocomposites with (a) 1.5 wt%, (b) 7 wt% clay [38].

TEM studies: The most common way to show the exfoliated/intercalated clay layers in nanoscale is done by the transmission electron microscope (TEM) image method. This method is widely applied for clay-thermoset and clay-thermoplastic nanocomposites studies. It gives evidence that the clay exfoliates in the thermoset matrix in some spots, and clearly demonstrates the clay layers. Figure 19 shows one example of TEM application in nanocomposites [41].

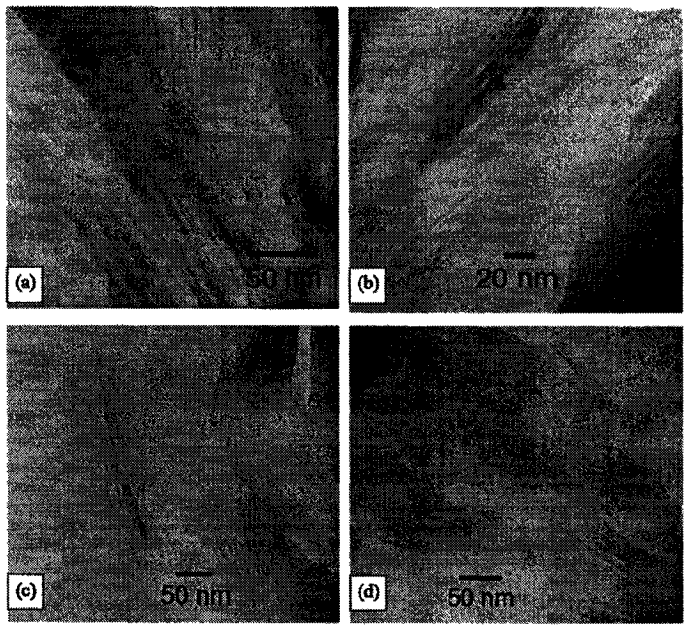

Figure 19: Transmission electron micrographs of clay/epoxy nanocomposites [41].

AFM studies: Some researchers have been using an atomic force microscope in TappingMode for revealing the nanoscale structures of nanocomposites.

Zilg et al [40] found that (1) compared with XRD, AFM analysis gave a high value of gallery space, and (2)clay layers seemed to be flexible and could be easily folded and scratched (see Figure 20 (a)).

Chin et al [42] use Kapton films to cover the bottom of their samples to investigate clay layer gallery height in clay/polyether nanocomposites containing 5wt% organoclay. Their results showed that the average distance between each stack was 20 nm (see Figure 20 (b)).

Becker et al [37] showed in their AFM images of clay/epoxy nanocomposites that at least part of the clay remained in tactoids or stacked in layers rather than forming a homogenous morphology through the whole matrix (see Figure 20 (c)).

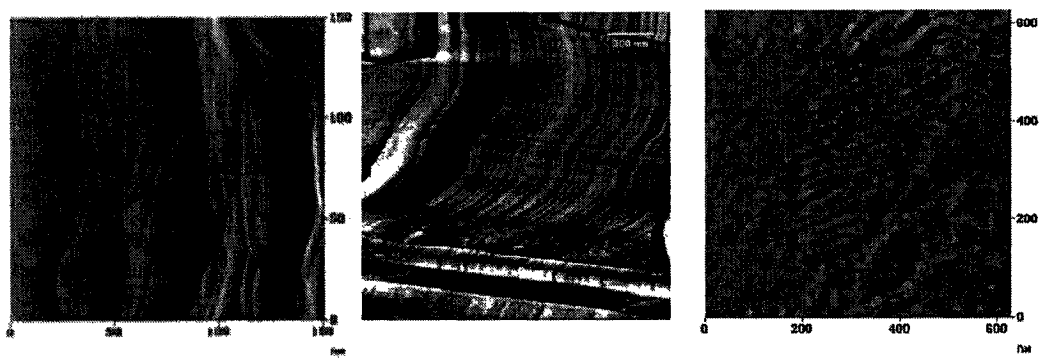

(a) (b) (c)

Figure 20: AFM phase images of clay/epoxy nanocomposites: (a) from Zilg et al [40].; (b) from Chin et al. [42]; (c) from Becker et al. [37].

2.3.3 Thermal properties

DSC is a tool for quantitative studies of chemical reactions, heat release/absorption, and glass transition temperatures (T_g) in epoxy-curing agent-organoclay systems. In clay/epoxy nanocomposites studies, combining DSC with other instruments such as XRD can give detailed information on clay exfoliation, factors for exfoliation, and variation of T_g.

Table 3 is the DSC data for the Epon 828/D2000 (curing agent)/clay system [10]. Note that 1) adding more clay can lower the onset temperature of the chemical

reaction, which was first observed by Wang and Pinnavaia [8]; 2) different clays possess different catalytic abilities for example, S30A in this system gave a lower onset temperature and a lower thermal release; 3) homopolymerization is not anticipated at epoxy curing temperature.

Table 3: DSC Data for Epon828/D2000/organoclay systems [10]

variation	T_{onset} (°C)	T_{max} (°C)	ΔH_{rxn} (cal/g)
Epon 828 Homopolymerization (no diamine)			
neat Epon 828	265	340	*a*
10% B34	316	329	*a*
10% S30A	304	315	56[b]
Epon 828 with D2000			
cold mix	132	190	29
75 °C mix	128	188	25
10% B34	125	190	21
10% S30A	98	166	16

[a] Difficult to integrate due to homopolymerization and degradation at same time. [b] Sharp, crisp, homopolymerization peak.

Kornmann et al [23] studied the effect of curing temperature on clay exfoliation. A higher temperature allows for better exfoliation. Under the catalytic effect of the intercalating agent a higher temperature increases the diffusion rate of the epoxy and the curing agent between the layers and favors the intragallery cure kinetics. As a result, the intragallery polymerization rate is faster than the polymerization rate in the extragallery, which leads to better exfoliation of the clay.

2.3.4 Rheological properties

Complex viscosity measurements can verify miscibility between clay and epoxy. A great increase (100 times) in viscosity can occur through successful epoxy

immigration into the clay layers [10], and the clay/epoxy mixture exhibits classic shear-thinning behavior, Figure 21.

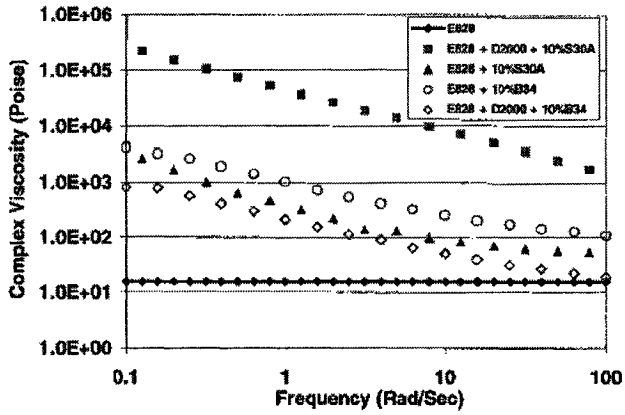

Figure 21: Complex viscosity of 10 wt% S30A and B34 in Epon 828 with and without diamine [10].

Small-strain stress relaxation under uniaxial deformation tests for glass clay/epoxy nanocomposites were also done by Lee and Lichtenhan [43]. Figure 22 illustrates time-dependent viscoelastic behavior of this nanocomposite, and shows modulus enhancement.

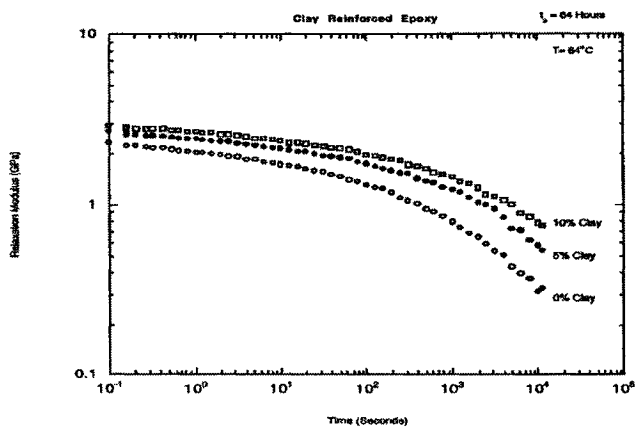

Figure 22: Small-strain stress relaxation modulus curves for DGEBA-D230-D2000-organoclay nanocomposites where applied strain is 0.001 [43].

2.3.5 Models

Clay/epoxy nanocomposite mechanical model

A three-phase model was developed to account for partial exfoliation and intercalation, the three phases being the matrix material, the exfoliated clay nano-layers and the intercalating nanoclay clusters. Luo and Denial [44] created a mechanical model to mathematically calculate the nanocomposite modulus and to describe the effect of clay concentrations, aspect ratios, exfoliation ratios, matrix modulus, and gallery spacings.

Monte Carlo simulations

This model is suitable for polymer melts filled with nanoparticles [45]. The systems simulated by a computer consist of three dimensionally periodic arrays of cubic cells containing N_p polymer chains and N_f filler particles. The simulation results showed that 1) the polymer units at the interface with the nanoparticles are arranged in a densely packed manner; 2) polymer chains become shorter; 3) each polymer chain connects several particles, and each particle is in contact with many different polymer chains. The nanoparticles behave as physical cross-links.

Other models

Analytical self-consistent field (SCF): A model to illustrate the interactions between the functional chains, the nonfunctional chains, and the clay layers [46].

Phase diagrams: This model uses a free energy function to express the complete phase diagram for the clay-polymer mixtures [47].

Mean-field lattice-based model: This model is used for making a clay-polymer melt intercalation prediction and it may give general guidelines for selecting potentially compatible polymer-organoclay systems [48, 49].

2.4 Study of epoxy

Epoxies are the mature products for industrial application, and are most widely used in composite material synthesis. Understanding the relationships between the microstructure and the properties of cured epoxy is inspiring interest in the area of composites, nanocomposites, and coatings [50].

VanLandingham et al [50] studied the Epon 828-PACM 20 curing agent system's microstructure, stoichiometry, and mechanical properties by using the AFM, the DMA and the density gradient column techniques (see Figure 23). In their system, a ratio of 28 phr curing agent for 100 phr Epon 828 yields the stoichiometric composition. They also investigated epoxy structural formation as a function of stoichiometry and

proposed a model for the formation of the two-phase structure. In their model, nucleus microgels form, grow and become hard phase and unreacted or partially-reacted prepolymer forms the soft dispersed phase.

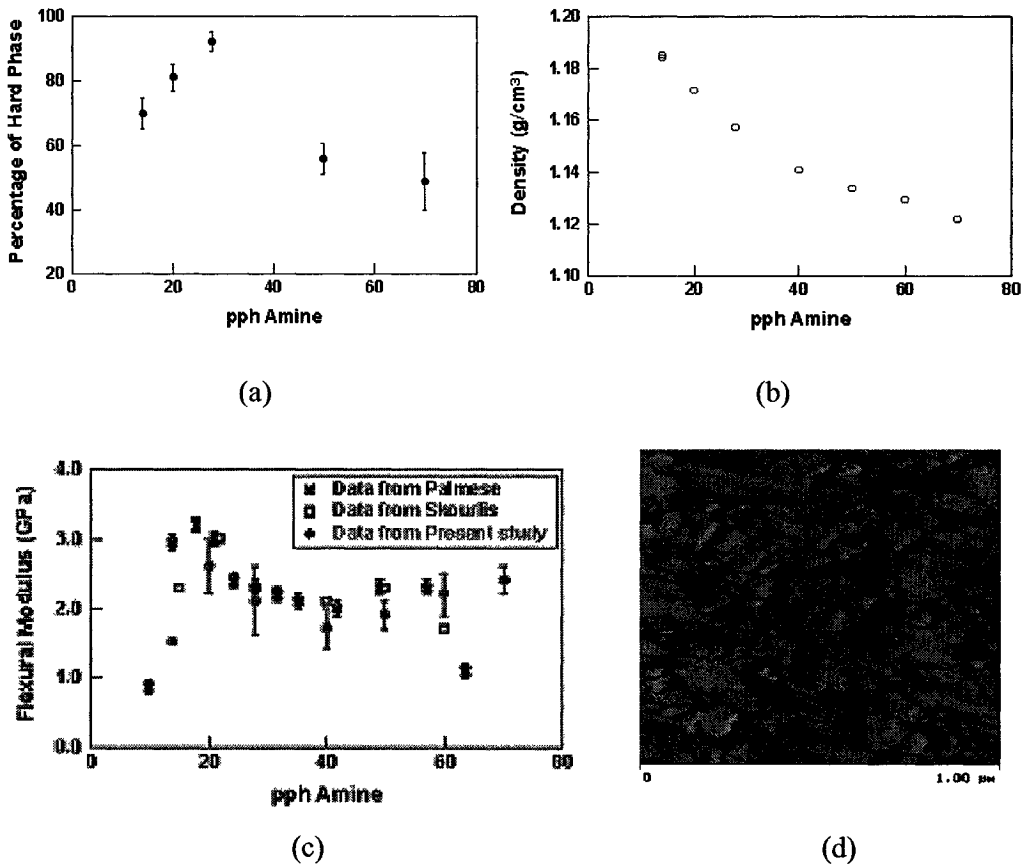

Figure 23: Illustration of Epon 828-PACM 20 amine system properties as the function of stoichiometry. (a) Bearing analysis of amount of hard-phase, (b) cured epoxy density, (c) flexural modulus at 30 °C, (d) AFM phase image at stoichiometric composition [50].

2.5 AFM application

The atomic force microscope (AFM) is a tool used to measure the nanoscale or atomic scale of non-conducting materials. The AFM is suitable for observing micro/nano structures of nonconductive materials with maximum resolution at around 1nm.

Usually in polymers, polymer composites, and biomaterials AFM studies [51, 52, 53, 54], topological and phase images are recorded at the same time. AFM topological images reflect the sample surface topological variance. In the phase pictures, the phase lag between the cantilever motion and its driving force is used to form phase images to illustrate the difference in viscosity/modulus, as well as topography.

The use of AFM in nanocomposites is just now in its beginning stage. Gu et al [55] used the AFM to study epoxy-air surface and epoxy-silicon interface. Substantial morphological and mechanical differences are observed between the surface and the interface for different crosslinked epoxies (see Figure 24).

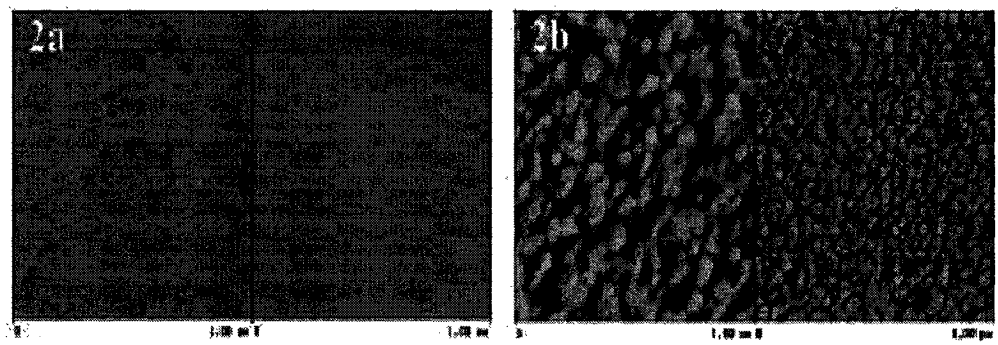

Figure 24: AFM topological image (left) and phase image (right) of epoxy coatings applied on silicon substrates: (2a) epoxy, air surface; (2b) epoxy-silicon interface. Scan size is 1 μm × 1 μm. Contrast variations from white to black are 10 nm for the topological image, and 90°for the phase image [55].

There are controversial views about epoxy surface morphology. Kocsis et al. [56] studied the microstructure of epoxy, vinylester/epoxy with the AFM, and their polished samples were eroded by Ar^+ ion bombardment. They found that the IPN (interpenetrating network) structure in vinylester/epoxy, and vinylester exhibited a two-phase microgel, but the epoxy showed a featureless homogeneous structure. The epoxies they used were of aliphatic and cycloapliphatic type, and curing agents were cycloapliphatic diamine and aliphatic diamine respectively. The question in this paper is that the sample surface roughness with z-range of about 750nm is too large and, therefore, not a good sample. Such a z-range means that surface topological factors prevent the details of the micro/nanoscale structures from being revealed.

Duchet et al. [57], in their AFM epoxy surface studies, tried to understand the microstructure of epoxy, and presented guidelines for the use of the AFM. They

showed their AFM investigation of DGEBA-amine systems surfaces, and concluded that the structure of Epoxy-amine was homogenous, that no nodules existed for cycloaliphatic and aromatic diamine cured epoxy, and that nodular structure existed in aliphatic amine epoxy systems and also in other thermoset polymers. In the first case (homogenous structure), the researchers regarded the nodular feature they observed to be raised from the topological variance and not due to the visco-elastic differences. In the second case (two-phase structure), they thought that the poor miscibility of long chain aliphatic amine with epoxy resulted in phase-separation. There are some questions about this paper: (1) in most cases, the authors used the sample's air-face for their AFM studies, which was not proper because the air-face structure is different from the inner structure; and (2) the detailed relationship between the surface roughness and its effect on the phase image were not well described.

We can see then, that there is still a need for continuing study of epoxy-amine system microstructure. For further AFM studies, refer to [58, 59, 60, 61, 62, 63] for relevant information.

3. Experiments

3.1 Methodology

In order to improve the properties of clay/epoxy nanocomposites, it is necessary to improve the interface between the clay and polymer matrix, improve the dispersion of clay and understand the change of matrix properties under the processing of nanocomposites.

For interface design, a multifunctional amine is used to synthesize intercalating agent, and then the primary clay is treated with this intercalating agent to obtain the new functional organoclay.

A series of studies on the new organoclay and organoclay/epoxy nanocomposites are done to understand the chemical and physical properties by using Fourier Transfer Infra-Red Spectroscopy (FT-IR), Differential Scanning Calorimetry (DSC), and X-ray diffraction (XRD), and to understand the performance properties by using DSC and mechanical tests.

As we know, advanced materials originate as liquids, this clue hints that it is necessary to avoid any dry state during the preparation of the clay/epoxy nanocomposites until the last stage (curing). A new synthesis method is developed to do this. The efficacy of this method was evaluated by studying the rheological

properties of the uncured clay/epoxy mixture and the cured clay/epoxy nanocomposites' mechanical properties (by DMA and compression test).

The optimal epoxy curing condition is changed when organoclay is added. A medium curing temperature is needed in order to achieve the best exfoliation of the organoclay. At this curing temperature the effect of epoxy-amine stoichiometric ratio is studied by using DSC, AFM, Nano indentation and NanoDMA, in order to find the best epoxy-amine ratio for preparing clay/epoxy nanocomposites. Further by this study, we can understand the relationship between the micro/nano-structure and mechanical properties.

3.2 Design of organoclay

It is known that in composites the interface plays a very important role. A stronger interfacial bond will greatly improve overall properties, such as tensile strength, inter-laminar shear strength, delamination resistance, toughness and corrosion resistance. Creating primary bonds between two phases is one of the most useful methods to improve the interface and thus, improve the properties of composites.

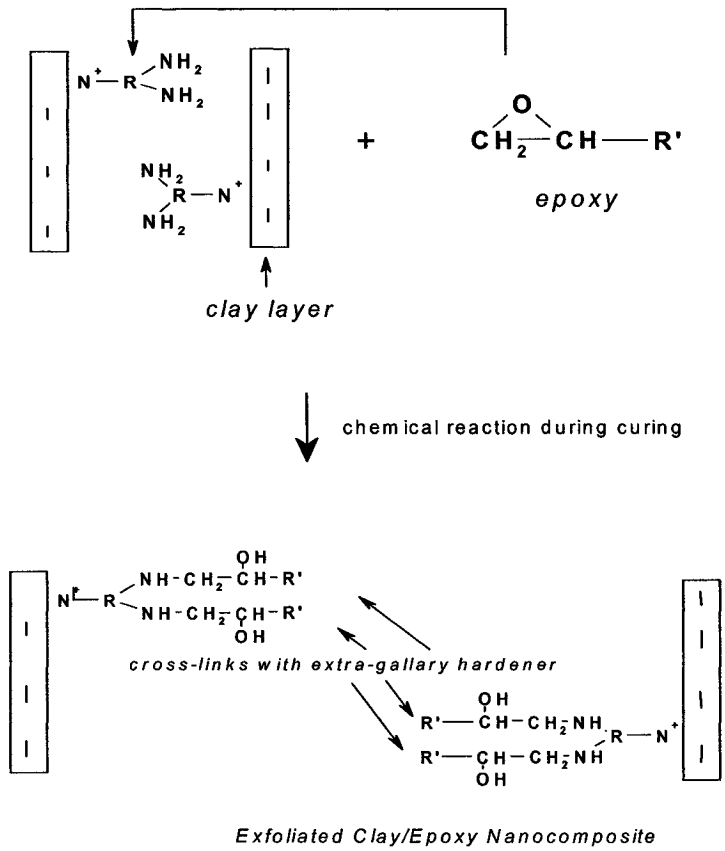

Figure 25: Illustration of the interface reinforcement mechanism.

Based upon the above considerations, a new type of multifunctional amine intercalating agent has been synthesized. A new type of organoclay, Triclay, is synthesized by the chemical reaction between montmorillonite and this new intercalating agent. The mechanism of reinforcement in the interface between the organo-clay and the matrix is shown in Figure 25.

3.3 Materials

Here is the list of all materials used in the experiments:

(a) Epoxy

The epoxy resin used was diglycidyl ether of bisphenol A, EPON 828, provided by Resolution Performance Products (Shell Chemicals), with a molecular weight of about 377, and an epoxide equivalent weight of about 189.

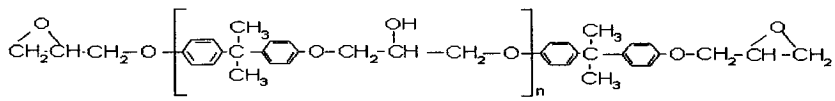

n=0 (88%); n=1 (10%); n=2 (2%).

(b) Curing agent

Epi-Cure 3046, an aliphatic diamine with an equivalent weight of about 90 is used as the curing agent. It was provided by Resolution Performance Products. Its composition is:

5—10% Ethanediamine, and 85—95% Triethylenetriamine (TETA) /tall oil fatty acid amido amine [CCOHS MSDS record number 2427156].

The stoichiometric quantity of Epi-Cure 3046 to Epon 828 is about 47 phr (parts amine per 100 parts epoxy is abbreviated as phr amine).

(c) Montmorillonite

The primary clay is a natural Na^+ rich montmorillonite (Cloisite Na+) purchased from Southern Clay Products [64]. Its Cation Exchange Capacity (CEC) is 92.6meq/100g clay;

Organoclay I.30E is a surface modified montmorillonite commercial mineral used for comparison with our synthesized Triclay and was provided by Nanocor Inc.

(d) Intercalating agent

JEFFAMINE® T-403 polyoxypropylenetriamine, supplied by the Huntsman Corporation was used to synthesize the intercalating agent. Figure 26 illustrates its chemical structure [65]. It's average molecular weight is about 438.

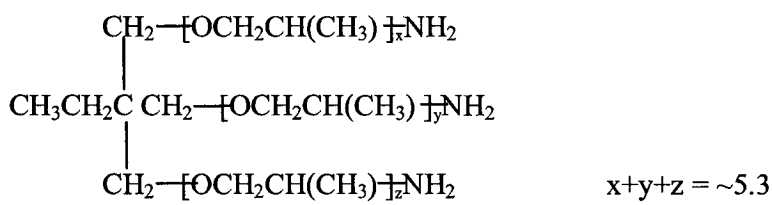

Figure 26: Chemical structure of T-403.

JEFFAMINE T-403 is light in color, low in viscosity and vapor pressure, high in primary amine content, and completely miscible in a wide variety of solvents, including water.

(e) Other Chemicals

Acid HCl (Hydrogen Chloride) is used to prepare the intercalating agent. 2N chemical grade HCl, and 0.1N $AgNO_3$ (Silver Nitrate) chemical grade were purchased from Daigger & Co.

3.4 Samples preparation

3.4.1 Organoclay synthesis

An amount of 9.473 grams of primary clay (Cloisite Na+) was dispersed into 750 ml of H_2O at 60 °C under 300 rpm, and stirred for about 30 minutes. The intercalating agent was prepared by titrating 0.013 mol of T-403 with 6.5 ml 2M HCl in 100 ml of distilled water. It was then poured into the primary montmorillonite hot water suspension and stirred for another hour at the same temperature. The precipitate was filtered and washed several times with a hot ethanol/water solution (50/50) until no Cl^- could be detected by one or two drops of 0.1N $AgNO_3$. After the powder was dried, it was ground and passed through a #325 sieve. This lab-synthesized organoclay is referred to as Triclay.

3.4.2 Epoxy preparation

Suitable amounts of Epi-cure 3046 were added to Epon 828. After mixing and outgassing, the Epon/Epi-cure viscous liquids were poured into a preheated silicone rubber mould that was packed with teflon film at its bottom. The processing curing cycle for the Epon828/Epi-cure 3046 was a two-hour cure at 95°C. A series of epoxy-amine samples were prepared (see table 4).

In Table 4, sample 100-47 means there are 47 parts of curing agent for 100 parts of Epon 828.

Table 4: Sample names and their corresponding compositions in epoxy-amine sample

Sample Name	Weight of epoxy (g)	Weight of amine (g)	Amine phr
100-25	11.417	2.845	24.9
100-35	11.517	4.019	34.9
100-47	19.220	9.028	47.0
100-52	13.423	6.976	52.0
100-60	13.502	8.100	60.0
100-80	11.646	9.318	80.0
100-120	16.523	19.843	120.0

3.4.3 Nanocomposites preparation

The most common way to prepare clay/epoxy nanocomposites is the direct mixing of organoclay with epoxy with or without solvent. The organoclay is in the dry state, thus it is very difficult to disperse it evenly in the matrix and most of the organoclay remains as agglomerates with radii far above 1 μm.

Using high shear force during flow to break the organoclay particles is an answer to above problem of agglomeration. The microfludiser is a high-pressure mixing machine which can effectively break solid particles down to less than 1 μm.

A new method is invented to synthesize organoclay/epoxy nanocomposites, which is hereafter called the L-L method. This method combines organoclay synthesis with organoclay/epoxy preparation, and solves the agglomeration problem caused by using dry organoclay. The new process is illustrated in Figure 27.

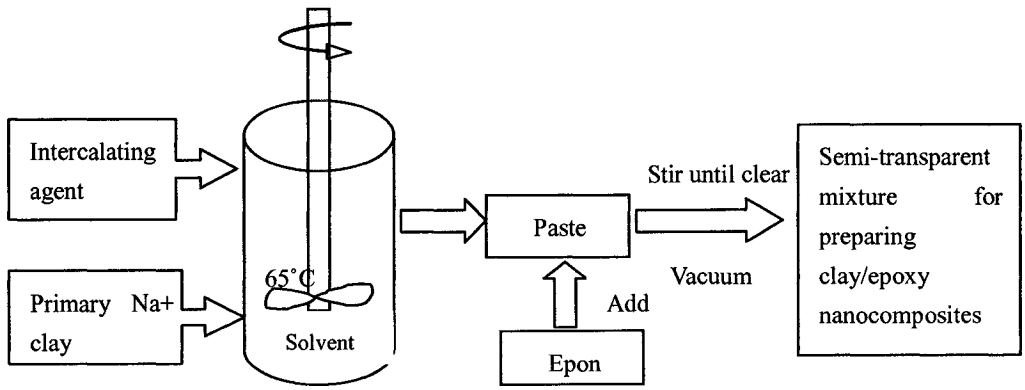

Figure 27: New L-L method for synthesizing organoclay/epoxy nanocomposites.

Direct mixing procedure:

The suitable amount of organoclay was added to the epoxy solution at 80 °C and stirred for 2 hours, followed by outgassing. Then the curing agent was added, cast into a preheated silicone mould and cured in an oven at a temperature of 95 °C or 125 °C. This direct mixing without solvent was used in the XRD study only.

Alternatively, the epoxy was premixed with organoclay in the presence of ethanol and stirred for about 16 hours at 25 °C. The ethanol solvent was evaporated by a 2 hour vacuum outgassing at 60 °C. The amount of solvent used was 50 % of the weight of the epoxy. After that, the curing agent was added and cured at an elevated temperature of 95 or 125 °C.

35 phr curing agent Epi-cure 3046 was used for all nanocomposites synthesized by direct mixing.

L-L method:

The amount of 10.0 grams of primary clay (Cloisite Na+) was dispersed into 750 ml of H_2O at 60-65°C under 300 rpm mechanical stirring for about 30 minutes. Then the intercalating agent was poured into the suspension and stirred for another hour. The precipitate was filtered and washed thoroughly with water (1 time), water/ethanol 50/50 (1 time) and several times (at least 3 times) with 99% ethanol. The organoclay/ethanol concentration in the resulting paste was about 6.4% measured by drying a small amount of the paste at 120°C in vacuum oven for at least 12 hours. Then the suitable amount of the paste and epoxy were mixed under rapid mechanical stirring at about 600 rpm until a clear high viscosity suspension was obtained. This suspension was outgassed at 120°C for 16 hours. Organoclay/epoxy nanocomposites were prepared for further analysis by adding 35phr Epi-cure 3046 curing agent.

Because we synthesize the organoclay and prepare the organoclay/epoxy both in the liquid without an intermediate drying step, this method is named the Liquid-Liquid method, abbreviated as L-L method.

Microfludiser method:

10 parts of I.30E organoclay and 40 parts of solvent (99% ethanol or acetone) were mixed and passed through microfludiser, and a pasty mixture was obtained. A

suitable amount of paste was mixed with Epon 828 and the curing agent to form a series of nanocomposites with different amounts of organoclay.

In summary we have used three ways to prepare clay/epoxy nanocomposites: direct mixing, mixing by microfludiser and Liquid-Liquid synthesizing of clay/epoxy mixture. The following table gives a comparison of their advantages and disadvantages.

Table 5: Comparison of three methods

Method	Advantages	Disadvantages
Direct Mixing	1. easy and quick 2. low viscosity and easy degassing	1. clay dispersion not good. 2. less exfoliation
Microfludiser	1. easy and quick 2. good dispersion of clay.	1. strict limit on size of clay particles. 2. lower clay aspect ratio because of clay breaking.
L-L synthesis	1. good dispersion of clay. 2. almost keep original clay aspect ratio	1. High viscosity. 2. longer time to remove solvent.

3.5 Characterizations

FT-IR

Powder FTIR analyses were done using a Thermol Nicolet 670 FT-IR. Three kinds of clay powder were under analysis: Closite Na+, Triclay and I.30E.

XRD

X-ray diffraction (XRD) was performed on a Philips PW1710 diffractometer with Cu (λ = 1.54 Å) irradiation. Samples were scanned at diffraction angles 2θ, from 2° to 10°, at a scanning rate of 1° per minute. The Bragg equation was used to calculate the gallery spacings (also called basal spacings).

DSC

Differential thermal scans were performed at a heating rate of 10 °C /min under a nitrogen atmosphere with a DSC 2010 of TA Instruments. Samples of 10—13 mg were used and sealed in aluminum pans.

DMA

Dynamic Mechanical Analyses were done on a TA983 Dynamic Mechanical Analyzer system. The measurement temperatures were from 30 °C to 180 °C, with a heating rate of 2 °C /min and a fixed frequency of 1 Hz in nitrogen atmosphere. The curve of Young's storage modulus, loss modulus, and tan delta as the temperature variation were obtained for the clay/epoxy system with different amounts of clay and different types of clay.

Mechanical Measurement

Tensile strength

The tensile strength of nanocomposites was tested using individually molded samples

at room temperature according to ASTM D638-98. A digitally controlled MTS servo hydraulic testing machine was used for this measurement. The samples were dog-bone-shaped, and dimension type V defined on the above standard. The results for five samples were averaged. The tensile ramp rate is 1mm/min. Two kinds of clay effects were under investigation - Triclay and I.30E.

Fracture tests

The plane-strain vs plane-stress fracture toughness and strain energy release rate of the nanocomposites were measured on a MTS servo hydraulic testing machine according to ASTM D 5045-96. A crosshead rate of 10mm/min was used. This test is also called toughness test. Single-edge-notch bending (SENB) samples were used in this study (Figure 28). The size parameters are:

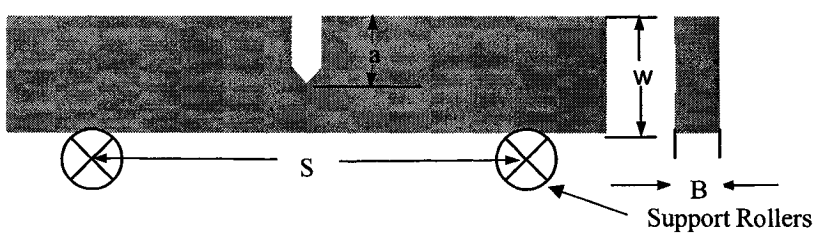

W=21.30mm, a=9.6mm, S=82.20mm. B is the specimen's thickness.

Figure 28: Specimen size for fracture tests.

Displacement correction specimens (unnotched) were used for the determination of the displacement correction in order to find the value of critical strain energy release rate G_{1c}.

K_{1c} and G_{1c} are calculated by following equations:

a) $K_{Ic} = (P_Q S/BW^{3/2})f(x)$

Where (0<x<1) x = a/w =0.4507, from table 1A of D5045, we can find $f(x) = 9.14$.

The unit of K_{1c} is $MPa.m^{1/2}$.

b) $G_{Ic} = U/(BW\phi)$

$U = U_Q - U_i$,

Where U_Q is the measured area under the force-displacement curve, U_i is the measured area under the force-displacement curve from uncracked specimen. Also from table 1A of ASTM D5045, $\phi = 0.274$. The unit of G_{1c} is kJ/m^2.

Compression tests

The tests were done on an MTS Servo Hydraulic Testing Machine, according to ASTM D695. The crosshead speed was 1.3 mm/min, the size of specimens was 12.7mm x 12.7mm x 25.4 mm. The specimens were postcured on 125 °C for 24 hours, and then conditioned at 23 °C for more than 2 days.

Rheological property

The instrument used is a Brookfield CAP2000+ viscometer with spindle #6, which is suitable for low viscosity materials. The software used is Capcalc V.20. The set temperature is 25°C, and 3 minutes was allowed for reaching temperature balance

between the sample and spindle. Viscosity was measured from 10 rpm to 770 rpm with a speed increment of 40, resulting in 20 points.

The Atomic Force Microscope (AFM)

Specimens (epoxy-amine series) for the Atomic Force Microscope study were cut from the cured epoxy without any further sample treatment, such as polishing. Three types of faces were studied—air faces (epoxy surface in contact with air), teflon-contacted faces (epoxy surface at the bottom that was in contact with the teflon film), and fracture faces (epoxy surface formed by breaking the sample under exterior force). Phase and topological images, corresponding to the amplitude and phase change, were recorded using a Digital Instruments NanoScope IIIa in TappingMode™. The probe used was a TESP silicon tip with the dimensions, 125x 35x 4 μm, a tip diameter of 5 nm and a resonance frequency of 285kHz. The setpoint voltage (A_{set}) for the tip was 70% of the cantilever free air vibration amplitude (A_0). Repeated scans were done to ensure that the observations were stable and repeatable.

Specimens of clay/epoxy nanocomposites were prepared by breaking the samples, sanding, and lightly polishing them. Sanding was done by using LECO 8 abrasive disc paper with grits of 600, 800, …, up to 1200. After sanding with the grit of 1200, further polishing was done using Nylon 8□ polishing cloths with 1μm alumina fine particles and 0.3μm alumina in the last step. The olympus

TGH+BH optical microscope was used to monitor the surface polishing results. The AFM instrument parameters were set the same as those for epoxy-amine series samples.

Nano Indentation (NanoDMA)

NanoDMA® was performed by using Triboscope® (Hysitron) under QSM mode. The applied force on the tip was 1000 μN, and the sweeping frequency was set from 1Hz to 300Hz, at room temperature. The epoxy-amine series samples were used. No surface treatment was done on the epoxy-amine series samples.

4 Results and Discussion

4.1 Organoclay properties

After the synthesis of Triclay, it is necessary to study the surface properties of this new organoclay. The easiest and most obvious way to do this is to use FT-IR to investigate the changes in surface chemical composition. Three types of clay powders were analyzed using FT-IR: Cloisite Na+, Triclay and I.30E.

Figure 29 shows the FT-IR spectra of the Cloisite Na+ clay, and then after the intercalating agent treatment—Triclay. Cloisite Na+ (top of Figure 29) exhibits three strong absorption peaks at 3624 cm^{-1}, 3408 cm^{-1} and 1636 cm^{-1}, which can be attributed to the strong –OH stretching vibration from the absorbed water in the clay layers [66, 67].

When this primary clay is modified by the organic onium ion, its FT-IR spectrum changes. New peaks indicate the change in surface chemistry. The most interesting peaks are at about 3263 cm^{-1}—3238 cm^{-1}, and 1377 cm^{-1}, which represent the vibration of $-NH_2$ and $-NH_3^+$ groups. Table 6 summarizes these peaks and their assignments.

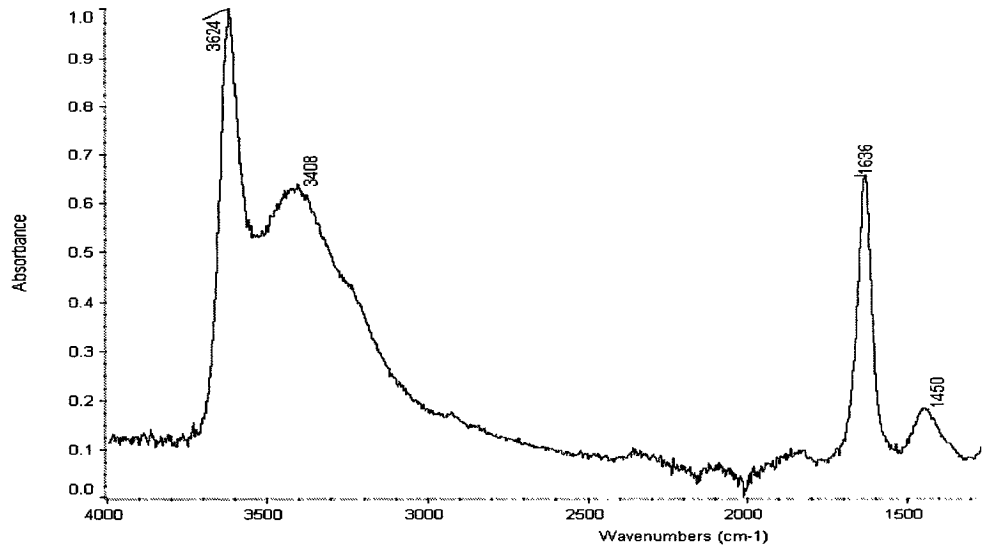

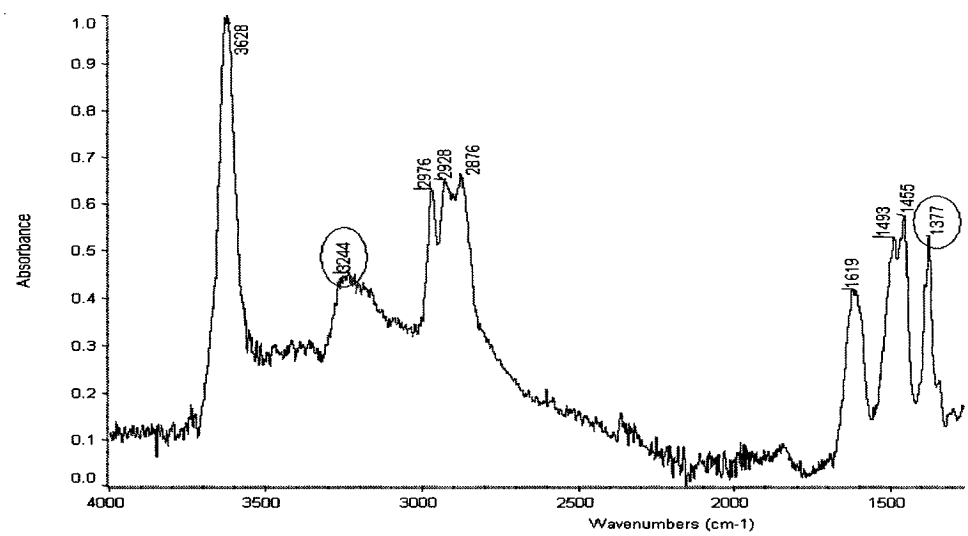

Figure 29: FTIR spectra of Cloisite Na+ (top) and Triclay (bottom) particles.

Table 6: The FTIR spectrum peaks assignment

Clay Type	wavenumber (cm^{-1})	Character	Assignments
Cloisite Na+	3624	sharp strong	—OH stretching on clay structure
	3429	broad medium	absorbed water, -OH stretching
	2362	medium	unknown
	1633	medium/strong	absorbed water, -OH stretching
	1425	medium	unknown
Triclay	3628	sharp strong	—OH stretching on clay structure
	3263—3238	broad, medium	$—NH_2$, $—NH_3^+$ stretching &deformation
	2976	medium	$—NH_3^+$ stretching &deformation
	2928, 2876	sharp, medium	$—CH_2—$ asymmetrical & symmetrical deformation.
	1619	medium/strong	absorbed water, —OH stretching
	1493	medium/strong	$—NH_3^+$ deformation
	1455	medium	$—CH_3$, $—CH_2—$, C—H deformation
	1377	medium	$—NH_3^+$ asymmetric deformation

Note that the FT-IR spectra of I.30E, seen in Figure 30, clearly shows two very strong peaks at 2920 cm^{-1} and 2848 cm^{-1}. These peaks can be attributed to the asymmetric and symmetric stretching of alkyl ($–CH_2–$) groups. From the FT-IR of I.30, it is clear that I.30E is a type of long alkyl ammonium onium modified clay.

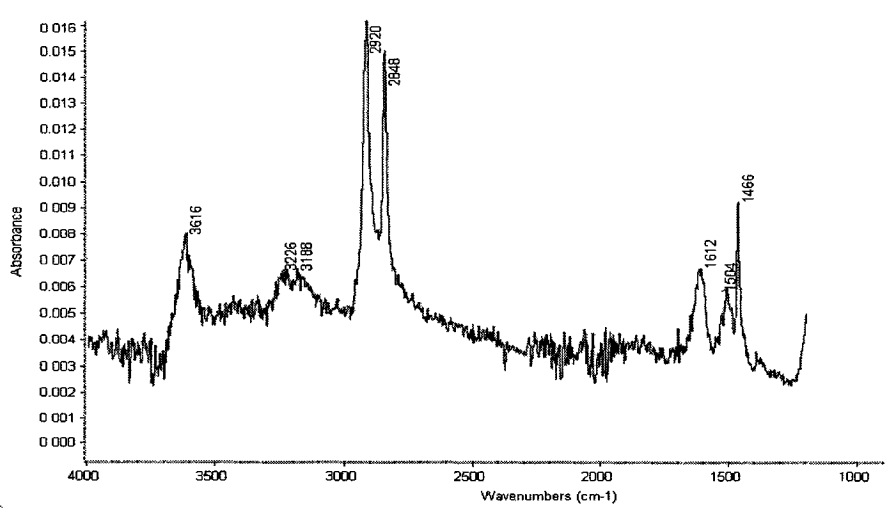

Figure 30: FT-IR of commercial I.30E organoclay

From the above differences in the FTIR spectra, it is clear that the surface chemical composition of the clay is changed by the modification of primary Cloisite Na+ clay. This change is illustrated by the distinct vibrations of $-NH_2$ and $-NH_3^+$. Therefore we conclude that the organic onium ions successfully substitute for inorganic cations and build ionic bonds between clay layers and the organic intercalating agent.

4.2 Clay/epoxy nanocomposites properties

4.2.1 Chemical/Thermal properties

After chemical modification, the intercalating agent was inserted into the clay galleries and deposited onto the surface of the clay particles. Since we use a tri-functional intercalating agent, there are free $-NH_2$ groups, which can take part in chemical reactions with the epoxy to form covalent bonds. The total heat of reaction ΔH_r from the clay/epoxy/curing agent system can be found from differential thermal scans by DSC. In order to observe the effect of the intercalating agent's amine groups on the total heat of reaction, we used the I.30E/epoxy/curing agent system for comparison.

First, let us discuss the effect of different clays on epoxy homopolymerization without curing agents. Epoxy can be cured not only by using curing agents, but also by epoxy-epoxy reaction (homopolymerization) that can take place in

suitable conditions, such as at high temperatures or with proper catalysts. Homopolymerization results in the formation of polyethers. Figure 31 shows the DSC of Epon828 homopolymerization with and without adding clay.

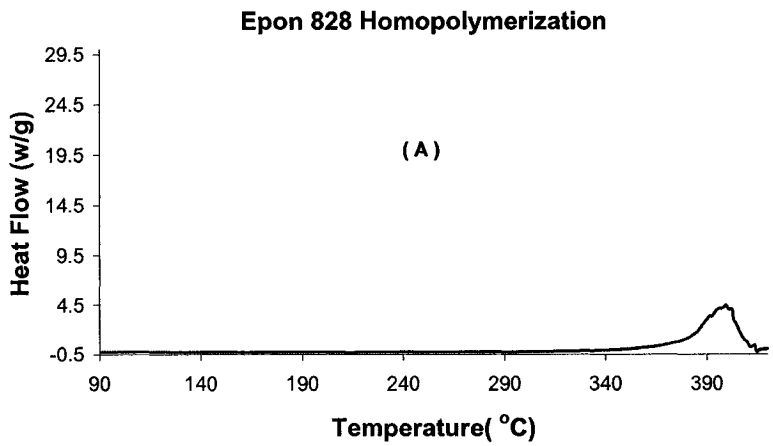

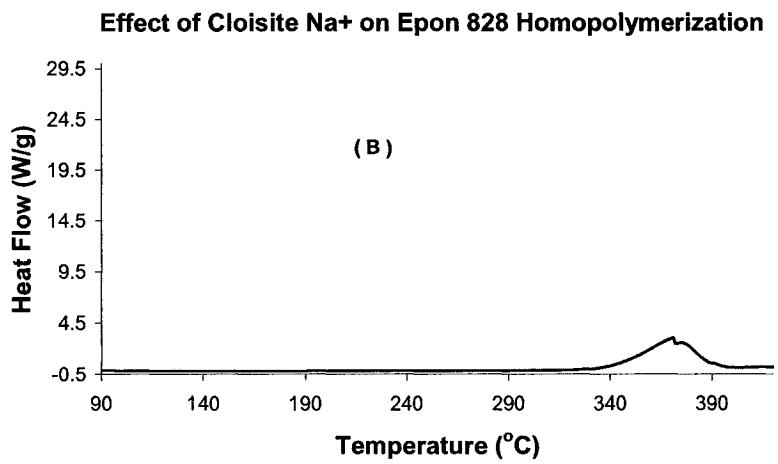

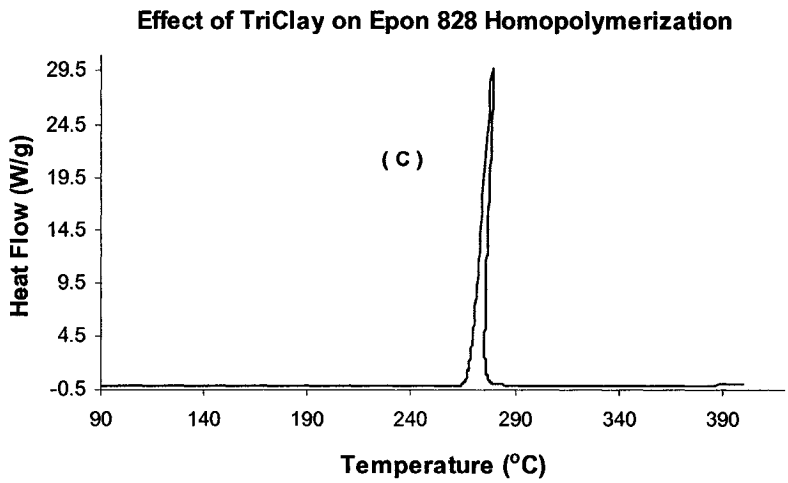

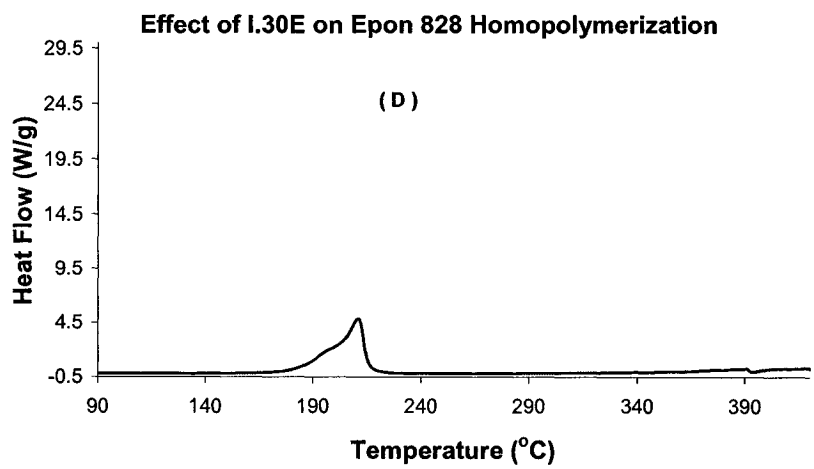

Figure 31: Epon828 homopolymerization at elevated temperature and the effect of different clay: (a)Epon828; (b)Epon828+10%Cloisite Na+; (c) Epon828+10%Triclay; (d) Epon828+10%I.30E.

Table 7 summarizes the effect of different clays on epoxy homopolymerization. It is obvious that organoclay has a catalytic effect on the epoxy polymerization because the onset temperatures of chemical reactions in epoxy-organoclay systems are lower than in pure epoxy homopolymerization. This catalytic effect

comes from the introduction of organic onium ions to clay, the hydroxyls on the surface of clay, and water residue in the clay [8, 10]. Compared to primary clay (without intercalating agent treatment), organoclay has a higher catalytic capability. The onset temperature is lower by about 110°C for Triclay, and 170°C for I.30E.

The differences between Epon828+10%Triclay and Epon828+10%I.30E can be observed in figures 31-C and 31-D. First, the exothermal peak of epoxy-Triclay is sharp with heat flow 5 - 6 times higher than that in epoxy-I.30E; second, the total heat released, ΔH, is different; epoxy-Triclay gives 12% more total heat release.

Table 7: The effect of different clays on the homopolymerization of Epon 828

Sample	T_{onset} (°C)	T_{peak} (°C)	ΔH (J/g)
Epon828	379.58	399.68	521.2
Epon828+10%Cloisite Na+	342.58	370.79	496.8
Epon828+10%Triclay	268.86	279.30	533.4
Epon828+10%I.30E	197.86	210.85	473.8

From the above analysis, the following characteristics of our lab synthesized Triclay are determined: (1) this organoclay is different from the common long alkyl ammonium onium ion treated clay, and more reactive – i.e. its amine groups reacts with the epoxide groups from epoxy; (2) its catalytic effect is lower than

that of I.30E.

Next, we look at the organoclay/epoxy/curing agent nanocomposite systems. Two systems (Triclay/Epoxy, and I.30E/Epoxy) with 3 wt%, and 5 wt% clay were studied.

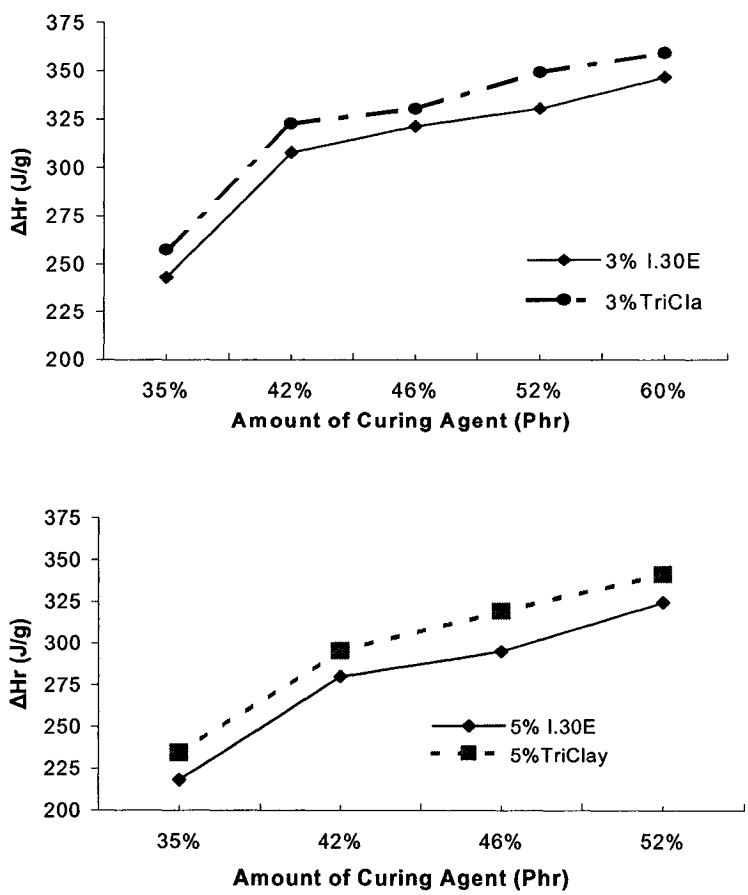

Figure 32: Comparison of total heat of reaction ΔH_r between the Triclay/epoxy system and the I.30E/epoxy system. Top picture - amount of organoclay is 3%; Bottom picture - amount of organoclay is 5%.

From Figure 32, it is clear that the total heat of the reaction ΔH_r is higher in the Triclay/Epoxy system than I.30E/Epoxy system by about 6%. This could be attributed to the free $-NH_2$ groups on the intercalating agent that take part in the chemical reaction and form covalent bonds with the thermoset matrix.

It is found that a higher content of organoclay leads to lower total heat of the reaction in the system. For example, with the same 46 phr 3046 curing agent, 3% of I.30E gives a ΔH_r of about 321 J/g, but 5% of I.30E gives 295 J/g, a difference of about 9%. Based upon Chin et al.'s conclusions [42], this change of energy could be due to exfoliation energy consummation. We summarize these values in Table 8.

Table 8: Heat of reaction of different clay/epoxy/curing agent systems

Organoclay		Amount of curing agent (phr)			
		35	42	46	52
3% I.30E	ΔH_r (J/g)	243.1	307.7	321.3	330.3
5% I.30E	ΔH_r (J/g)	217.9	279.8	295	324.4
Difference		-10%	-9%	-8%	-2%
3%Triclay	ΔH_r (J/g)	257.5	322.7	330.4	349.2
5%Triclay	ΔH_r (J/g)	234.2	295.6	319.3	341.5
Difference		-9%	-8%	-3%	-2%

The effects of the amount of organoclay, and of the amount of curing agent on the

cured nanocomposite glass transition temperature were also studied. Figure 33 shows the glass transition temperatures of Triclay/Epon/Epi-cure3046 and I.30E/Epon/Epi-cure 3046 nanocomposites. Neither shows any obvious improvement in T_g, revealing that the epoxy-based nanocomposites have similar glass transition temperatures to cured epoxy. Therefore we conclude that the epoxy local movements are not affected by the presence of organoclay.

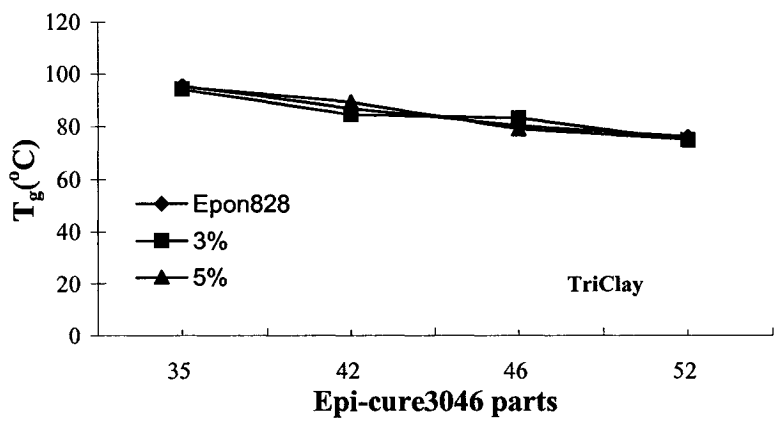

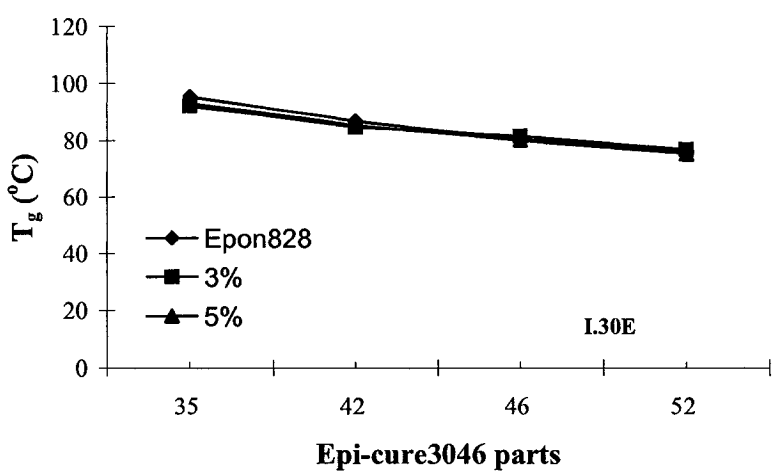

Figure 33: Illustration of glass transition temperatures of Triclay (top) and I.30E (bottom) epoxy nanocomposites.

From the DSC analysis, it is proved that:

(1) The amine groups from the Triclay layer surface can take part in chemical reactions with epoxy, and thus increase the total heat release of the system.

(2) Compared with I.30E the Triclay catalytic effect is lower, but the onset temperature is still greatly decreased compared to primary Cloisite Na+.

(3) No improvement in T_g is observed in any clay/epoxy nanocomposites.

4.2.2 Micro/nano structures

4.2.2.1 XRD study

It is commonly regarded [23, 32, 41] that the clay exfoliation process can be explained as: (1) an intercalating agent treatment that changes the primary clay from hydrophilic to hydrophobic and also increases clay gallery distance; (2) a swelling of clay by epoxy monomers, which provides an environment for curing agents to migrate into the clay interlayer region; and (3) a temperature controlled curing process which results in the final nanocomposite. During the last stage, the balance of the extragallery and intragallery curing speed is needed to permit the formation of exfoliated clay layers in the epoxy matrix. If the temperature is too low, the rate of epoxy and curing agent intercalation will be too slow, and then the extragallery polymerization will be faster than the intragallery polymerization and intercalated nanocomposites will form. Therefore, a moderate increase of curing temperature is beneficial to the formation of exfoliated nanocomposites.

There are also some other methods used to improve exfoliation, such as using chemical solvents to mix the clay with the epoxy, using lower amounts of curing agents, and using a higher curing temperature. We used these methods and discuss them in detail below. Direct mixing (DM) method was used in preparing all specimens for XRD measurements.

First we consider the gallery spacing of the organoclay. Figure 34 shows the X-ray diffraction pattern of Triclay powder. From this picture, we can see that after ion exchange, the basal spacing is ~15 Å calculated by the Bragg equation. We also investigated the I.30E powder, and found it to have a basal spacing of about 22 Å. The difference comes from the chain length of the intercalating agent; I.30E contains long alkyl ammonium onium which gives increased clay gallery height.

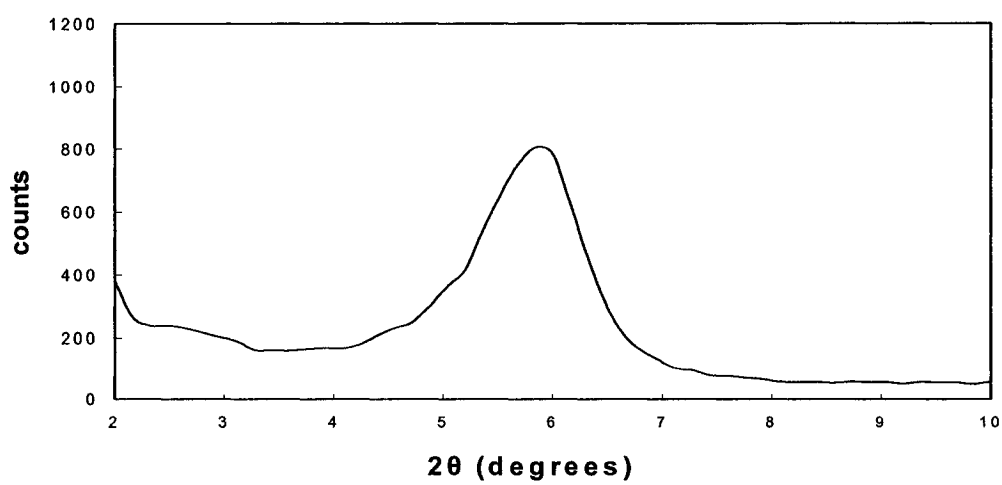

Figure 34: X-ray diffraction of Triclay.

Processing conditions greatly affect the degree of exfoliation in nanocomposites, because the exfoliation of clay layers depends upon the kinetics of the curing reaction and the migration of the polymer precursors into the clay galleries. If the intragallery polymerization rate is comparable to that of the bulk, exfoliation can take place. Therefore the curing temperature and the amount of curing agent affect the exfoliation and thus the properties of the nanocomposites.

Here two different curing temperatures (95°C and 125°C) and two different amounts of curing agent (35 phr and 47 phr) were used. Also ethanol was used in the clay/epoxy nanocomposites' sample preparation, which improves the exfoliation because it lowers the viscosity during the mixing of clay with epoxy. Figure 35 illustrates the effect of these factors on the gallery spacing of the resulting composites. From this figure, it is found that higher temperatures and lower amounts of curing agent improve the exfoliation process because the peak in the curve 35phr-125C is the lowest compared with the other 3 curves. Therefore the optimum conditions are 35 phr of curing agent and 125 °C curing temperature, which were used in all of our studies.

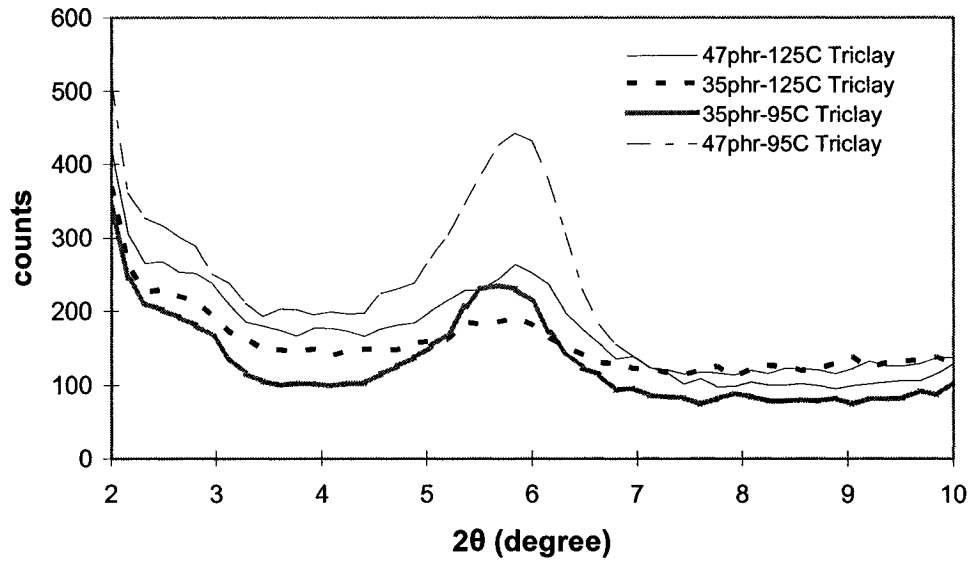

Figure 35: X-ray diffraction patterns of four Triclay/Epoxy specimens: 47phr-95C represents the sample cured at 95 °C with a curing agent amount of 47 phr; 47phr-125C represents the sample cured at 125 °C with a curing agent amount of 47 phr; 35phr-95C represents the sample cured at 95 °C with a curing agent amount of 35 phr; 35phr-125C represents the sample cured at 125 °C with a curing agent amount of 35 phr. All of the above specimens contain 3% of organoclay and were prepared using ethanol in the premixing of the Triclay and the epoxy.

Now we compare the spectrum of a Triclay nanocomposite with that in the I.30E/Epoxy nanocomposite (Figure 36). The I.30E/Epoxy nanocomposite can be regarded as good exfoliation, from the viewpoint of the XRD, because there is no sharp peak on its X-ray diffraction pattern. From this figure, we can see that by combining different condition - using a lower amount of curing agent, a higher curing temperature, and solvent mixture technology, the Triclay/epoxy gives

satisfactory results.

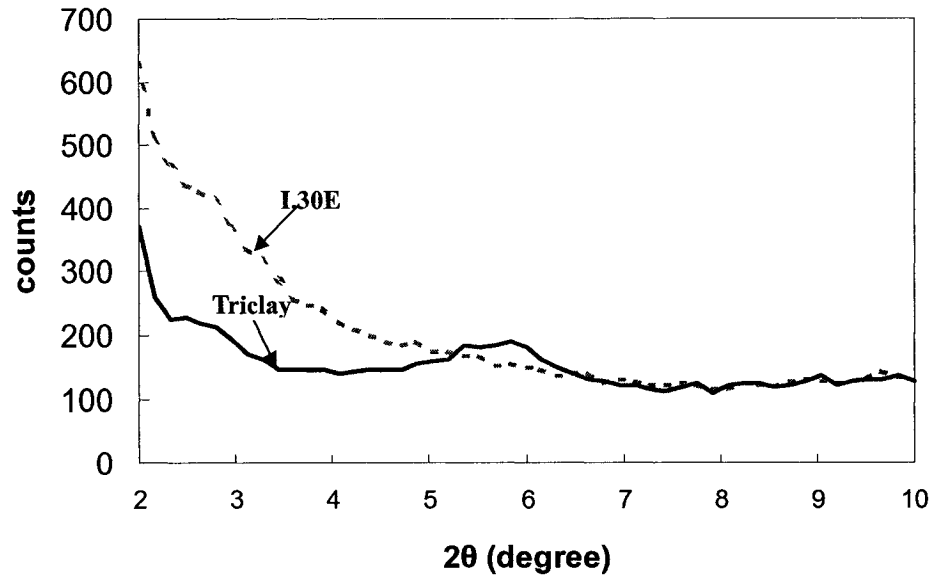

Figure 36: X-ray diffraction patterns of 3% I.30E/Epoxy nanocomposite and 3% Triclay/epoxy nanocomposite.

From the XRD, the following conclusions can be drawn:

(1) A low amount of curing agent and a suitably high curing temperature are the keys to attain the best degree of exfoliation.

(2) Mixing epoxy with clay using a suitable solvent allows even clay distribution and improves the exfoliation process.

4.2.2.2 Atomic Force Microscopy (AFM) study

Organoclay:

It is interesting to use the AFM to observe the structure of different clays such as, Cloisite Na+, Triclay and I.30E (see Figure 37). It is clear that the clays are

packed in a layered structure (37-a, b) and have a smooth surface. When the Closite Na+ is treated with an intercalating agent, chemical material deposits on its surface and changes its chemical properties (37-c, d, e).

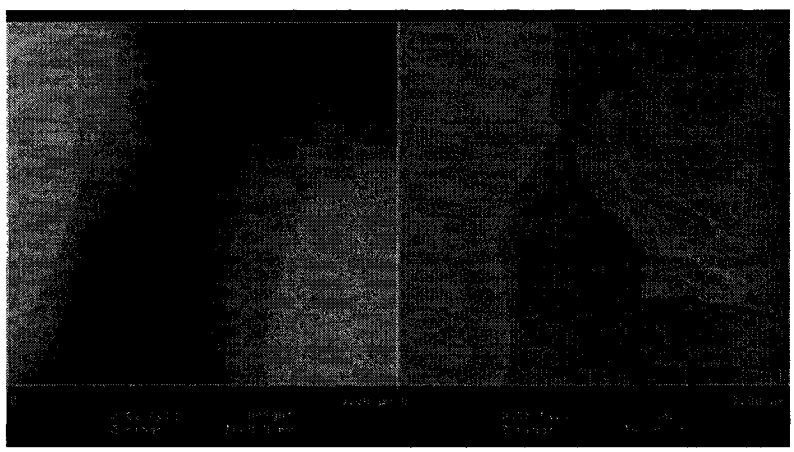

(a)

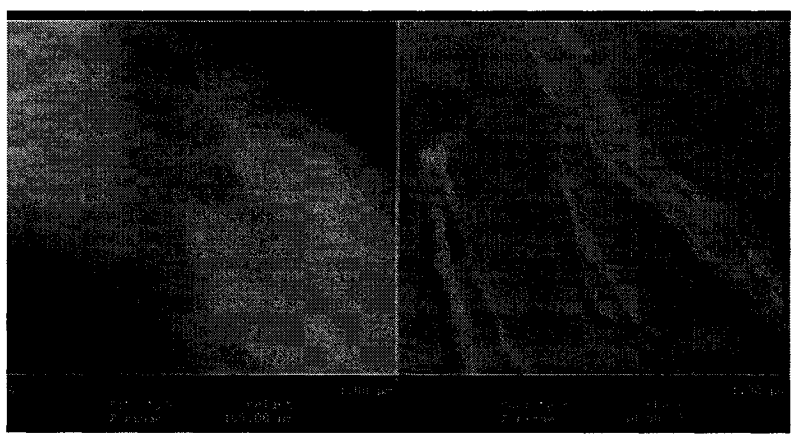

(b)

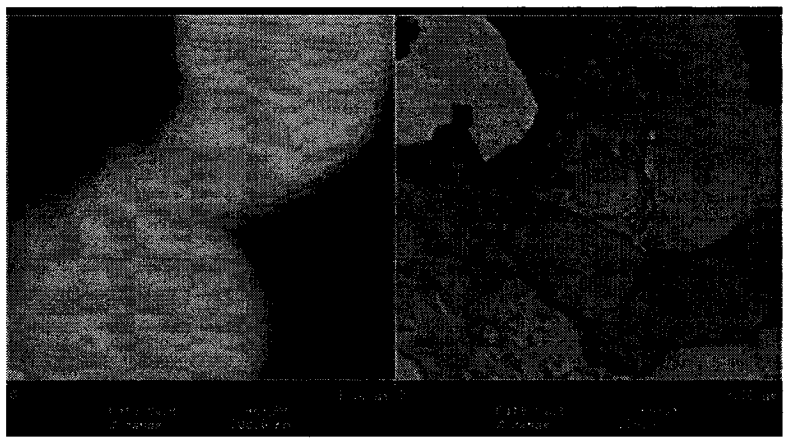

(c)

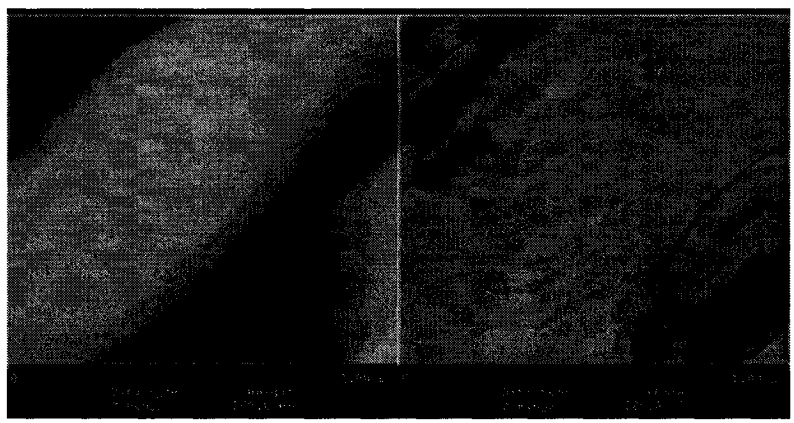

(d)

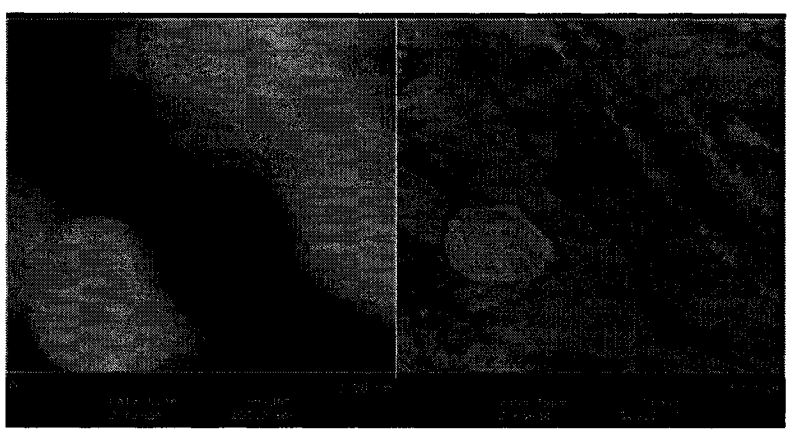

(e)

Figure 37: AFM images of (a) Cloisite Na+, size 3μm x 3μm; (b) Cloisite Na+, size 1μm x 1μm; (c) Triclay, size 3μm x 3μm; (d) Triclay, size 1μm x 1μm; (e) I.30E, size 3μm x 3μm.

Clay/epoxy nanocomposites:

The AFM is a powerful tool to investigate the micro/nano-structure of nanocomposites, offering a nanometer scale measurement. The material preparation process for the AFM requires a very slight surface cleaning and polish. Careful attention should be paid to avoid dragging the clay particles out of the epoxy matrix during the polish. The phase images, presented in Figure 38, show the very large phase contrast of 180° (maximum value). The z range of the topological images is about 800nm, which is large compared to a very smooth fracture epoxy surface (about 50nm), so we cannot see the microstructure of the matrix (epoxy) because of the topological interference on the phase image.

In this AFM observation, the set-point amplitude ratio $r_{sp} = A_{sp}/A_0$ is set to 0.70, which is considered moderate. Because image contrast can be reversed at different r_{sp} ratios and A_0, it is difficult to assign the features to chemical components. Based on the references [51-56], we assign the white phase to represent the hard clay and the dark phase to represent the soft epoxy.

By using the AFM in TappingMode, we can see the intercalated/exfoliated layers are still organized in a lamellar structure (Figure 38). From these pictures, we can roughly measure the gallery height to be about 15-20 nm.

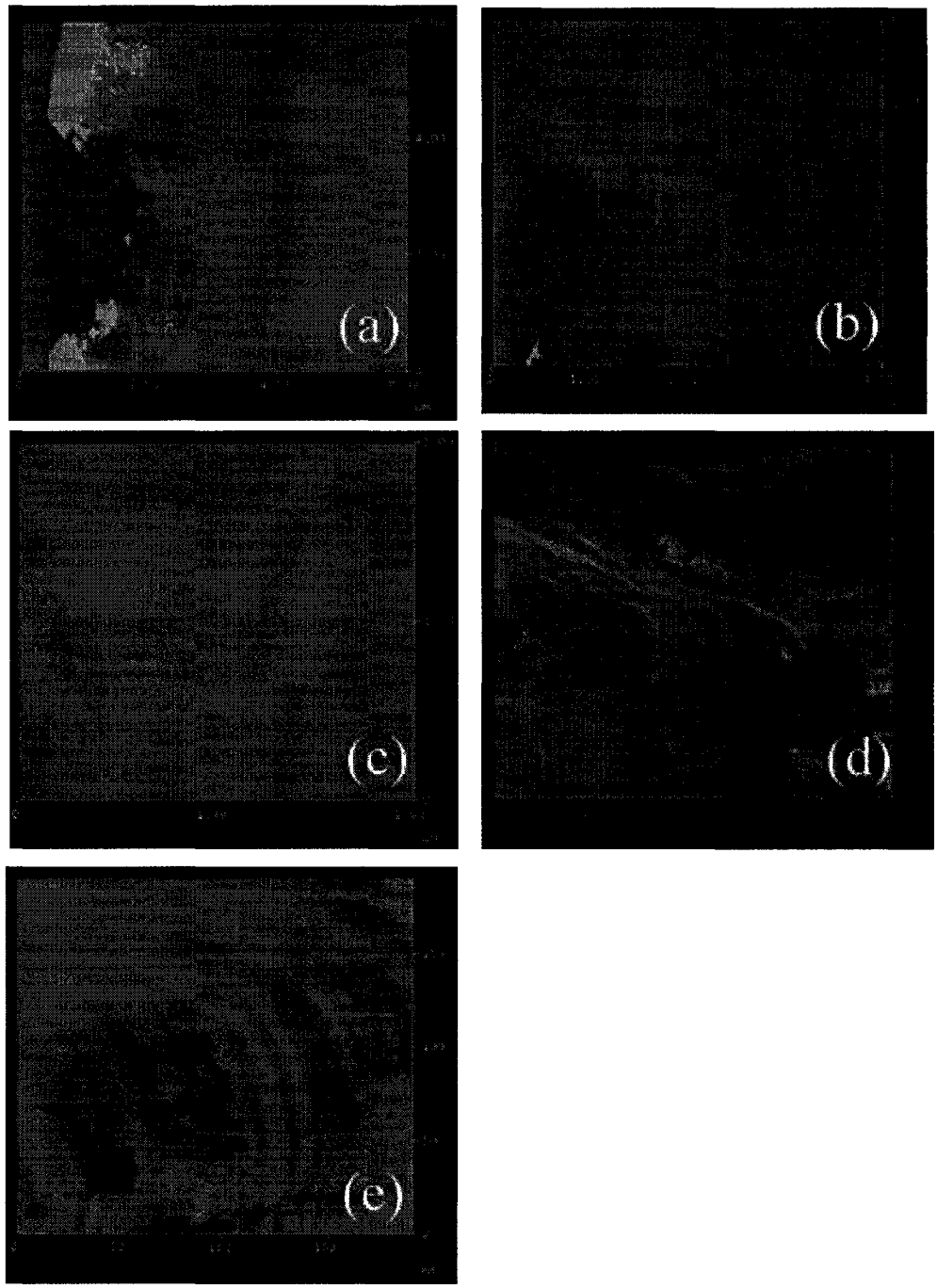

Figure 38: AFM images of clay/epoxy nanocomposite, organoclay content 3% (direct mixing): (a) image size 6μm x 6μm; (b) image size 4μm x 4μm; (c) image size 2μm x 2μm; (d) image size 800nm x 800nm; (e) image size 200nm x 200nm;

4.2.3 Mechanical properties

4.2.3.1 Tensile Tests

Mechanical improvement is one of the most important goals in the study of nanocomposites. Composite strength and modulus are two key indexes in material analysis. The specimens studied here were 1) Triclay/epoxy nanocomposites prepared by direct mixing; 2) I.30E/epoxy nanocomposites prepared by direct mixing; 3) I.30E/epoxy nanocomposites prepared by using the microfludiser. Table 9 gives the tensile strength measurement data of Triclay/epoxy nanocomposites and I.30E/epoxy nanocomposites prepared by direct mixing.

Just as we discussed in section 3.1, the goal of our organoclay design is to create primary bonds between epoxy and organoclay. Successful preparation of this interface should have the ability to transfer the load from the epoxy to the clay, thus increasing the tensile and other mechanical properties of the nanocomposite.

Table 9: Comparison of tensile strength between two different clay/epoxy nanocomposites using same preparation method (direct mixing)

I.30E %	0	1	3	5	7
Strength MPa	46.8	45.6	47.9	41.0	43.4
S.D	3.4	5.9	6.1	3.9	2.1
Triclay %	0.0	1.0	3.0	5.0	7.0
Strength MPa	46.8	53.7	45.0	49.2	45.4
S.D	3.4	3.4	3.6	3.0	1.8
Comparison %		17.8	-6.1	19.9	4.7

From the table above, it is found that adding I.30E decreases the tensile strength of nanocomposites, Figure 39. For example, epoxy tensile strength is 46.8MPa, and when 5% I.30E is added, its tensile strength decreases by about 12%. This phenomenon can be explained by the inferior interface between the clay and the matrix, where added clay I. 30E particles decrease the effective cross sectional area, therefore lowering the composite tensile strength.

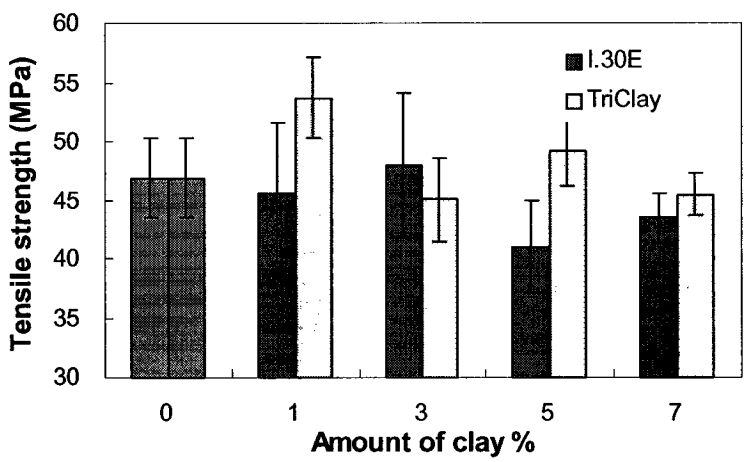

Figure 39: Comparison of tensile strength between I.30E/expoxy and Triclay/epoxy nanocomposites.

It appears that the tensile strengths of the Triclay/epoxy nanocomposites are improved as compared with I.30E/epoxy nanocomposites, especially with the clay amounts of 1% and 5%. For the 3%Triclay/epoxy nanocomposite, the strength is less than I.30E/epoxy nanocomposite. But it is noticed that the standard deviation is larger for the 3% I.30E/epoxy sample and its strength (47.9MPa) is above the strength of the pure epoxy. Normally this data should be less than 46.8MPa due to the inferior

interface as explained before.

Further, the tensile specimens of I.30E/epoxy prepared by the microfludiser were studied to understand the effect of clay dispersion. From Figure 40, we found that there is more decrease in tensile strengths compared with the specimen prepared by direct mixing (Figure 39). The reason is that the microfludiser breaks the agglomerated clay particles and thus greatly increases the viscosity of the organoclay/epoxy paste, which in turn will inevitably result in the introduction of air bubbles in the system when the clay/epoxy mixture and curing agent are mixed together. The final material's tensile property is very sensitive to the presence of voids in the material; and the nanocomposite's tensile strength will decrease.

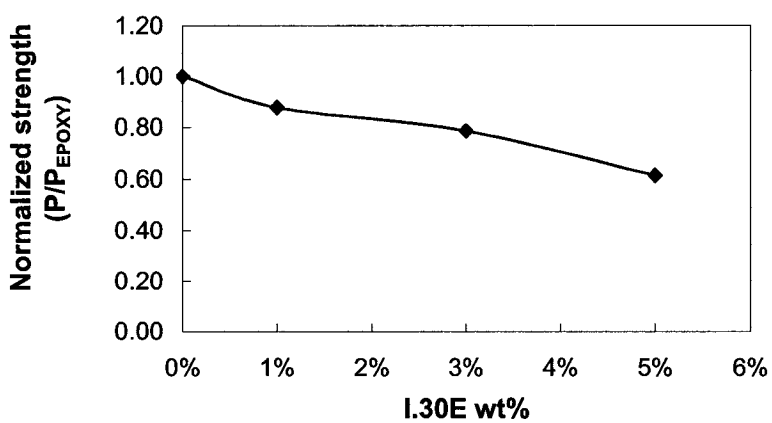

Figure 40: Tensile strength of I.30E/Epoxy nanocomposites prepared by the microfludiser procedure

Generally the use of Triclay shows its advantage in tensile strength improvement, which is an effect that cannot be achieved in I.30E/epoxy nanocomposites.

This improvement directly demonstrates that our interface design gives better results than the commercial clay. Using multifunctional intercalating agents changes the clay surface chemical composition and the amine groups react with epoxide groups forming covalent bonds which effectively transfer part of the exterior force to the high strength, high modulus clay layers, and thus improve the mechanical properties of nanocomposite.

4.2.3.2 Compression Tests

From the compression test, we can obtain the maximum strength (or ultimate strength), yield strength and modulus. Also this test can show better the effect of organoclay than by tensile strength test, because compression test results are less sensitive to voids in the material. Figure 41 shows compression stress-strain curves for 5% Triclay/epoxy nanocomposites. Here we compare the effect of two preparation methods: the L-L method and the direct mixing method. Table 10 gives the details of the compressive properties of Triclay/epoxy nanocomposites.

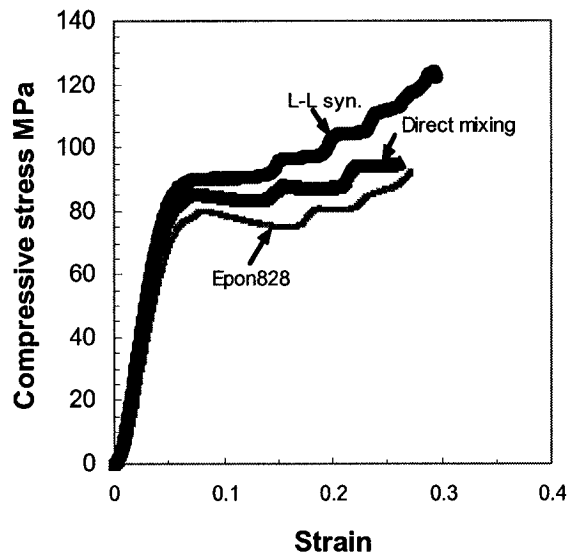

Figure 41: Compression test results of 5% Triclay/epoxy nanocomposites

Table 10: Compressive test results of Triclay/epoxy nanocomposites

	Maximum stress (MPa)		Yield stress (MPa)		Modulus (MPa)	
Triclay wt%	L-L	Direct Mixing	L-L	Direct Mixing	L-L	Direct Mixing
0	89.02	89.02	82.18	82.18	1831	1831
1	107.67	101.82	86.13	85.36	2011	2028
5	129.22	97.66	90.90	87.13	2298	2109

It is observed that the nanocomposites prepared by the L-L method show the following advantages:

1) There is a 20% increase in maximum stress, a 5% increase in yield stress and a 10% increase in modulus with only 1% Triclay. These improvements were

caused by the improved dispersion of organoclay and the good interface between the clay and the matrix.

2) The best improvement is at 5% clay which gives a 45% increase in maximum stress, a 10% increase in yield stress and a 26% increase in modulus. There is one reference related to the improvement in clay/epoxy compression strength [68], where they found the 29%, 6%, and 25% increases in maximum strength, yield strength and modulus respectively at 6 % I.30E organoclay.

The results from the two different methods—direct mixing and L-L methods are compared in Figure 42. For 1%, and 5% organoclay nanocomposites, the L-L method always gives better mechanical properties due to its better dispersion of organoclay in the matrix.

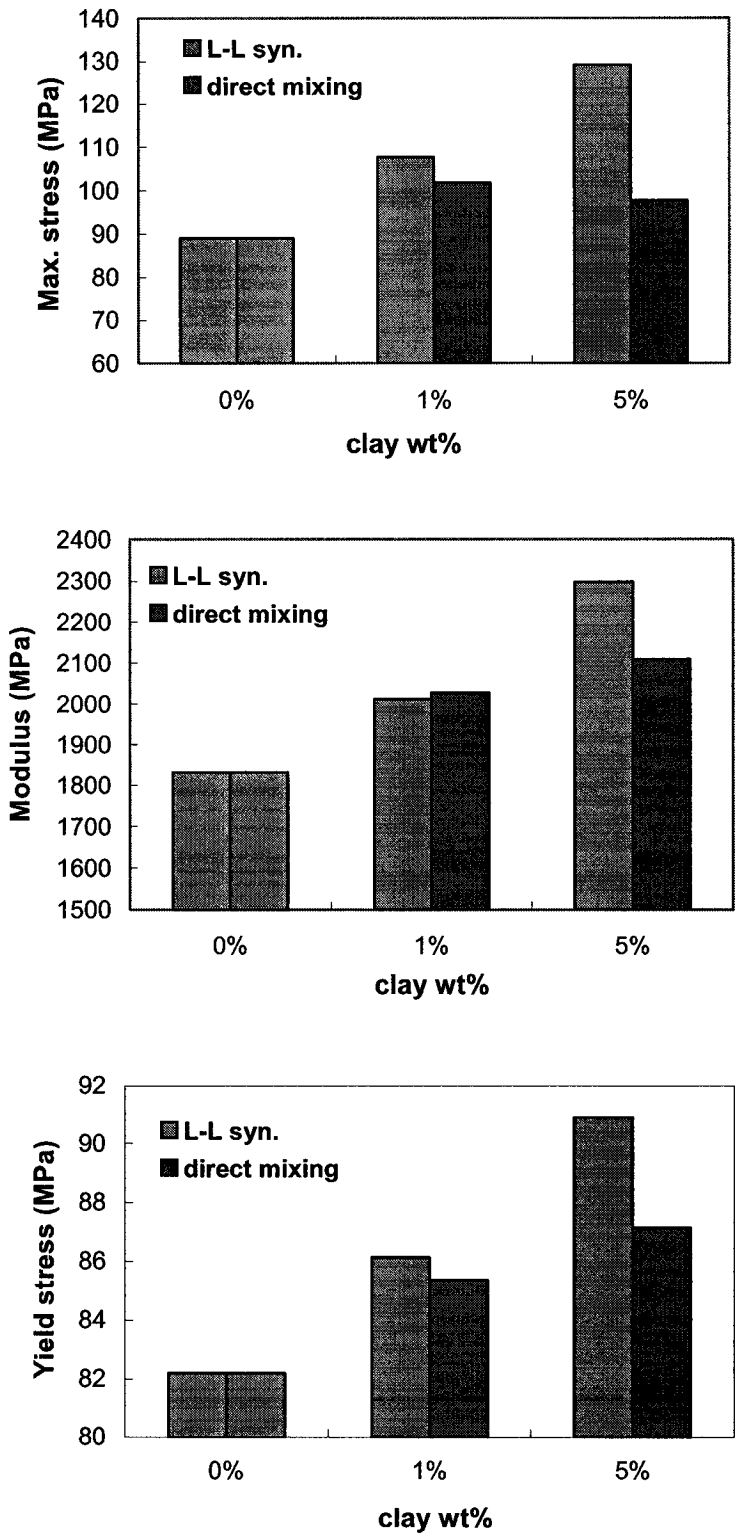

Figure 42: Compression properties of Triclay/epoxy nanocomposites

4.2.3.3 DMA tests

Dynamic Mechanical Analysis (DMA) is used to measure the modulus, and loss tangent of materials. The samples studied here were prepared using 1) Triclay by direct mixing; 2) I.30E by direct mixing; 3) Triclay by L-L method; 4) I.30E by using microfludiser. Figure 43 shows the DMA modulus curves (E') of Triclay/epoxy and I.30E/epoxy nanocomposites with 1%, 3%, and 5% amount of organoclay, both nanocomposites were prepared by direct mixing.

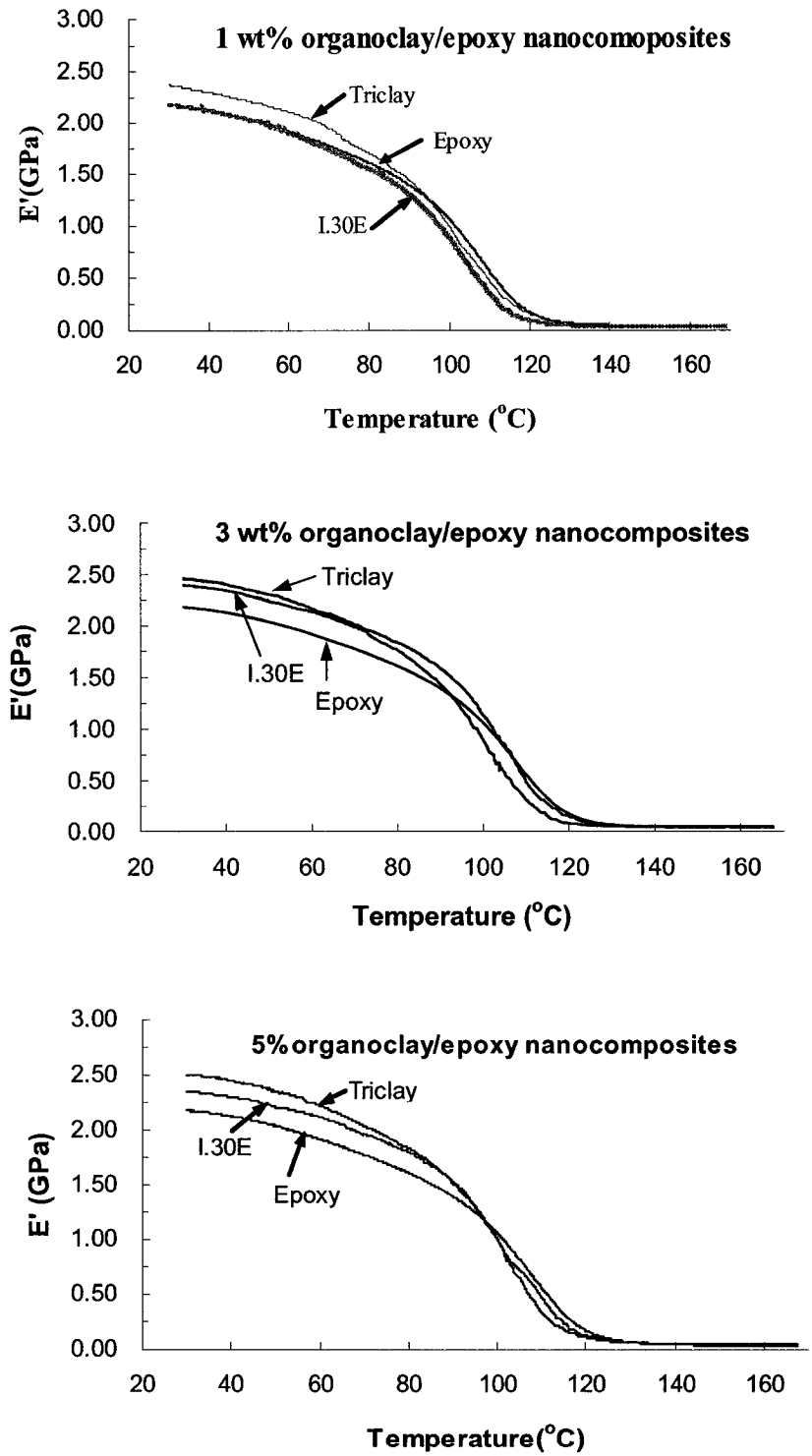

Figure 43: DMA curves of nanocomposites with different amount of organoclay (1%, 3%, 5%), prepared by direct mixing (DM).

In the above graphs, the clay reinforcement factor can be clearly seen. Table 11 summarizes the organoclay reinforcement factors by comparing the storage modulus at 35°C.

Table 11: Comparison of storage modulus for different organoclay reinforcement results at 35°C (DM)

	35°C				Increase Δ			
Clay wt %	0	1	3	5	0	1	3	5
I.30E/epoxy E' (GPa)	2.159	2.155	2.374	2.331	–	-0.2%	10.0%	8.0%
Triclay/epoxy E' (GPa)	2.159	2.342	2.440	2.483	–	8.5%	13.0%	15.0%

From Table 11, it is clear that a small amount of organoclay can increase the modulus. For example, the modulus of cured epoxy (Epon828 with 35phr Epi-cure3046) is 2.159 GPa at 35°C. When we add just 3wt% I.30E to the system, the material's modulus increases by 10%.

The effect of reinforcement is determined mostly by the amount of organoclay. We used the L-L method and the microfludiser to improve the exfoliation of organoclay in the matrix, and then measure its modulus (Figure 44). Both specimens show almost the same reinforcement—about 10% increase in modulus for 3% organoclay loading nanocomposites, which is the same as the value we found for the specimens prepared

by direct mixing.

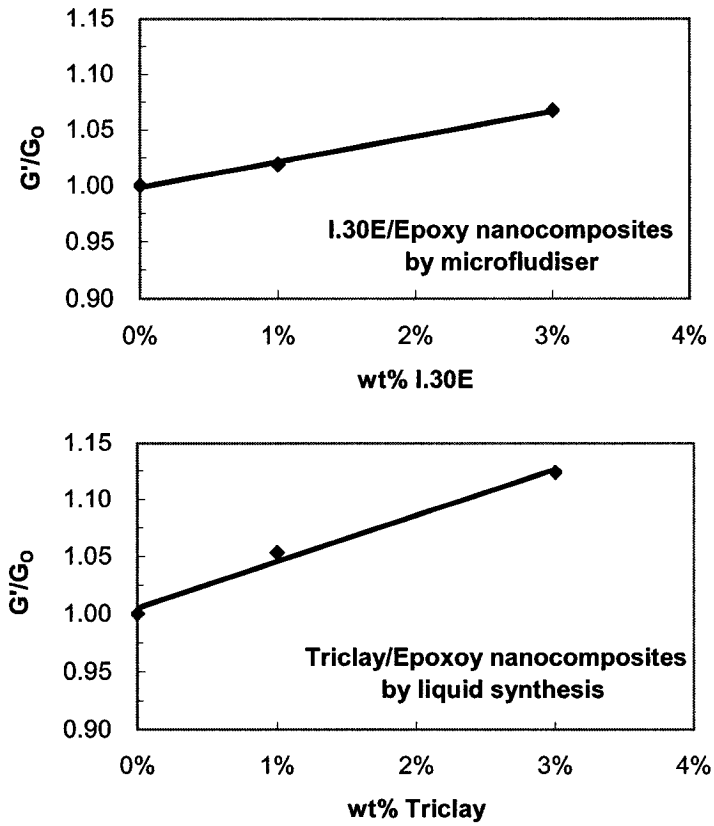

Figure 44: Normalized storage modulus of I.30E/epoxy (microfludiser) and Triclay/Epoxy (L-L method) nanocomposites.

DMA can also be used to measure the glass transition temperatures of polymers. Figure 45 shows the T_g of Triclay/epoxy nanocomposites with different weight amounts of Triclay. From this figure, we can see that there is no obvious change in the glass transition temperature. The difference between T_g measured in DSC and DMA can be explained because of the (1) different measuring systems, (2) different heating rates: DSC 10K/Min, DMA 2K/Min, and (3) different curing conditions - DSC epoxy cures in-situ, DMA 2hr cure in oven and conditioning before

measurement.

By using DMA and DSC, it is clear that the glass transition temperature is not improved in clay/epoxy nanocomposites. This has also been observed by other researchers.

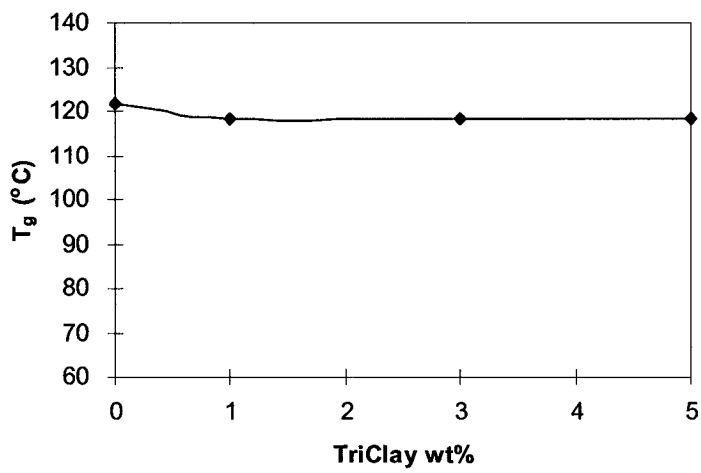

Figure 45: Glass transition temperature of Triclay/epoxy nanocomposites.

4.2.3.4 Fracture tests

From fracture tests, we can see that there is no improvement of toughness with the addition of organoclay. The Epon828/Epi-cure 3046 matrix itself has good toughness characteristics, and it is obviously not affected by the organoclay (Figures 46 and 47), in our case the critical stress intensity factor K_{IC} and the critical strain energy release rate G_{IC} even decrease when more organoclay are added.

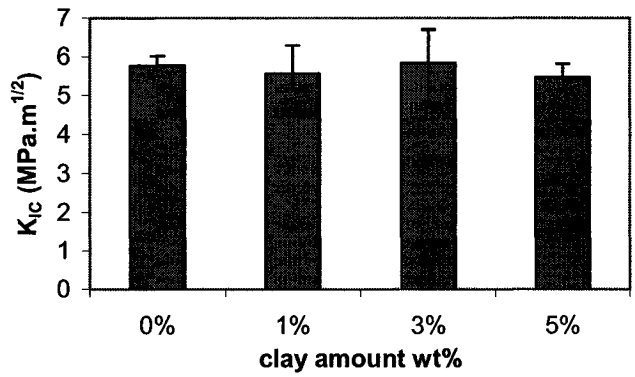

Figure 46: The critical-stress-intensity factor, K_{IC} of Triclay/epoxy nanocomposites (direct mixing).

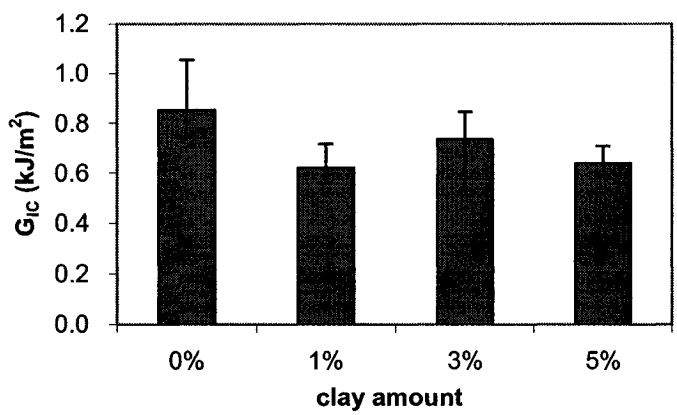

Figure 47: The critical strain energy release rate, G_{IC} of Triclay/epoxy nanocomposites prepared by direct mixing.

<u>Here we make observations from the mechanical measurements</u>:

1) The tensile strength of Triclay/epoxy nanocomposites increases by 20% compared to I.30E/epoxy nanocomposites. The increase comes from the reinforcement of the interface.

2) The compressive properties are improved by adding Triclay to the matrix. There is a 45% increase in maximum stress, a 10% increase in yield stress and a 26%

increase in modulus for 5 % clay/epoxy nanocomposite prepared by the L-L method.

3) Adding a small amount of organoclay can improve the modulus (DMA) of an epoxy. For example, there is a 10 % increase in the modulus when 3 wt% of organoclay (Triclay or I.30E) is added to the system. The method of preparing nanocomposites has less effect on the improvement of the modulus.

4) Adding organoclay doesn't improve the glass transition temperature of a nanocomposite. Also organoclay does not improve the toughness of the Epon828/Epi-cure3046 system.

5) The L-L method for synthesizing nanocomposites improves their compressive properties.

4.2.4 Rheological properties

4.2.4.1 Clay dispersion analysis (percolation)

In order to produce clay/epoxy nanocomposites of the highest quality, it is necessary to improve the dispersion of clay in the matrix, especially to achieve maximum exfoliation of the clay layers. It is believed that a more exfoliated clay structure will reinforce many properties of nanocomposites, such as the mechanical properties and chemical properties. Therefore it is very important to understand the clay dispersion status in the matrix. In this section percolation theory and rheological tests are used to investigate the dispersion.

Assuming that a single clay layer is a circular disk with diameter D, thickness t, and the average number density of this type disk is n, the volume fraction is [23]:

$$V = \pi D^2 tn/4$$

The clay layer aspect ratio is $\alpha = D/t$. Every randomly exfoliated clay layer occupies a volume of D^3. When the system reaches the percolation point, $nD^3 = 1$, the critical volume fraction for percolation is:

$$V_c = \pi D^2 tn/4 = \pi n D^3/(4\alpha) = \pi/(4\alpha) \approx 0.8/\alpha.$$

This is a useful equation for understanding the dispersion of particle filled polymers. Here are some cases to be discussed:

1) Natural clay has aspect ratios distributed between 100 –1000 [32]. If we take the average of this distribution $\alpha = 200$ [10], and assume that few clay layers were broken under intercalating agent treatment, the clay content for percolation under complete exfoliation is around 0.4%. Beyond this percolation point, the viscosity of the uncured epoxy nanocomposites should increase dramatically.

2) If more clay is added to the system, some clay layers must transform to a clustered (layered) structure adopting a lower aspect ratio.

3) When the clay is mixed with a polymer, if only the gallery height increases and no exfoliation takes place (a kind of intercalated state), the aspect ratio is

low, which leads to low viscosity. For example, for a typical stack of 100 layers, which results in a low aspect ratio to around 2, and lower the system viscosity.

It is clear that ideal exfoliated-clay/epoxy nanocomposites can only exist in the system with less than 0.4% volume fraction of clay. Increasing the content of clay will lead to a lower exfoliation state such as an intercalating and/or conventional filled composite. If the clay layers are very well exfoliated in the matrix, the high viscosity makes it very difficult to prepare nanocomposites because bubbles are introduced into the matrix when adding curing agent to the clay/epoxy mixture.

4.2.4.2 Viscosity of organoclay uncured epoxy mixtures

All clay/epoxy mixtures exhibit shear thinning behavior, Figure 48. We note:

1) The clay/epoxy mixture prepared by the L-L method has a much higher viscosity. Using the microfludiser can also effectively disperse the clay into the matrix, but not as effectively as the L-L method.

2) The percolation point for the Triclay/uncured epoxy appears to be at a point higher than 1% because the of viscosity-shear rate behavior of this system does not show the characteristic effect of percolation seen in the curves of the 3% and 5% Triclay/uncured epoxy mixtures. Our theoretical calculations indicate that percolation should occur at 0.4% Triclay if the assumptions that we made about the

geometry of the layers were correct. In particular, a somewhat lower aspect ratio could explain the behavior we observed.

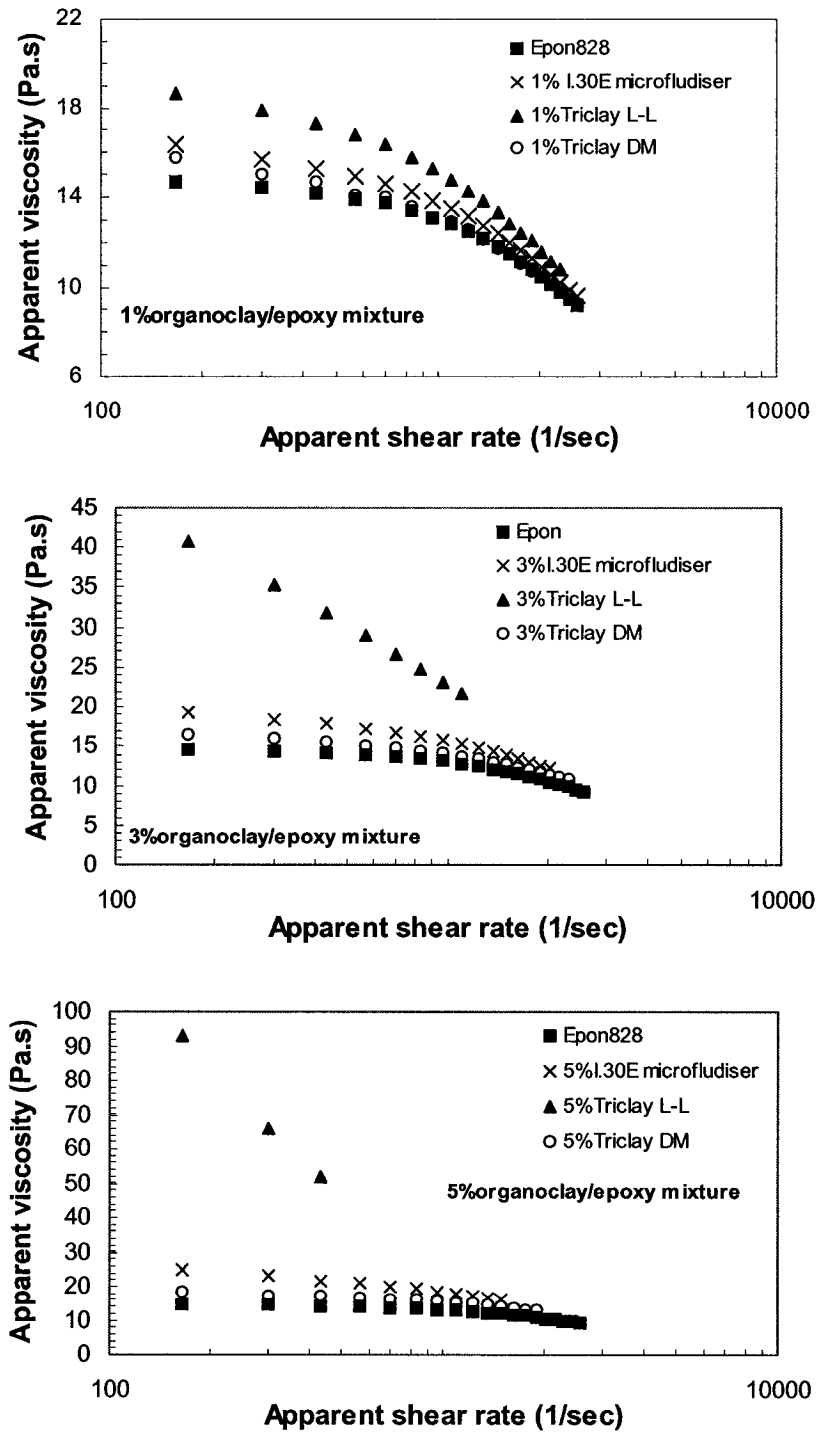

Figure 48: Viscosity of organoclay/epoxy mixtures prepared by different methods.

In our experiment, we tried to make Triclay/epoxy mixtures with more than 10% organoclay, producing an almost solid paste which cannot be handled for further addition of curing agent to synthesize nanocomposites.

The increase in viscosity can be more clearly observed in Figure 49, which shows the apparent viscosity at 50 rpm. For example, the viscosity increases more than 6 times for the 5% mixture prepared by the L-L method, while there is only less than 50% increases for the same organoclay content (I.30E and Triclay) prepared by microfludiser and direct mixing.

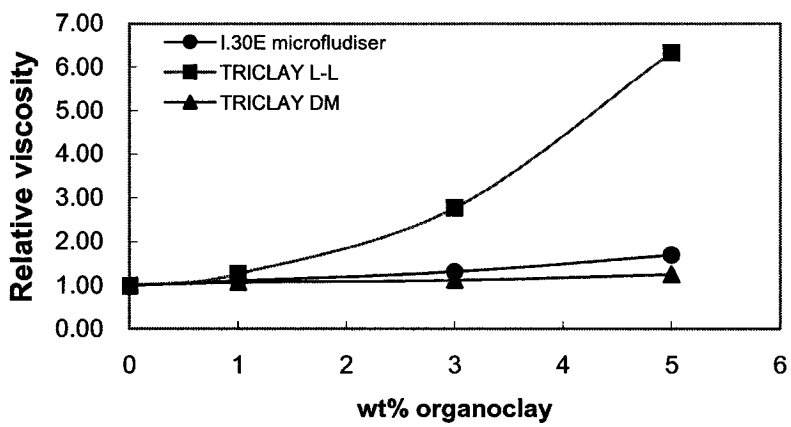

Figure 49: Relative viscosity of organoclay/epoxy mixture with different preparation methods, at apparent shear rate 167/s (50rpm).

There are two models which can describe viscosity of particle filled polymers: the Krieger-Dougherty model and the Einstein model, we describe these models below:

Krieger-Dougherty Model

This model indicates that there is an increase in the viscosity when particles are added. This increase depends on the concentration of the particles:

$$\frac{\eta}{\eta_o} = \left(1 - \frac{\phi}{\phi_m}\right)^{-[\eta]\phi_m}$$

where the intrinsic viscosity, $[\eta]$, is equal to 2.5 for spheres and is determined by the shape of the particle, ϕ is the volume fraction of particles, ϕ_m the volume fraction at maximum packing, η is the viscosity of the suspension and η_0 is the viscosity of the medium.

Volume fraction, ϕ, can be calculated from the clay weight ratio w, clay density ρ_c and the matrix density ρ_m:

$$\phi = (w/\rho_c) / (w/\rho_c + (1-w)/\rho_m)$$

Einstein model

For a dilute solution, only pair interactions (such as collisions) are considered. At low shear rates, the increase in viscosity can then be described as

$$\eta/\eta_0 = 1 + 2.5\phi + 6.2\phi^2.$$

It is found that the Krieger-Dougherty model can describe the clay/uncured-epoxy mixture system better. The following parameters for the Krieger-Dougherty model can best fit the data, Table 12.

Table 12: Parameters for Krieger-Dougherty model.

	Φ_m			[η]		
Shear rate	167 s^{-1}	300 s^{-1}	433 s^{-1}	167 s^{-1}	300 s^{-1}	433 s^{-1}
Triclay L-L	0.08	0.11	0.2	22	22	22
I.30E microfludiser	0.2	0.2	0.3	9	8	8
Triclay DM	0.1	0.1	0.1	3	3	3

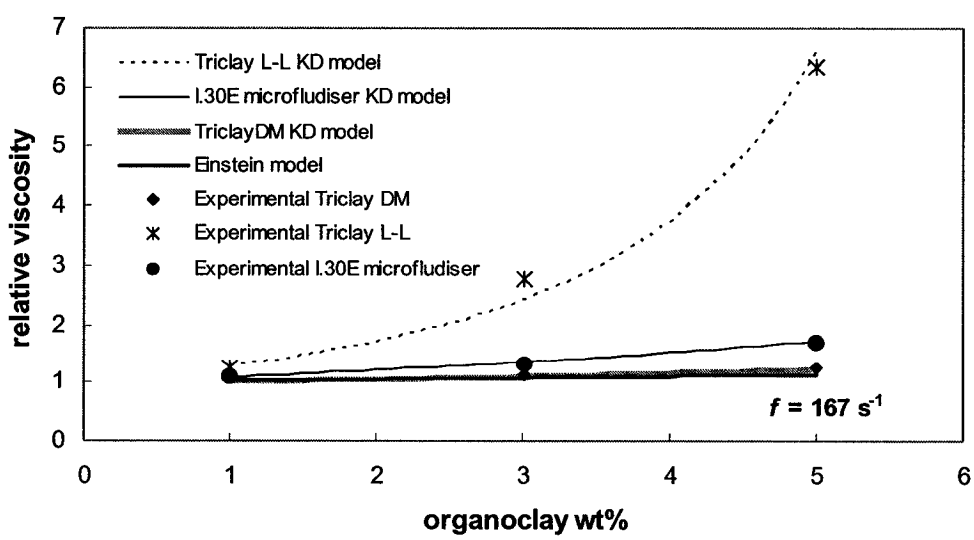

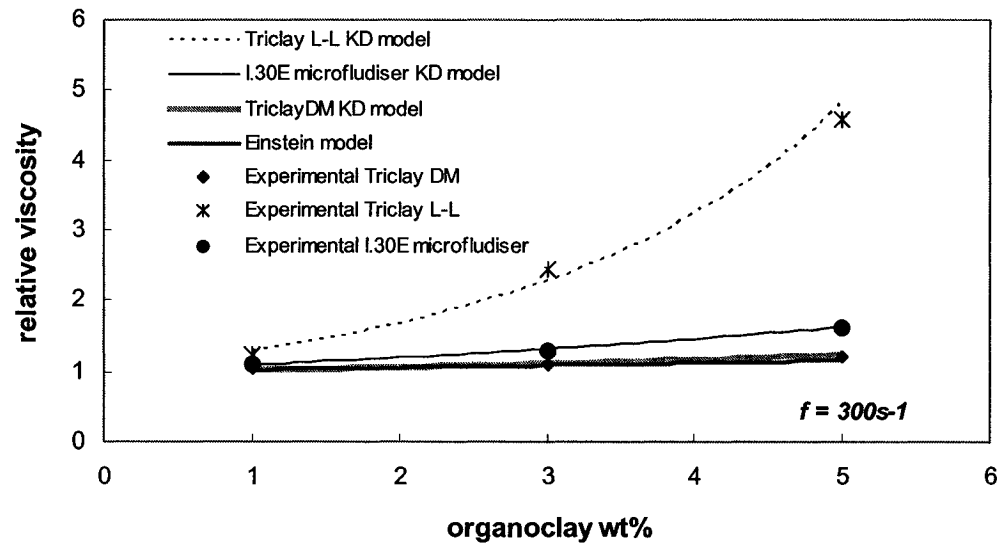

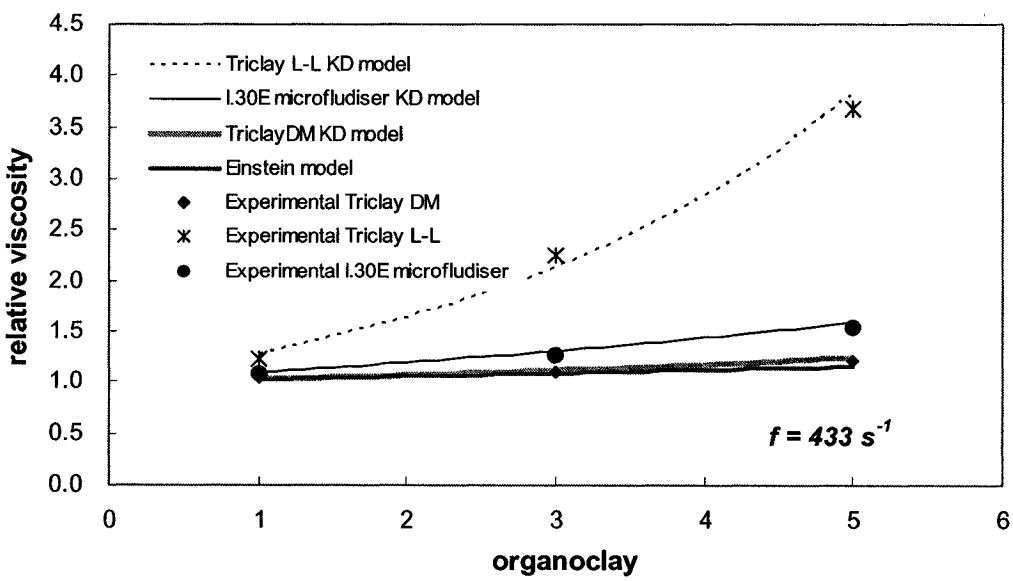

Figure 50: Krieger-Dougherty (KD) model for clay/uncured-epoxy mixture.

Figure 50 illustrates the use of the Krieger-Dougherty model and the Einstein model to reveal some properties of the clay/uncured-epoxy mixtures. First, the Krieger-Dougherty model can very well describe the organoclay/uncured-epoxy mixtures. The fitted intrinsic viscosities are 22, 9 and 3 for the mixtures prepared by

the L-L method, microfludiser and direct mixing (DM) respectively, and this value is almost not affected by the apparent shear rate. It is interesting to note that the intrinsic viscosity of the Triclay DM system is very close to 2.5, which represents the spherical particle shape. Therefore we conclude that direct mixing cannot disperse the clay layers evenly into the matrix, and the clay particles are still agglomerated in an almost spherical geometry. With the microfludiser and the L-L methods, the intrinsic viscosity increases greatly, which reveals that the clay layer dispersion is improved, and thus we can produce better nanocomposites due to the better exfoliation of clay layers.

4.3 Epoxy matrix properties

In clay/epoxy nanocomposites, epoxy plays an important role as the matrix for combining the clay layers and transferring exterior forces to the clay layers. Having a clear understanding of its micro/nano-structures, epoxy-amine stoichiometry and its mechanical /chemical properties is key to achieving improved materials.

Recently, atomic force microscopy (AFM), with its scales in nanometers, has become a very important instrument to study the material surfaces. The most useful mode for studying polymer and polymer composites using AFM, is TappingMode® from which the topological and phase images can be obtained. TappingMode AFM, which can give very high resolution on most samples (1nm to 5 nm), is operated by

scanning a tip attached to the end of an oscillating cantilever across the sample surface.

Another interesting mechanical probing tool is nanoDMA® that dynamically measures nanoscale mechanical properties. By controlling the force applied to the tip, the indent depth can be set according to the experimental requirements. NanoDMA® can give surface nanoscale mechanical information that is difficult to obtain using common methods and it reveals valuable information about micromechanical properties.

Here our research object is to show and explain the relationships among epoxy/curing agent stoichiometry, micro/nano-structures, and their properties by using DSC, atomic force microscopy (AFM) and NanoDMA. As well, AFM is used to investigate the micro/nano-structure of clay/epoxy nanocomposites. Epon828/Epi-cure3046 system with different stoichiometric ratios is used here.

4.3.1 Chemical/physical properties of epoxy-amine system

First, let us consider the chemical properties of Epi-cure 3046. The manufacturer's MSDS indicates that it is a mixture of two different ethyleneamines - ethylenediamine and triethylenetriamine (TETA). Its chemical structure can be written in the general form:

$$H_2N(CH_2CH_2NH)_xH$$

Where x=1, Ethylenediamine, and x=3, Triethylenetriamine (TETA).

Because of its low molecular weight, the viscosity is low and it has a high vapor pressure [69]. The poor compatibility of Epi-cure 3046 with Epon828 gives a sample cured at room temperature an oily tacky air surface, because the amine exudes to the surface of the epoxy-amine mixture before the cure can trap the amine in the matrix.

A typical cure mechanism of epoxy-amine is the reaction between epoxy resins and all primary and secondary amines. The cure possesses the following reaction characteristics: (1) the speed of the reaction is faster than with cycloapliphatic and aromatic polyamines, and (2) it can be cured at room temperature. Because of its short molecular chain length, Epi-cure 3046 can give high cross-linkage networks that result in a good balance of solvent resistance, mechanical strength, and low flexibility.

In order to avoid the escape of Epi-cure 3046 that causes the sample surface to be tacky, we increased the curing temperature so that the curing agent in the matrix is trapped before it can migrate to surface. Raising the curing temperature also leads to a higher chemical reaction rate between the epoxy and the amine, and shortens the operation time. In 2 hours curing time, very smooth and highly transparent samples can be obtained. Here we study the effect of stoichiometry on the final samples by noting the properties and the etherification chemical reactions that have taken place at this elevated temperature (see Figure 51).

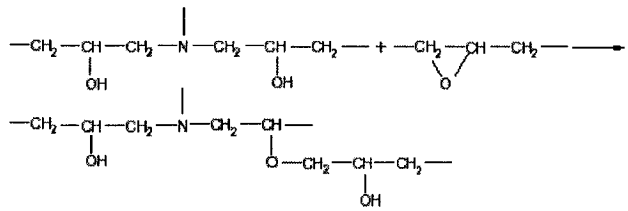

Figure 51: Etherification reaction in epoxy-rich system.

Two questions have been addressed here: 1) when will etherification take place, and 2) at what condition will it be initiated? For these questions, we need to consider two different epoxy-amine ratios at elevated temperatures:

1) In the case of excess epoxy, chemical reactions between first and second amines with epoxide groups take place. After the amine is depleted, etherification between the reacted epoxy groups and unreacted epoxide groups takes place slowly (diffusion controlled process) at the cure temperature near to or higher than T_g, which allows the formation of a high cross-linking density and a higher T_g.

2) For the case of excess amine, the epoxy-amine reaction is quicker and the highest epoxy conversion rate can be reached. Unlike the epoxy-rich case, spare amines exist in the cured epoxy as the original small molecules leading to low hardness and low T_g.

In order to understand the properties of this epoxy-amine system, we have used DSC, AFM and Nano-indentation (NanoDMA). The results are discussed below.

4.3.2 DSC study of epoxy-amine system

For the experiments, a series of samples of different epoxy-amine ratios were studied: 35phr, 41phr, 46phr, 52phr, 60phr, 80phr, 100phr and 140phr. The total weight of sample in the DSC alumina pan was about 10~16 mg, the heating rate was 10 K/min under N_2 atmosphere, and the temperature range was from 40 to 220°C. The total heat release H_r was measured and analyzed. Table 13 gives data from the DSC curves of the above samples.

Table 13: The total heat release in Epon828/Epi-cure3046 system

Epi-cure3046 phr	35	41	46	52	60	80	100	140
H_r (J/g)	259.0	315.8	357.8	358.4	358.4	345.2	324.4	265.7
H_r per epoxide group (kcal/mol)	15.75	20.19	23.52	24.53	25.82	27.98	29.22	28.72

In the above table, the H_r per epoxide group is calculated by using following equation:

$$Hr\ per\ epoxide\ group = Hr*M_{epon}*(1+amine\ phr/100)/N_{epoxide}*4.186$$

Where M_{epon} is 377g/mol, and $N_{epoxide}$ is the number of epoxide group per epoxy molecule, here it is 2.

Figure 52 shows the relationship between the amount of curing agent and the total heat released. It is clear that the total heat released reaches its maximum value of 358 J/g at the epoxy-amine ratio of one amine to one epoxide group. In epoxy rich cases, there is less amine so the total heat released is less. Adding more amine allows more free epoxide groups to convert into a hard network. For amine rich samples there are many free-active, small molecular weight amines that are left in the

network reducing the total heat release and also make the sample softer.

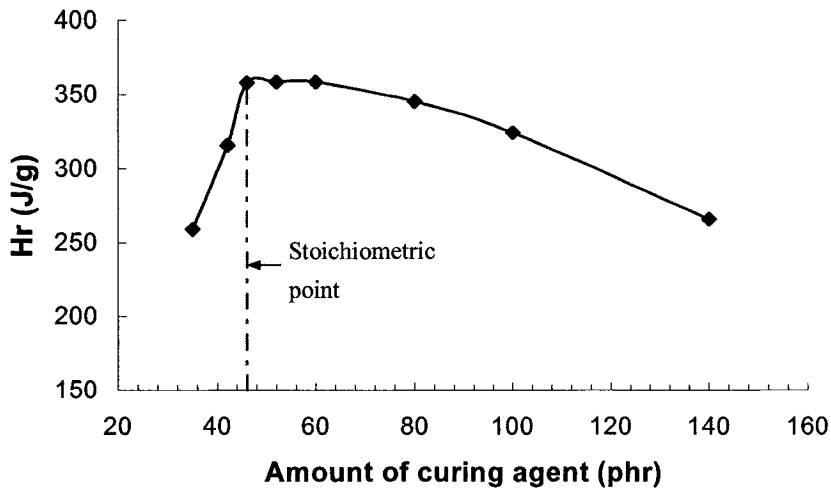

Figure 52: The relationship between the amount of curing agent and the total system heat released.

The glass transition temperature reflects the local movements of the polymer chains. If we can improve a glassy polymer's T_g, the mechanical behavior of the material at elevated temperatures is more stable.

For the above epoxy-amine system, glass transition temperatures are measured after the first epoxy-amine reaction in DSC pan. The amount of curing agent was limited to below 60phr because a higher amount of curing agent (greater than 80phr) will lead to an uncured state of epoxy-amine mixtures after the first run of the DSC thermal cycle. The effect of the amount of curing agent on the cured epoxy T_g can be clearly seen in Figure 53. Note that the maximum T_g is not at a 1:1 hydrogen/epoxide ratio (46phr), but at 35 phr, and when more amine is added the glass transition temperature

decreases monotonically. The difference in glass transition temperatures between 35 phr (maximum T_g) and 46phr is more than 15°C.

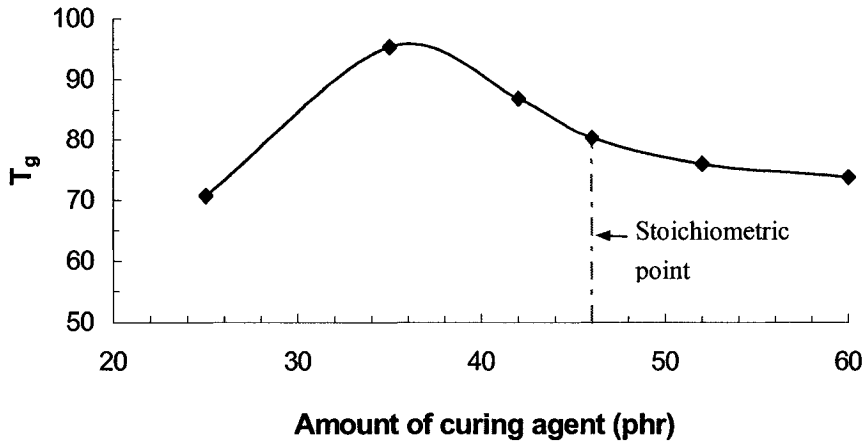

Figure 53: Illustration of the effect of amount of the curing agent (≤60 phr) on the glass transition temperatures.

Figure 53 demonstrates that further reduction of the curing agent will lead to a decrease in glass transition temperature. The reason for the decrease in T_g can be explained as following:

For an amine-rich system, where the amine amount is larger than 46phr, no free epoxide groups are available because all of them have been taken up in the chemical reaction with the active primary and secondary hydrogens. Thus, more amine means more residue of unreacted curing agent (low molecular weight) in the cured system, which gives a lower glass transition temperature.

For epoxy-rich samples where the amine amount is less than 46phr, etherification must be considered. There are unreacted epoxide groups that can undergo

etherification which is a molecular diffusion controlled process. More free epoxide groups need much more time to complete this etherification reaction. Based on the properties of materials as discussed by B.Ellis [69], it is known that etherification can give a high glass transition temperature. Also in Figure 53 we see that the 25phr amine-epoxy system has a much lower T_g than the 35phr amine-epoxy system. The explanation for this difference is that in 25phr amine-epoxy sample there are too many free epoxide groups after the limited curing time. In the 35phr amine-epoxy sample fewer epoxide groups remain unreacted and most of the available epoxide groups could take part in the etherification and, thus, form polyether, which has high glass transition temperature. Therefore, 35phr amine-epoxy sample gives highest T_g compared with other samples.

4.3.3 Micro/nano structural study of Epoxy-amine System

Some researchers found that a two-phase structure exists in a cured epoxy-amine system: a high density, high modulus phase is surrounded by a low density, low modulus phase. If so, this two-phase structure should have an effect on the properties of cured epoxy and epoxy-based nanocomposites [50,52,55]. However, some researchers question the validity of the above observation and have found no granular structure in cured epoxy systems [56,57].

This controversial topic should play an important role in understanding the microstructure and chemical/physical behaviors of cured epoxy. Here I give my

observations and try to explain what I observed. Further systematic study and theoretical explanation is necessary to fully understand the micro/nano structure of the epoxy system and its nanocomposites.

In our research, the air-faces, teflon-faces, and fracture-faces were studied by atomic force microscopy and nanoDMA in order to understand the micron/nanometer size structure and properties of this epoxy system. In this way we could further design clay/epoxy nanocomposites with optimum epoxy-amine ratios.

4.3.3.1 AFM Study

Figure 54 shows the air-face AFM images of different stoichiometric ratio epoxy samples with a size of 1 μm x 1 μm. It was found that the sample air faces were very smooth. In the topological images, the z-range (peak-to-valley difference in height values within the analyzed region) was less than 50 nm except in sample100-120 (120 phr of Epi-cure 3046). For the phase images, a very large phase difference (180°) was observed in our samples. One thing to note is that epoxy two-phase nodular structure is not always apparent in its air face, and the epoxy air-face micro/nano-structure is sensitive to the amount of curing agent. It was found that the nodular size increased when the amine amounts changed from 25 phr (Figure 54-a) to 47 phr (Figure 54-c). In Figure 54-d (sample 100-52), there seems to be a thin film on the surface which might explain the difficulty in clearly revealing the surface

images of the sample. The phase image makes it appear as though the sample is immersed in water. The nodular particle size increases from Figure 54-e to Figure 54-g when more amine is added to epoxy in the case of amine-rich situation.

I regard the air-face of cured epoxy as a special case because the moisture, carbonate, amine migration, oxygen, and surface thermal gradient may change the properties of the cured surface skin. All of these factors can cause the air-face skin properties to be different from the inner bulk properties.

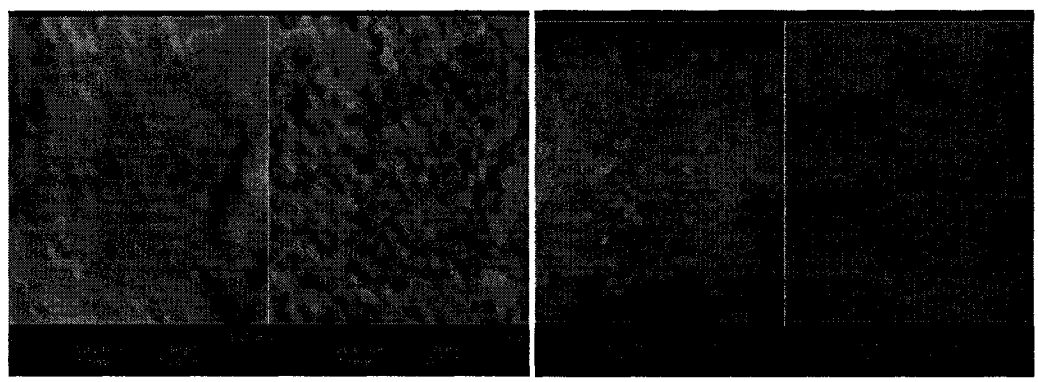

(a) (b)

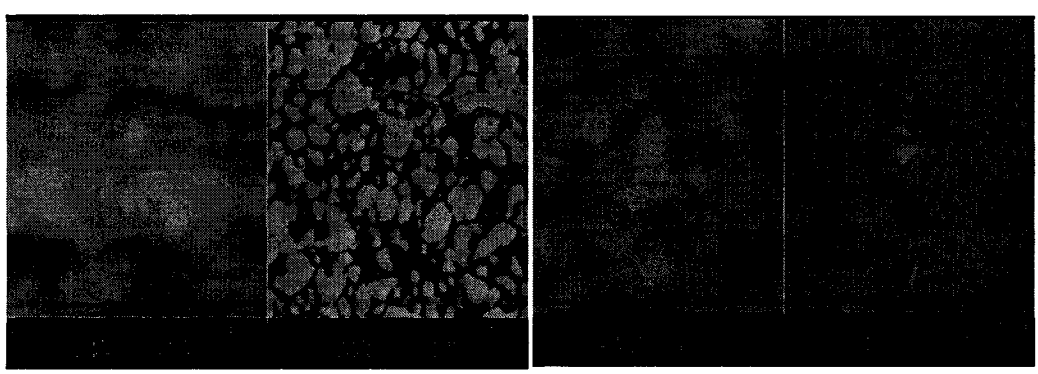

(c) (d)

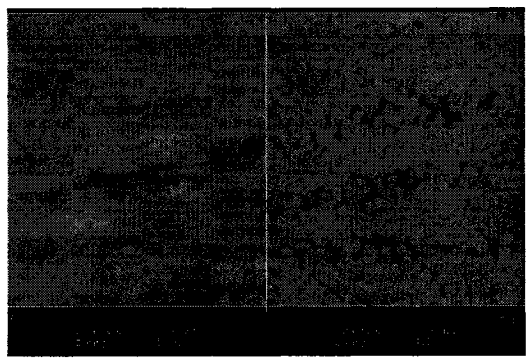

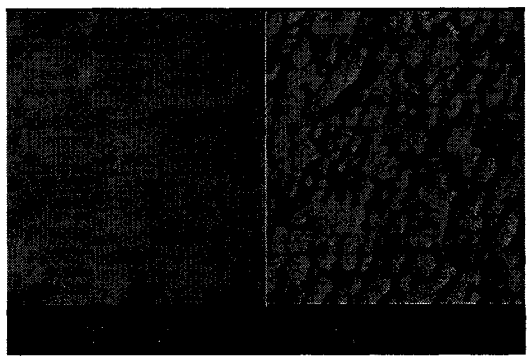

(e) (f)

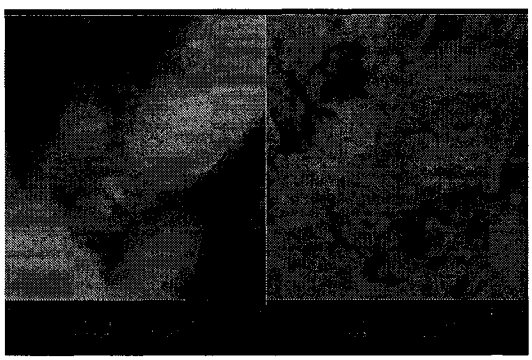

(g)

Figure 54: AFM topological (left) and phase (right) images of air-faces in epoxy with different amine amounts: (a) 100-25 sample; (b) 100-35 sample; (c) 100-47 sample; (d) 100-52 sample; (e) 100-60 sample; (f) 100-80 sample; (g) 100-120 sample. The phase difference is 180 °; the topological difference range (a to f) is less than 50 nm, and 100nm for sample 100-120 (g). Image size: 1 μm x 1 μm.

Fracture surfaces present the inner structure of cured epoxy which determines the macro-properties of cured epoxy. Figure 55 gives AFM images of these different stoichiometric ratio epoxy resins on a micron-size scale. The fracture surfaces of the samples are also very smooth. Unlike the air-face structure, the two-phase nodular

structure appears clearly in every sample at all stoichiometric values. In epoxy rich samples, the size of the nodules decreases when more amine is added (Figure 55-a, Figure 55-b). In the case of amine-rich samples (>46 phr), and the stoichiometric point (46 phr), the nodular sizes also decrease when the content of amine increases (Figure 55-c to Figure 55-g). This decrease in size can be explained as the effect of nucleation. More nuclei will generate when more amines are added. Thus the nodular size decreases.

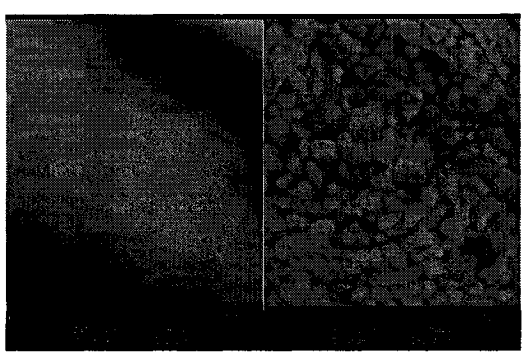

(a)

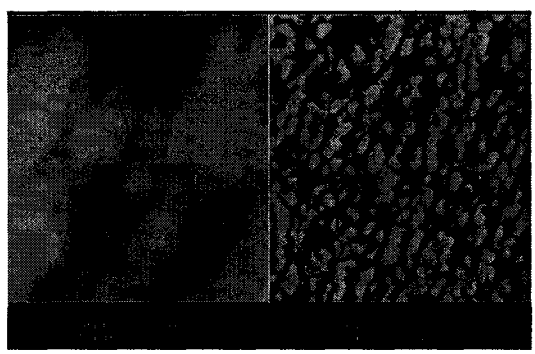

(b)

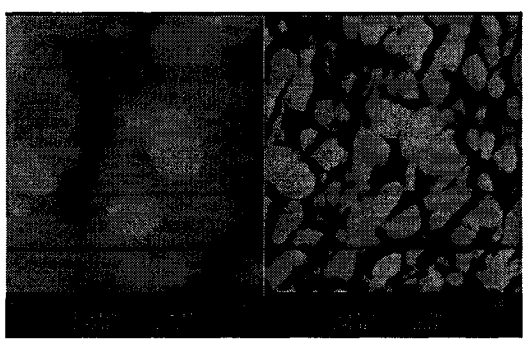

(c)

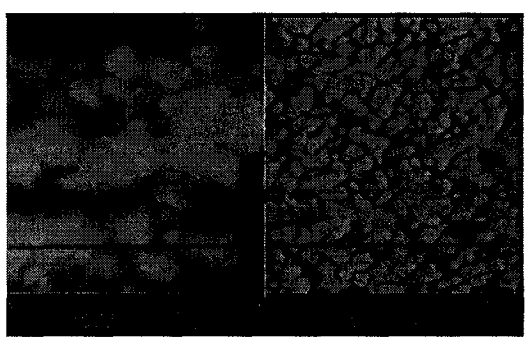

(d)

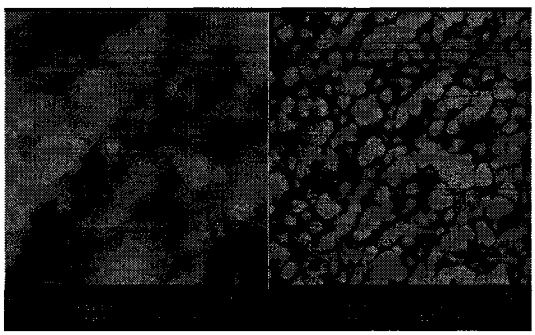

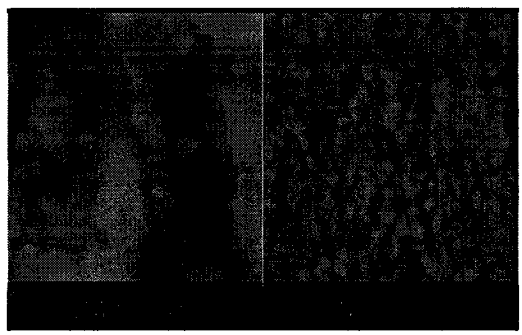

(e) (f)

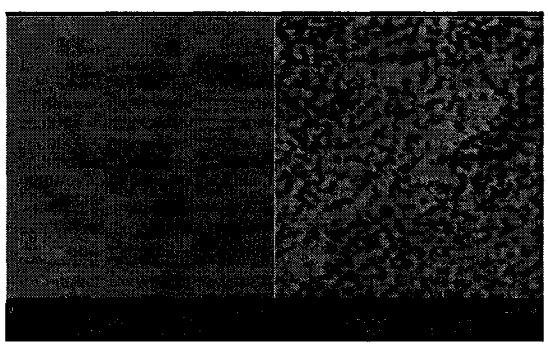

(g)

Figure 55: AFM topological (left) and phase (right) images of fracture-faces in epoxy with different amine amounts: (a) 100-25 sample; (b) 100-35 sample; (c) 100-47 sample; (d) 100-52 sample; (e) 100-60 sample; (f) 100-80 sample; (g) 100-120 sample. The phase difference range is 180 °; the topological difference range is 50 nm. Image size: 1 μm x 1 μm.

The bearing function is one of the most important tools in AFM image analysis. It provides a method to measure how much of the surface lies below or above a given height. Here height can mean the topological variance or phase variance. The bearing function gives a depth histogram, which plots depth versus percentage of

occurrence of data at different depths. Figure 56 illustrates the Epon828-35phr Epi-cure3046 bearing depth histogram. Here we can define a phase value to be the given height, and then we can use the bearing function to calculate how many hard-phase (high phase angles) and soft- phase (low phase angles) exist in the cured epoxy system.

Here phase images of the fracture samples (from Figure 55) are used to quantify the hard and soft phase distribution by applying the bearing tool. The depth histograms of the fracture samples show that a significant break exists between the hard-phase and the soft-phase. Here we arbitrarily define the distinction between hard and soft phases in these images as 70°.

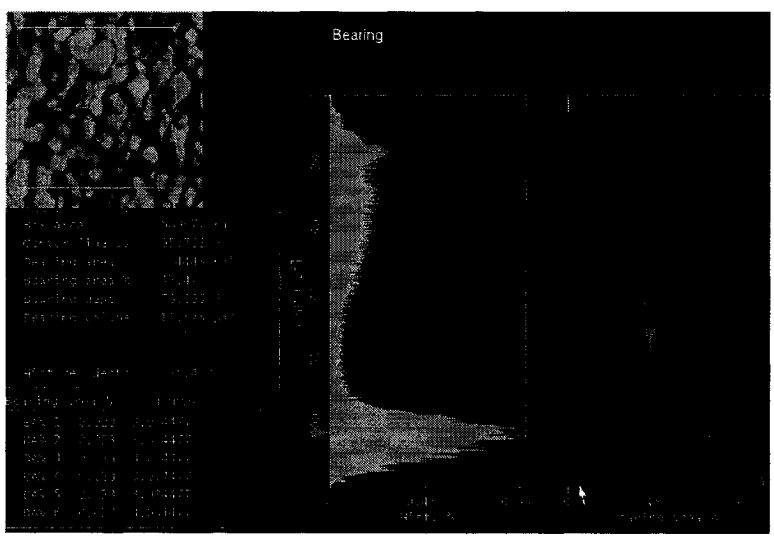

Figure 56: Application of bearing function on Epon828-35phr Epi-cure3046.

After analysis, we attain the relative amounts of the two phases as a function of epoxy-curing agent stoichiometry (see Figure 57). The maximum percentage of hard

phase occurs at 35phr, which is in accord with the T_g results attained in the DSC analysis. The curve shape is also the same as the shape of the T_g DSC curve. This adds additional proof that the highest T_g value is not at 47phr amount of curing agent, because of etherification that takes place at elevated temperatures.

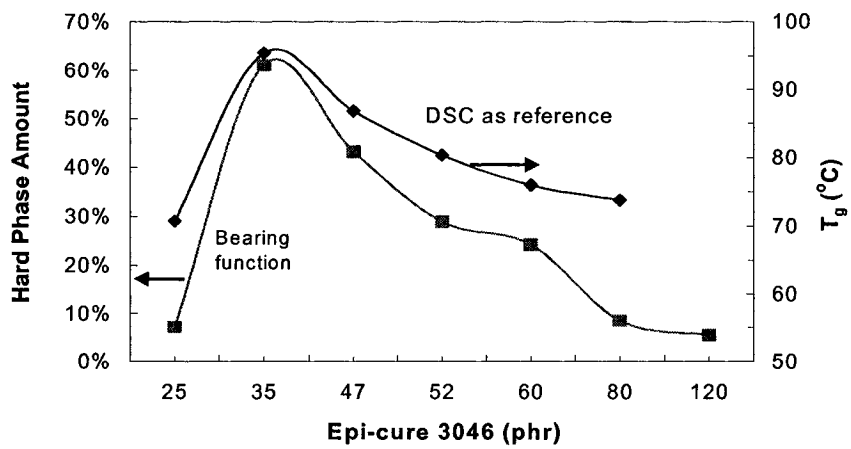

Figure 57: Amount of hard phase as a function of the amount of curing agent, DSC data from Figure 53 as reference.

Now let us consider the teflon-face AFM images of these samples (see Figure 58). The faces on the teflon film side are coarser than the air-face. It is obvious that the nodular particles are much larger than on the air-face and fracture-face, and that the two-phase nodular structure exists in all samples. The smallest nodular size appears in sample 100-35 (Figure 58-b) which also represents the smallest nodular size on the fracture face on the AFM image.

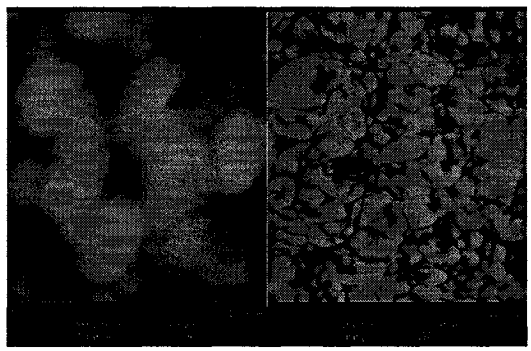

(a)

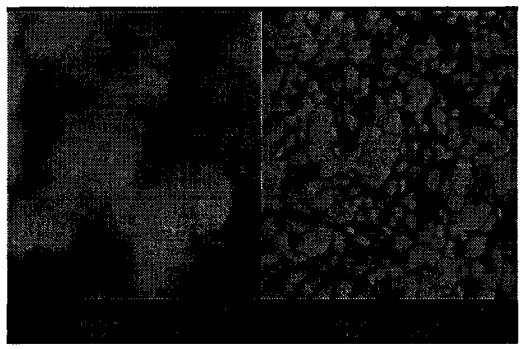

(b)

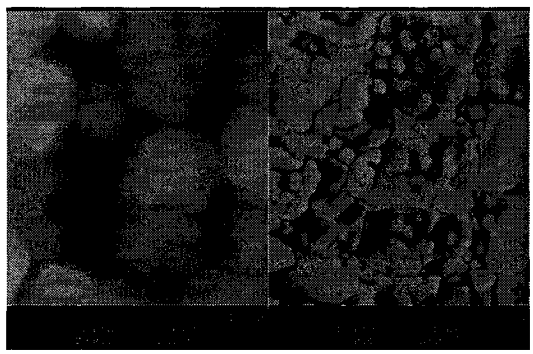

(c)

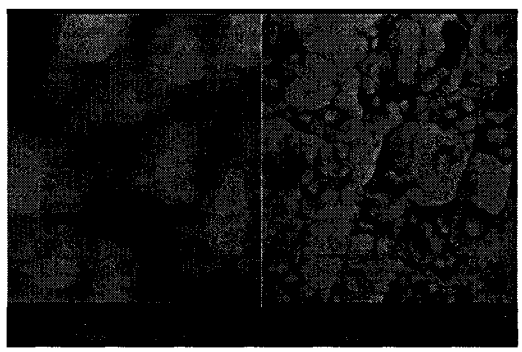

(d)

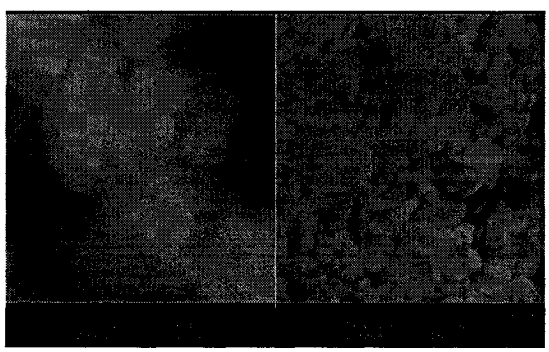

(e)

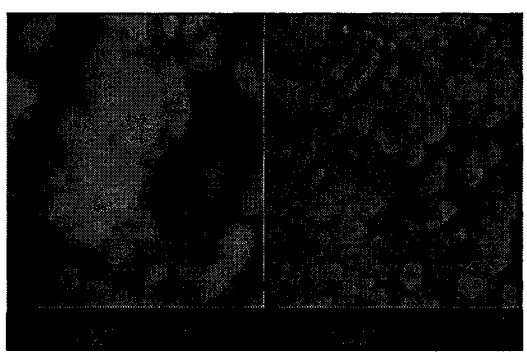

(f)

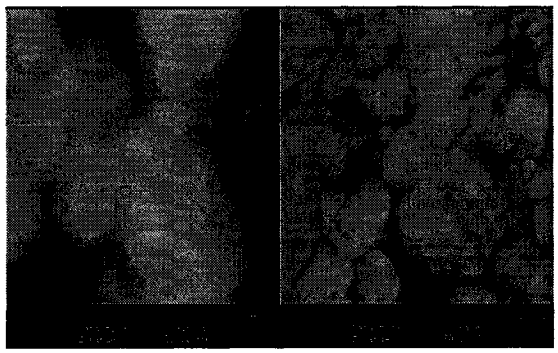

(g)

Figure 58: AFM topological (left) and phase (right) images of teflon faces in epoxy with different amine amounts: (a) 100-25 sample; (b) 100-35 sample; (c) 100-47 sample; (d) 100-52 sample; (e) 100-60 sample; (f) 100-80 sample; (g) 100-120 sample. The phase difference range is 180 °; the topological difference range is less than 200nm. Image size: 1 μm x 1 μm.

Some observations from AFM studies of cured epoxy:

1) Through the AFM study of the fracture-face and teflon-face of cured epoxy, the nodular structure is observed. For some samples we cannot see the nodular structure on the airface. We attribute this lack of visibility to the formation of a special skin layer that is caused by carbonates, moisture, oxygen, and thermal gradients during the curing process.

2) The fracture-face which presents the internal structure, can give the most valuable information about cured epoxy structures. This internal structure causes the basic physical/mechanical behaviors of epoxy.

3) The bearing function analysis for the fracture-face samples indicates the same optimal epoxy-amine ratio at elevated temperatures as DSC studies do. Both the

bearing function analysis and the Tg study results indicate that the optimal value is 35 phr instead of 47phr Epi-cure3046.

4) More research needs to be done to clarify the controversy about the structure of cured epoxy. We should consider the effect of tip radius, force level, cantilever vibration amplitude, and different methods of sample preparation.

4.3.3.2 Nano indentation & NanoDMA

The following study was performed to understand more about the relationship between the micro-/ nano-structure of the matrix and its mechanical properties. Additionally it is interesting to use the AFM and nano indentation to reveal the material surface characteristics as such studies are rare in the literature.

First, let us consider the use of indentation on the cured epoxy-amine samples. During our experiments, an indenter tip is driven into the sample by applying an increasing normal load. When reaching a preset maximum value, the normal load is kept constant for a preset time, and then reduced until partial or complete relaxation occurs (see Figure 59). This form of applying force is called the loading function.

For each loading function cycle, the applied load value is plotted with respect to the corresponding position of the indenter. The resulting load-displacement curves provide data specific to the mechanical nature of the material under examination.

Established models are used to calculate quantitative hardness and modulus values from such data (see Figure 60).

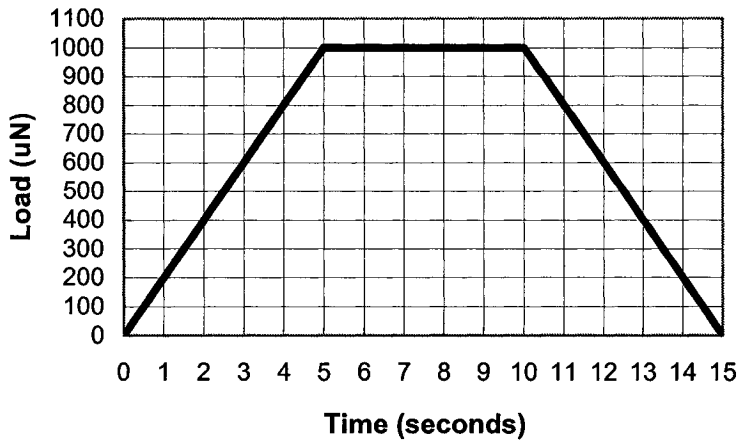

Figure 59: The loading function of Nano indentation: first stage - raise force from zero to 1000μN in five seconds; second stage - keep force constant for five seconds; last stage - withdraw force from 1000μN to zero.

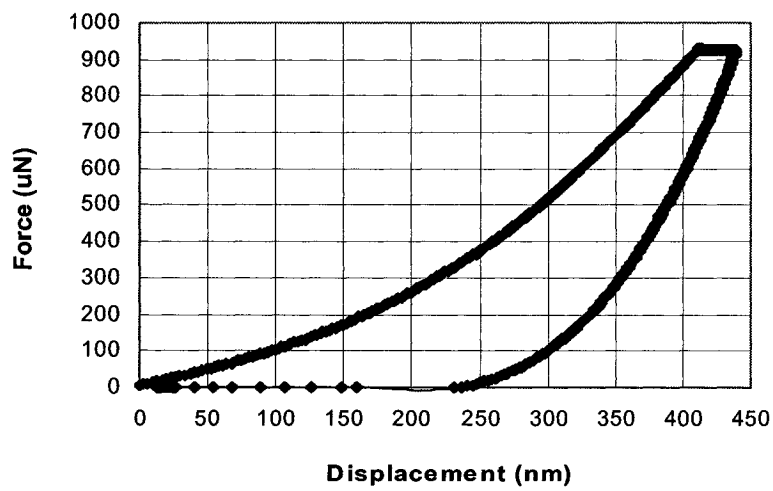

Figure 60: Nano indentation load-displacement curve (Epon828-Epicure3046, applied force 1000μN).

Here we used different maximum forces to measure the relationship between the maximum force and the indent depth. The forces used were 500μN, 800μN, 1250μN, 2500μN, and 15000μN. We used the same loading times for the three stages of the loading function: five seconds for raising the force, five seconds for holding the force constant, and five seconds to withdraw the force. The indention on the Epon-amine sample is shown in Figure 61. We used a Berkovich tip, which is standard for nano indentation. The radius of curvature of the tip is between 100nm and 200nm. The indentation marks on the sample are clearly shown in the AFM images (Figure 61).

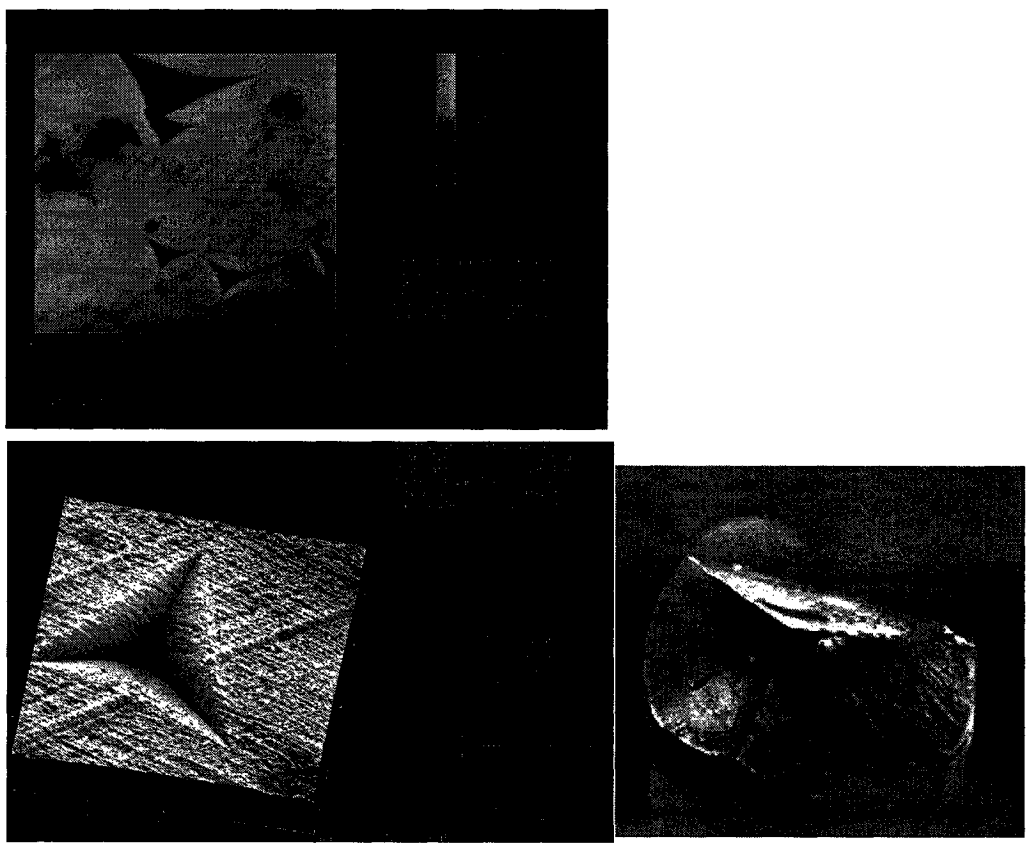

Figure 61: Indentation on the Epon828-35phrEpicure3046 sample (top), its 3D image and the shape of the Berkovich tip (right).

The section function from the AFM software is applied to the nano indentation images from which we analyze the depth of indentation with different applied forces. In Figure 62 a cross-sectional line is drawn across the image in order to allow for the calculation of the depth of the indentation. The vertical profile along that line is displayed at the upper left side of the picture and the measurements are displayed in the right text boxes that give the information on the surface distance, vertical height between the two triangle cursors, and the surface roughness of the sample at the image scale.

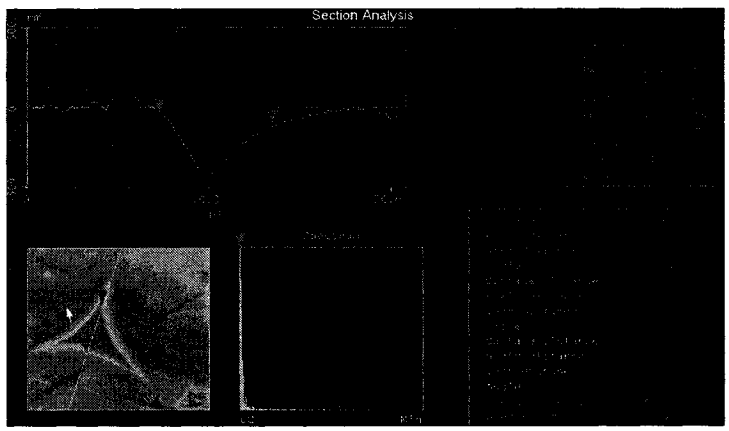

Figure 62: Section analysis of the indentation depth, sample is Epon828-35phr Epi-cure3046, applied force 15000μN.

We applied the section function to all indentations and attained the data shown in Table 14. Here Max Length is chosen as the maximum length of 3 triangle sides from the image. From this table, we draw Figure 63 to illustrate the relationship between the applied force and indentation characteristics.

Table 14: Indentation depth and length measured by the section function

Force (μN)	*500*	*800*	*1250*	*2500*	*15000*
Depth (nm)	77	95	122	175	530
Max Length (μm)	2.3	3.1	4.3	6.4	15.5

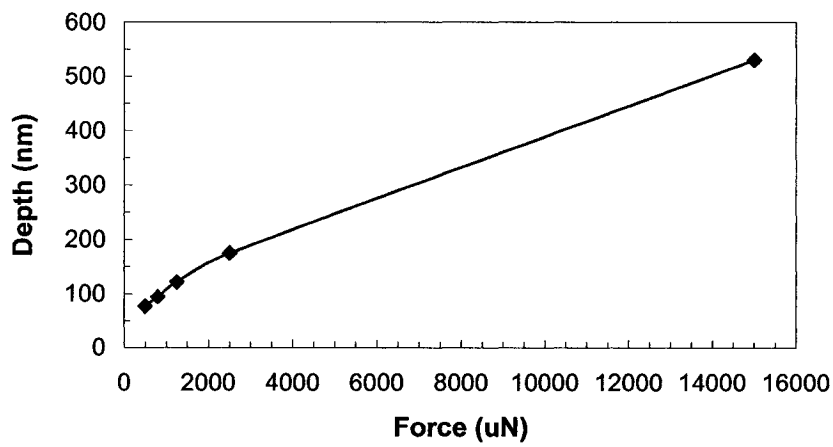

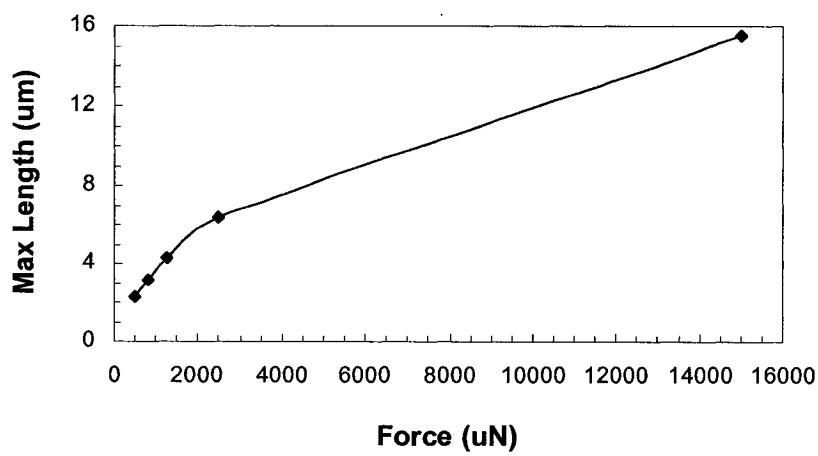

Figure 63: Illustration of the relationship between the applied force and indentation characteristics, sample: Epon828-35phr Epi-cure3046.

Now let us consider the use of the NanoDMA for micro/nano scale mechanical property measurement. The force we applied was 1000μN and the frequency ranged from 1 - 300Hz. The indent depth under this force was about 110nm (for sample 100-35). The curve showing the storage modulus, loss modulus, and tan delta is illustrated in Figure 64.

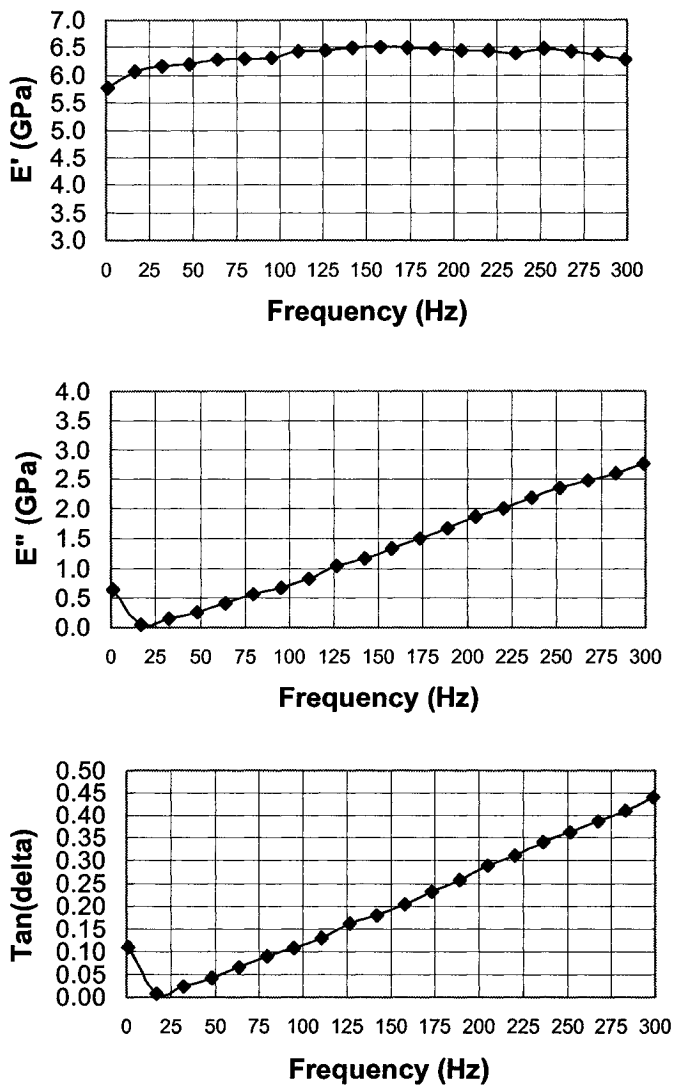

Figure 64: NanoDMA measures the storage modulus E' , loss modulus E" and Tan Delta as the function of frequency, sample: Epon828-35phr Epi-cure 3046 (sample 100-35).

After using NanoDMA to measure the mechanical properties of the air-face and the bottom-face of the epoxy-amine sample, Figure 65 was drawn.

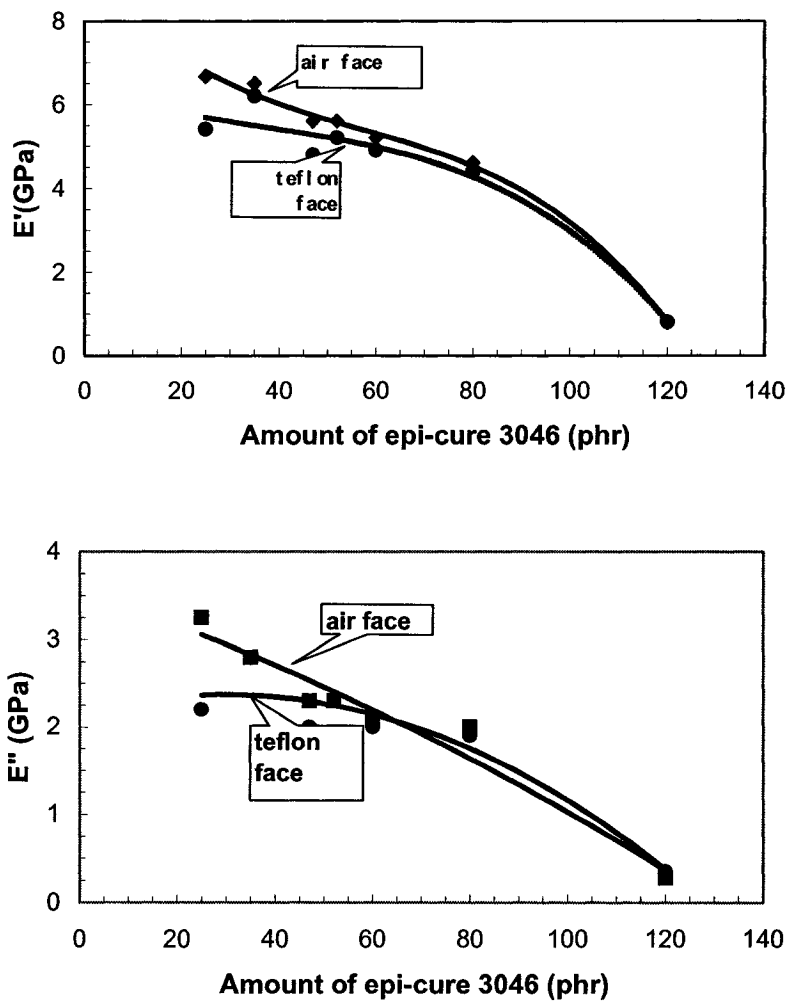

Figure 65: Comparison of the maximum storage /loss modulus of epoxy air face and teflon face as functions of the amount of curing agent: the solid line represents the air face modulus, the dotted line represents the teflon face modulus.

The micro /nano-mechanical properties shown above give some hints to the properties of the outermost epoxy skin layer. For the maximum storage modulus (E') and maximum loss modulus (E"), it was found that the modulus decreased monotonically with increasing curing agent. Sample 100-25 demonstrates high E' and E". This result could be due to the etherification reaction completing more at the surface than at the inner core because of a higher temperature at surface. The fact that the air-face skin shows a higher modulus than the teflon bottom skin layer could also be explained by the difference in temperature on the air-face and on the teflon-face.

4.4 Future work

Further work should be done on the following areas:

1) Investigate the L-L method, clarify the factors which will affect this new method, such as the type of solvent, type of intercalating agent, temperature for removing solvent and the effect of residue solvent on the final properties.
2) Investigate this method in regards to improvement of other properties such as fire retardation and barrier properties.
3) Use XRD and SEM to understand the exfoliation of organoclay of Triclay/epoxy nanocomposites prepared by L-L method.
4) Clarify the validity of Kreiger-Dorgerhty model for organoclay/ uncured epoxy mixture.

5. Conclusions

Newly developed organoclay—Triclay:

1) The successful synthesis of the functional organoclay is proved by FT-IR, AFM and DSC. DSC demonstrated more thermal energy release during curing in the new nanocomposite system, indicating chemical bonds are forming between the new organoclay and the epoxy. The bonds can form because of the change of surface chemical properties of the new Triclay.
2) Triclay shows its advantage over commercial I.30E organoclay in tensile strength. There is no decrease in tensile strength (even a slight improvement is seen) in the Triclay/epoxy nanocomposites, but the I.30E/epoxy nanocomposites show a decrease in the strength.

Synthesis methods:

1) As well as conventional direct mixing, the new Liquid-Liquid (L-L) method and the advanced high-pressure mixing—microfludiser were used in the study. The L-L method and the microfludiser are better than the conventional method because both effectively disperse organoclay into the matrix, avoiding conglomeration of dry clay particles.
2) The L-L method gives a high viscosity in the uncured system compared to the use of the microfludiser, and gives the better mechanical properties. But the high viscosity makes it very difficult to prepare nanocomposites.

3) Kreiger-Dorgherty model successfully describes the dispersion of clay layers in the uncured epoxy.

4) Curing temperature and amount of curing agent affect the exfoliation process. A high curing temperature and lower amount of curing agent are beneficial to the clay exfoliation.

For the use of interface design and L-L method:

The compressive properties of triclay/epoxy nanocomposites are greatly improved over the cured epoxy. 5% Triclay nanocomposites exhibit a 45% increase in maximum stress, a 10% increase in yield stress and a 26% increase in modulus.

The epoxy-amine system:

1) At the curing temperature optimum for clay exfoliation in nanocomposites the best epoxy/curing agent ratio is at 35phr, and not the 47phr point which gives a 1:1 epoxide/H^+ ratio.

In the epoxy-rich system, etherification takes place at the temperature required by the clay exfoliation in clay/epoxy nanocomposites. Etherification is a diffusion controlled process, which leads to the highest amount of hard phase in the cured epoxy system not at the stoichiometric point, but at the point where the amount of amine is less than the

stoichiometric point.

2) It is clear that the surfaces of cured epoxy possess different structures when compared with the inner structures, resulting in different mechanical and chemical properties

Contributions

In order to improve the interface between the clay and the matrix, a new kind of organoclay is synthesized by using a multi-functional intercalating agent. The tests show that covalent bonds are created between the organoclay and the epoxy, resulting in an improvement in the compression and tensile properties of the nanocomposites.

Dry organoclay tends to conglomerate and is very difficult to disperse evenly into the matrix. The clay particles can be seen with standard microscopy instruments, and most of the clay particles have radii much larger than 1 μm. A new method to synthesize clay/epoxy nanocomposites is developed, called the *L-L method.* This method combines organoclay synthesis with organoclay/epoxy preparation, and solves the defects caused by using dry organoclay. This method can make the clay layers more evenly dispersed into the matrix, as a result, the mechanical properties of the organoclay are improved.

References

1. C.C. Koch, "Nanostructured Materials, Processing, Properties and Potential Application", William Andrew Publishing, Now York (2002).
2. G. Lagaly, "Introduction: from clay mineral-polymer interactions to clay mineral-polymer nanocomposites", Applied Clay Science, 15, 1 (1999).
3. C.N.R. Rao, A.K. Cheetham, "Science and technology of nanomaterials: current status and future prospects", Journal of Materials Chemistry, 11, 2887 (2001).
4. A. Usuki, M. Kawasumi, Y. Kijima, A. Okada, T. Kurauchi, O. Kamigaito, "Synthesis of Nylon 6-Clay Hybrid", J. Mater. Res., 8, 1179 (1993).
5. W.A. Zisman, "Improving the performance of reinforced plastics", Industrial and Engineering Chemistry, 57, 27 (1965).
6. B.K.G. Theng, "Formation and Properties of Clay-Polymer Complexes", Developments in soil science 9, Elsevier Scientific Pub. Co. (1979).
7. J.K. Lu, Y.C. Ke, Z.N. Qi, X.S.Yi, "Study on Intercalation and Exfoliation Behavior of Organoclays in Epoxy Resin", J. Polym. Sci.: Part. B: Polym. Phys., 39, 115 (2001).
8. M.S. Wang, T.J. Pinnavaia, "Clay-Polymer Nanocomposites Formed from Acidic Derivatives of Montmorillonite and an Epoxy Resin", Chem. Mater., 6, 468 (1994).
9. P.B. Messersmith, E.P. Giannelis, "Synthesis and Characterization of Layered Silicate-Epoxy Nanocomposites", Chem. Mater., 6, 1719 (1994).
10. J.M. Brown, D.Curliss, R.A. Vaia, "Thermoset-Layered Silicate Nanocomposites.

Quaternary Ammonium Montmorillonite with Primary Diamine Cured Epoxies", Chem. Mater, 12, 3376 (2000).

11. G. Galgali, C.Ramesh, A.Lele, "A Rheological Study on the Kinetics of Hybrid Formation in Polypropylene Nanocomposites", Macromolecules, 34, 852 (2001).
12. G.M. Chen, Y.M. Ma, Z.N.Qi, "Preparation and Morphological Study of an Exfoliated Polystyrene/Montmorillonite Nanocomposites", Scripta mater., 44, 125 (2001).
13. J. X. Ren, A.S. Silva, R. Krishnamoorti, "Linear Viscoelasticity of Disordered Polystyrene-Polyisoprene Block Copolymer Based Layered-Silicate Nanocomposites", Macromolecules, 33, 3739 (2000).
14. K.Yano, A. USUKI, A.Okada, T. Kurauchi, O.Kamigaito, "Synthesis and Properties of Polyimide-Clay Hybrid", J. Polym. Sci.: Part A: Polymer Chemistry, 31, 2493 (1993).
15. H.L. Tyan, C.M. Leu, K.H. Wei, "Effect of Reactivity of Organics-Modified Montmorillonite on the Thermal and Mechanical Properties of Montmorillonite /Polyimide Nanocomposites", Chem. Mater., 13, 222 (2001).
16. Y.I. Tien, K.H.Wei, "High-Tensile-Property Layered Silicates/Polyurethane Nanocomposites by Using Reactive Silicates as Pseudo Chain Extenders", Macromolecules, 34, 9045 (2001).
17. C.J.G. Plummer, L.Garamszegi, Y. Leterrier, M. Rodlert, J.A.E. Manson, "Hyperbranched Polymer Layered Silicate Nanocomposites", Chem. Mater, 14, 486 (2002).

18. J.A.E. Manson, C.J.G. Plummer, M.Rodlert, "Dentritic Polymers for Nanostructured Composite Materials", TOP NANO 21 (2002).

19. J.S. Chen, M.D. Poliks, C.K.Ober, Y.M.Zhang, U.Wiesner, E.Giannelis, "Study of the interlayer expansion mechanism and thermal-mechanical properties of surface-initiated epoxy nanocomposites", Polymer, 43, 4895 (2002).

20. D.Kong, C.E.Park, "Real Time Exfoliation Behavior of Clay Layers in Epoxy-Clay Nanocomposites", Chem. Mater., web.no: cm0205837 (2002).

21. Y.C. Ke, J.K.Lu, X.S.Yi, Z.N.Qi, "The Effects of Promoter and Curing Process on Exfoliation behavior of Epoxy/Clay Nanocomposites", J. Appl. Polym. Sci., 78, 808 (2002).

22. X. Kornmann, H. Lindberg, L.A. Berglund, "Synthesis of epoxy-clay nanocomposites: influence of the nature of the clay on structure", Polymer, 42, 1303 (2001).

23. X. Kornmann, H. Lindberg, L.A.Berglund, "Synthesis of epoxy-clay nanocomposites. Influence of the nature of the curing agent on structure", Polymer, 42, 4493 (2001).

24. T.J.Pinnavaia, T.Lan, Z. Wang, H.Z. Shi, P.D. Kaviratna, "Clay-Reinforced Epoxy Nanocomposites: Synthesis, Properties, and Mechanism of Formation", Nanotechnology—Molecularly Designed Materials, Chapter 17, ACS Symposium Series 622 (1996).

25. J.F. Timmerman, B.S. Hayes, J.C. Seferis, "Nanoclay reinforcement effects on the cryogenic microcracking of carbon fiber/ epoxy composites", Composites

Science and Technology, 62, 1249 (2002).

26. B.P. Rice, C.G. Chen, L. Cloos, "Organoclay-Aerospace Epoxy Nanocomposites, Part I, SAMPE Journal, 37, 5, 7 (2001).
27. C.G. Chen, D. Curliss, "Resin Matrix Composites: Organoclay-Aerospace Epoxy Nanocomposites, Part I, SAMPE Journal, 37, 5, 11 (2001).
28. B.K.G. Theng, The chemistry of clay-organic reactions, Wiley, New York [1974].
29. J.C. Dai, J.T. Huang, "Surface modification of clays and clay-rubber composite", Applied Clay Science, 15, 51 (1999).
30. L. Margulies, H. Rozen, S. Nir, " Model For Competitive Adsorption of Organic Cations on Clays", 36, 270 (1988).
31. S.J. Park, D.I. Seo, J.R. Lee, "Surface Modification of Montmorillonite on Surface Acid-Base Characteristics of Clay and Thermal Stability of Epoxy/Clay Nanocomposites", J. Colloid & Interface Sci., 251, 160 (2002).
32. T. Lan, P.D. Kaviratna, T.J. Pinnavaia, "Mechanism of Clay Tactoid Exfoliation in Epoxy-Clay Nanocomposites", Chem. Mater, 7, 2144 (1995).
33. C. Zilg, R. Thomann, J. Finter, R. Mülhaupt, "The influence of silicate modification and compatibilizers on mechanical properties and morphology of anhydride-cured epoxy nanocomposites", Macromol. Mater. Eng., 280/281, 41 (2000).
34. D.J. Suh, O.O. Park, "Nanocomposite Structure Depending on the Degree of Surface Treatment of Layered Silicate", J. Appl. Polym. Sci., 83, 2143 (2002).
35. H.L. Tyan, C.M. Leu, K.H. Wei, "Effect of Reactivity of Organics-Modified

Montmorillonite on the Thermal and Mechanical Properties of Montmorillonite/ Polyimide Nanocomposites", Chem. Mater., 13, 222 (2001).

36. H.L. Tyan, K.H. Wei, T.E. Hsieh, "Mechanical Properties of Clay-Polyimide (BTDA-ODA) Nanocomposites via ODA-Modified Organoclay", J. Polym. Sci.: Part B: Polym. Phys., 38, 2873 (2000).
37. O. Becker, R.Varley, G. Simon, "Morphology, thermal relaxations and mechanical properties of layered silicate nanocomposites based upon high-functionality epoxy resins", Polymer, 43, 4365 (2002).
38. A.S. Zerda, A.J. Lesser, "Intercalated Clay Nanocomposites: Morphology, Mechanics, and Fracture Behavior", J. Polym. Sci.: Part B: Polym. Phys., 39, 1137 (2001).
39. Z. Wang, T.J. Pinnavaia, "Hybrid Organic-Inorganic Nanocomposites: Exfoliation of Magadiite Nanolayers in an Elastomeric Epoxy Polymer", Chem. Mater., 10, 1820 (1998).
40. C. Zilg, R. Mulhaupt, J. Finter, "Morphology and toughness/stiffness balance of nanocomposites based upon anhydride-cured epoxy resins and layered silicates", Macromol. Chem. Phys., 200, 661 (1999).
41. C.S. Triantafillidis, P.C.LeBaron, T.J. Pinnavaia, " Homostructured Mixed Inorganic—Organic Ion Clays: A New Approach to Epoxy Polymer-Exfoliated Clay Nanocomposites with a Reduced Organic Modifier Content", Chem. Mater., 14, 4088 (2002).
42. I.J. Chin, T.Thrun-Albrecht, H.C. Kim, T.P. Russell, J. Wang, "On exfoliation of

montmorillonite in epoxy", Polymer, 42, 5947 (2001).

43. A. Lee, J.D. Lichtehan, " Thermal and Viscoelastic Property of Epoxy-Clay and Hybrid Inorganic-Organic Epoxy Nanocomposites", J. Appl. Polym. Sci., 73, 1993 (1999).
44. J.J. Luo, I.M. Daniel, "Characterization and modeling of mechanical behavior of polymer/clay nanocomposites", Composites Science and Technology, 63, 1607 (2003).
45. M. Vacatello, "Monte Carlo Simulations of Polymer Melts Filled with Solid Nanoparticles", Macromolecules, 34, 1946 (2001).
46. A.C. Balazs, C. Singh, E. Zhulina, "Modeling the Interactions between Polymers and Clay Surfaces through Self-Consistent Field Theory", Macromolecules, 31, 8370 (1998).
47. V.V. Ginzburg, A.C. Balazs, "Calculating Phase Diagrams of Polymer-Platelet Mixtures Using Density Functional Theory: Implications for Polymer/Clay Composites", Macromolecules, 32, 5681 (1999).
48. R.A. Vaia, E.P. Giannelis, "Lattice Model of Polymer Melt Intercalation in Organically-Modified Layered Silicates", Macromolecules, 30, 7990 (1997).
49. R.A. Vaia, E.P. Giannelis, "Polymer Melt Intercalation in Organically-Modified Layered Silicates: Model Predictions and Experiment", Macromolecules, 30, 8000 (1997).
50. M.R. VanLandingham, R.F. Eduljee, and J.W. Gillespie, Jr., "Relationships Between Stoichiometry, Microstructure, and Properteis for Amine-Cured

Epoxies", J. Appl. Polym. Sci., 71, 699 (1999).

51. G. Bar, Y. Thomann, R. Brandsch, H.-J. Cantow, "Factors Affecting the Height and Phase Images in Tapping Mode Atomic Force Microscopy. Study of Phase-Separated Polymer Blends of Poly(ethene-*co*-styrene) and Poly(2,6-dimethyl-1,4-phenylene oxide)", Langmuir, 13, 3807 (1997).
52. D. Raghavan, M. VanLandingham, X. Gu, T. Nguyen, "Characterization of Heterogeneous Regions in Polymer Systems Using Tapping Mode and Force Mode Atomic Force Microscopy", Langmuir, 16, 9448 (2000).
53. J. P. Cleveland, B. Anczykowski, A. E. Schmid, V. B. Elings, "Energy Dissipation in Tapping-Mode Atomic Force Microscopy", Applied Physics Letters, 72, 2613 (1998).
54. M. Rafailovich, S. Stony, B. R. Eby, "AFM Topography/Phase Imaging Study of Clay Additives in Polymer Blends", Veeco Metrology Group, Veeco Inc. (2002).
55. X. Gu, D.L. Ho, L. Sung, M.R. VanLandingham, T. Nguyen, "Nanocharacterization of Surface and Interface of Different Epoxy Networks", Mat. Res. Soc. Proc., MRS Symposium DD Polymer Interfaces and Thin Films, Materials Research Society, Volume 710, Editors: A. Karim, C.W. Frank, T.P. Russell, P.F. Nealey (2002).
56. J. K. Kocsis, O. Gryshchuk, S. Schmitt, " Vinylester/epoxy-based thermosets of interpenetrateing network structure: An atomic force microscopic study", J. Mater. Sci., 38, 413 (2003).
57. J. Duchet, J.P. Pascault, "Do Epoxy-Amine Networks Become Inhomogeneous at

the Nanometric Scale", J. Polym.Sci.: Part B: Polymer Physics, Vol. 41, 2422 (2003).

58. J.K. Kocsis, O. Gryshchuk, J. Frőhlich, R. Műlhaupt, "Interpenetrating vinylester/epoxy resins modified with organophilic layered silicates", Composites Science and Technology, 63, 2045 (2003).

59. M.S. Bischel, M.R. Vanlandingham, R.R. Eduljee, J.W. Gillespie, Jr., J.M. Schultz, " On the use of nanoscale indentation with the AFM in the identification of phases in blends of linear low density polyethylene and high density polyethylene", J. Mater. Sci., 35, 221 (2000).

60. Q.P. Guo, R. Thomann, W. Gronski, R. Staneva, R. Ivanova, B. Stűhn, "Nanostructures, Semicrytalline Morphology, and Nanoscale Confinement Effect on the Crystallization Kinetics in Self-Orfanized Block Copolymer/Thermoset Blends", Macromolecules, 36, 3635 (36).

61. Q.P. Guo, R. Thomann, W. Gronski, T. Thurn-Albrecht, "Phase Behavior, Crystallization, and Hierarchical Nanostructures in Self-Organized Thermoset Blends of Epoxy Resin and Amphihilic Polyethylene oxide)-block-poly(propylene oxide)-bloc-poly(ethylene oxide) Triblock Copolymers", Macromolecules, 35, 3133 (2002).

62. C. Serré, M. Vayer, R. Erre, C. Ollive, "Morphology of the outermost layer of a compression molded composite based on unsatureated polyester resin", J. Mater. Sci., 34, 4203 (1999).

63. M. Vayer, C. Serré, N. Boyard, C. Sinturel, R. Erre, "Surface morphologies of

composites based on unsaturated polyester pre-polymer", J. Mater. Sci, 37, 2043 (2002).

64. Closite Data Sheet from the website of Southern Clay Products: http://www.nanoclay.com/data/Na.htm.

65. Technical Bulletin from Huntsman website: http://www.huntsman.com/ performance_chemicals/Media/JEFFAMINET403.pdf.

66. D. Dolphin, A. Wick, Tabulation of Infrared Spectral Data, New York, Wiley, (1977).

67. K.A. Carrado, L.Q. Xu, R. Csencsits, J.V. Mutean, "Use of Organo- and Alkoxysilandes in the Synthesis of Grafted and Pristine Clay", Chem. Mater., 13, 3766, (2001).

68. W.P. Liu, S.V. Hoa, M. Pugh, "Morphology and Performance of Epoxy Nanocomposites Modified with Organoclay and Rubber", Polym. Eng.& Sci., 44, 1178, (2004).

69. B. Ellis, "Chemistry and Technology of Epoxy Resins", Blackie Academic & Professional, (1993).